

Chapter 10

Pyroclastic Flows, Lahars, and Mixed Avalanches Generated During the 2006 Eruption of Augustine Volcano

By James W. Vallance,¹ Katharine F. Bull,² and Michelle L. Coombs³

Abstract

Each of the three phases of the 2006 eruption at Augustine Volcano had a distinctive eruptive style and flowage deposits. From January 11 to 28, the explosive phase comprised short vulcanian eruptions that punctuated dome growth and produced volcanowide pyroclastic flows and more energetic hot currents whose mobility was influenced by efficient mixing with and vaporization of snow. Initially, hot flows moved across winter snowpack, eroding it to generate snow, water, and pyroclastic slurries that formed mixed avalanches and lahars, first eastward, then northward, and finally southward, but subsequent flows produced no lahars or mixed avalanches. During a large explosive event on January 27, disruption of a lava dome terminated the explosive phase and emplaced the largest pyroclastic flow of the 2006 eruption northward toward Rocky Point. From January 28 to February 10, activity during the continuous phase comprised rapid dome growth and frequent dome-collapse pyroclastic flows and a lava flow restricted to the north sector of the volcano. Then, after three weeks of inactivity, during the effusive phase of March 3 to 16, the volcano continued to extrude the lava flow, whose steep sides collapsed infrequently to produce block-and-ash flows.

The three eruptive phases were each unique not only in terms of eruptive style, but also in terms of the types and morphologies of deposits that were produced, and, in particular, of their lithologic components. Thus, during the explosive phase, low-silica andesite scoria predominated, and

intermediate- and high-silica andesite were subordinate. During the continuous phase, the eruption shifted predominantly to high-silica andesite and, during the effusive phase, shifted again to dense low-silica andesite. Each rock type is present in the deposits of each eruptive phase and each flow type, and lithologic proportions are unique and consistent within the deposits that correspond to each eruptive phase.

The chief factors that influenced pyroclastic currents and the characteristics of their deposits were genesis, grain size, and flow surface. Column collapse from short-lived vulcanian blasts, dome collapses, and collapses of viscous lavas on steep slopes caused the pyroclastic currents documented in this study. Column-collapse flows during the explosive phase spread widely and probably were affected by vaporization of ingested snow where they overran snowpack. Such pyroclastic currents can erode substrates formed of snow or ice through a combination of mechanical and thermal processes at the bed, thus enhancing the spread of these flows across snowpack and generating mixed avalanches and lahars. Grain-size characteristics of these initial pyroclastic currents and overburden pressures at their bases favored thermal scour of snow and coeval fluidization. These flows scoured substrate snow and generated secondary slurry flows, whereas subsequent flows did not. Some secondary flows were wetter and more lahatic than others. Where secondary flows were quite watery, recognizable mixed-avalanche deposits were small or insignificant, and lahars were predominant. Where such flows contained substantial amounts of snow, mixed-avalanche deposits blanketed medial reaches of valleys and formed extensive marginal terraces and axial islands in distal reaches. Flows that contained significant amounts of snow formed cogenetic mixed avalanches that slid across surfaces protected by snowpack, whereas water-rich axial lahars scoured channels.

Correlations of planimetric area (A) versus volume (V) for pyroclastic deposits with similar origins and characteristics exhibit linear trends, such that $A=cV^{2/3}$, where c is a constant for similar groups of flows. This relationship was tested and

¹U.S. Geological Survey, Cascades Volcano Observatory, 1300 SE Cardinal Court, Vancouver, WA 98683.

²Alaska Volcano Observatory, Alaska Division of Geological and Geophysical Surveys, 3354 College Road, Fairbanks, AK 99709.

³Alaska Volcano Observatory, U.S. Geological Survey, 4200 University Drive, Anchorage, AK 99508.

calibrated for dome-collapse, column-collapse, and surgelike flows using area-volume data from this study and examples from Montserrat, Merapi, and Mount St. Helens. The ratio $A/V^{2/3} = c$ gives a dimensionless measure of mobility calibrated for each of these three types of flow. Surlike flows are highly mobile, with $c \approx 520$; column-collapse flows have $c \approx 150$; and dome-collapse flows have $c \approx 35$, about that of simple rock avalanches. Such calibrated mobility factors have a potential use in volcano-hazard assessments.

Introduction

The 2006 eruption of Augustine Volcano spanned less than 4 months, yet the snowclad, unglaciated Alaskan island volcano erupted in a range of eruptive styles characterized by diverse deposit types, each with distinctive morphology, grain size, and lithologic composition. Within 3 months, three eruptive phases produced at least four lava domes and two lava flows, ranging in composition from low- to high-silica andesite (57.3–63.2 weight percent SiO_2 ; Larsen and others, this volume). During each eruptive phase, pyroclastic flows produced deposits with the same four predominant rock types; however, the flow deposits of each phase had distinctive morphology and proportions of lithologic components. Only the initial explosive phase generated lahars and mixed-rock-and-snow avalanches.

The morphology, lithologic composition, and areal extent of deposits were initially estimated during the eruption by utilizing onsite Web cameras, satellite imagery, aerial surveillance, and occasional field-based observations (Coombs and others, this volume). These early estimates provided important groundwork for later, field-based mapping, as well as for understanding the eruption chronology. Later field investigations revealed that the deposits were uniformly more abundant, widespread, and varied than suggested by preliminary estimates.

This chapter describes the flow deposits of the 2006 eruption of Augustine Volcano in terms of their morphology, lithologic composition, and sedimentology and discusses possible mechanisms for their flow generation and transport. Our study complements other chapters in this volume that discuss the eruption chronology, seismic interpretation of flow timing, tephra falls, and petrogenesis (Coombs and others, McNutt and others, Wallace and others, and Larsen and others). In particular, this chapter is a companion to that by Coombs and others, which presents a detailed chronology of the events that produced the on-island deposits, as well as a 1:20,000-scale map of the 2006 deposits. The detailed monitoring of Augustine Volcano enabled us to establish a fairly accurate chronology of flowage events (Coombs and others, McNutt and others, Power and Lalla, this volume), allowing us to show how composition and texture of erupted material and morphology of deposits changed during the course of the eruption. We show that lithologic components of clastic deposits, distinct in composition and texture, were produced throughout the eruption, though

in proportions that varied systematically with eruptive phase and style. In addition, the distinctive morphologies and relations between pyroclastic-current, lahar, and mixed-avalanche deposits of the initial, explosive phase suggests that deposition on and incorporation of snow were primary controlling factors in the sheetlike morphology of the initial pyroclastic currents, the production of mixed avalanches, and the release of melted ice and snow to produce lahars.

Flowage Phenomena and Recognition of Their Deposits

“Pyroclastic current” is defined here as a general term meaning any pyroclastic density current, regardless of origin, mechanism of transport, or particle concentration. Genesis may be plume-column collapse, or fracturing and collapse of a dome or lava flow. A pyroclastic current is a hot mixture of rock (lithics, pumice, or both lithics and pumice), ash, and gas that flows rapidly away from its source. In this study, the high-solids-fraction end member of the pyroclastic-current spectrum is a pyroclastic flow, and the dilute end member is a pyroclastic surge. In pyroclastic currents, both dense and dilute, the fluid phase, gas, provides at least partial support for the particulate phase and lends such flows their mobility. We define “block-and-ash flows” as pyroclastic flows derived from fracturing and collapse of lava domes or lava flows.

A “lahar” is defined here as a rapidly flowing, gravity-driven mixture of rock debris and water from a volcano. A lahar event may include, in order of increasing proportion of water, debris-flow, hyperconcentrated-flow, and stream-flow or flood phases, but the term “lahar” itself includes only sediment-rich debris flow and intermediate hyperconcentrated flows (Vallance, 2000). The fluid at least partly supports the solid particles in lahar flows.

We define volcanic “mixed avalanche” as a flow or avalanche of rock particles, water, and snow or ice in which snow and ice provide partial support for the solid particles. Such flows, variously termed “mixed avalanches” (Pierson, 1994) and “hybrid flows” (Waitt, 1995) are most common where pyroclastic currents sweep across the extensive snow and ice covering the flanks of a volcano. These phenomena are transitional between snow-rich avalanches and debris flow and commonly behave partly as sliding and partly as flowing mixtures. Waitt and others (1994) describe genetically related sequences of such flows generated by pyroclastic eruptions comprising initial relatively dry debris and snow flows, followed by debris-rich slushy flows and, finally, by watery laharc flows. We report similar sequences of pyroclastic currents, mixed avalanches, and lahars during the 2006 eruption of Augustine Volcano.

At Augustine deposits of pyroclastic flows and lahars are distinctive and commonly well preserved, whereas those of pyroclastic-currents emplaced on snow, mixed avalanches of snow and debris, and lahars that contained substantial snow are ephemeral and can be difficult to distinguish as little as

2 years after the 2006 eruption. Archetypal pyroclastic-flow deposits display coarse levees and digitate margins, and individual flow units are as thick as 2 m. Some more energetic flow deposits thicken to many meters on gentle axial slopes but may thin or be absent on steep slopes and commonly thin to a fine-grained featheredge at deposit margins. In contrast, lahar deposits at Augustine commonly comprise isolated blocks on scoured surfaces bounded by low-aspect blocky levees. Where they funnel into drainages, lahars leave scoured surfaces with faintly stratified deposits, as much as 2 m thick in favorable pockets. Both pyroclastic-current deposits emplaced on snow and mixed-avalanche deposits display soft irregular surfaces crisscrossed with cracks and have thin margins containing lapilli and blocks and commonly lack prominent levees, but ephemeral features like irregular surfaces and cracks disappear in a few years time. Each type of deposit commonly drapes large blocks and vegetation at its margins, suggesting flows that were of greater depth than thin remnants might suggest. These two types of deposit are more distinctive where the flows moved into vegetation. Pyroclastic currents stripped and singed vegetation above the snow level but left it unaffected below, whereas mixed avalanches broke exposed vegetation into uncharred stem and branch fragments but similarly preserved lush vegetation below the emplacement snow surface. In addition, mixed-avalanche deposits are emplaced downslope of cogenetic pyroclastic currents but commonly form genetically related marginal levees for lahars. In such cases, the marginal mixed-avalanche deposits form thick, poorly sorted fills with abundant scattered wood fragments, and the lahar deposits consist of scattered blocks and debris remnants on a scoured, axial channel surface that commonly has vegetation battered and bent over in the flow direction.

Geologic Background and Eruptive History

Augustine is an island volcano, approximately 8 by 11 km, in lower Cook Inlet, 280 km south-southwest of Anchorage, Alaska (fig. 1). The volcano, which is one of the more active volcanoes in Alaska, has had six major eruptions in the 2 centuries before 2006 (1812, 1883, 1935, 1963–64, 1976, 1986; Coats, 1950; Johnstone, 1978; Miller and others, 1998). It has a central vent and comprises a series of domes, lava flows, pyroclastic flows, and debris-avalanche deposits that overlie Jurassic and Cretaceous sedimentary rocks of the Naknek Formation exposed on the south side of the island (Dettermen and Reed, 1980; Waitt and Begét, 1996 and 2009). Johnston (1978) suggests that the onset of volcanism was during the Moosehorn glacial advance, 19.0–15.5 ka. Hummocky topography along the north coastline is evidence for numerous catastrophic collapses of the summit dome, the most recent of which, in 1883, generated a tsunami that reached the east shores of Cook Inlet (Begét and Kienle, 1992; Siebert and others, 1995; Begét and Kowalik, 2006; Waitt, this volume).

Recent historical eruptions of Augustine have followed sequences similar to that in 2006. Eruption sequences have typically begun with explosive activity that produced ash plumes to higher than 10 km above mean sea level (asl) and pyroclastic flows, followed by effusive activity that built lava domes and lava flows and caused block-and-ash flows (Kienle and Forbes, 1977; Johnston, 1978; Kienle and Swanson, 1985; Swanson and Kienle, 1988). Lavas and juvenile clasts have consistently been crystal-rich, vesicular to dense, two-pyroxene+amphibole+olivine, low- through high-silica andesite and dacite (56–64 weight percent SiO_2), with banded clasts of the same rock types (Johnston, 1978; Daley, 1986; Harris and others, 1987; Miller and others, 1998, p. 14).

The well-studied 1976 and 1986 eruptions of Augustine were particularly similar to the 2006 eruption in terms of sequence, deposit distributions, and magma compositions (Swanson and Kienle, 1988; Power and others, 2006; Coombs and others, this volume). Before the 1976 eruption, precursory seismic activity began in May 1975, and the volcano erupted explosively on January 22. Explosions continued for about 3 days, produced ash plumes as high as 14 km asl, and generated pyroclastic flows and lahars on all flanks of the volcano (Kienle and Forbes, 1977; Johnston, 1978). At least one of the pyroclastic flows burned and damaged a research station on the northern tip of the island, and another reached the sea to the east of there. Activity resumed on February 6, and the volcano erupted almost continuously until February 16. Pyroclastic flows also occurred during the continuous phase of ash emission. A lava dome emerged February 11–12. After a

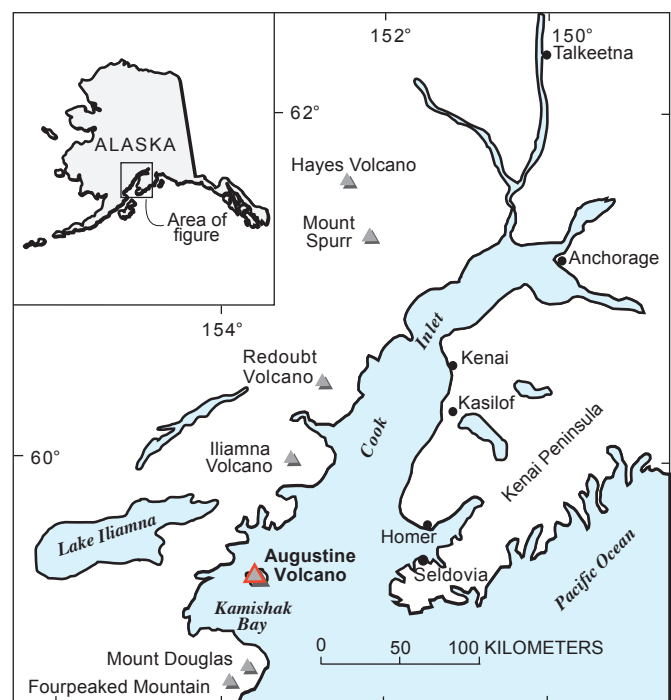


Figure 1. Index map of southern Alaska, showing location of Augustine Volcano in lower Cook Inlet.

repose period, renewed effusion occurred in August. The total volume of pyroclastic-flow deposits from the 1976 eruption was estimated at 0.05 km³ (Kienle and Swanson, 1985).

Seismic activity precursory to the 1986 eruption began in July 1985, and the explosive phase began in late March 1986. Ash plumes rose as high as 12 km asl but, unlike during previous eruption, pyroclastic flows moved only northward, some reaching the sea (Swanson and Kienle, 1988). Ash reached surrounding communities, including Anchorage, March 27–31. During April 23–28, the continuous phase was marked by effusion and resulted in a short, blocky lava flow. Encroachment of the lava flow and a growing dome on steep slopes generated scattered block-and-ash flows. A 4-month repose followed the April activity. Renewed effusion August 30–31 accelerated dome growth and sent block-and-ash flows down the north flank of the volcano.

The 2006 Eruption Sequence

Slowly escalating, shallow seismicity (increasing from ~4–8 to 20–35 earthquakes per day) initiated precursory activity at Augustine in late April 2005 (Jacobs and McNutt, this volume; Power and Lalla, this volume). Seismicity increased through fall 2005. Inflation at the volcano began in midsummer 2005, marked by lengthening along a north-south baseline between stations located at 100 and 200 m asl, and continued at a steady rate until late November (Cervelli and others, 2006). Inflation reached a maximum by mid-December, suggesting intrusion of a northwest-striking dike at shallow levels (Cervelli and others, 2006; Cervelli and others, this volume). In mid-December, phreatic explosions produced a thin layer of ash on the winter snowpack within about 1 km of the vent (Power and others, 2006; Wallace and others, this volume). Small explosions continued through December.

From January to March 2006, distinct eruptive styles and deposits characterized each of the three eruptive phases (table 1). During the explosive phase, from January 11 to 28, 13 discrete vulcanian explosions, from 1 to 11 minutes in duration, initiated pyroclastic flows, and during quiescent intervals between explosions, three lava domes effused (Coombs and others, this volume). Initial pyroclastic currents of the explosive phase were widespread and deposited onto snow. Varying amounts of snow incorporated by the flows, or that underlay their still hot deposits, produced mixed avalanches and lahars (fig. 2A). Subsequent pyroclastic flows moved across previous deposits rather than snow and did not generate secondary flows (figs. 2A, 2B). None of the pyroclastic flows reached the sea, although near Rocky Point the last explosive-phase pyroclastic flow came within 100 m of the water (fig. 2B). During the continuous phase, from January 28 to February 10, continuous rapid effusion and nearly constant collapse of a high-silica-andesite lava dome punctuated by small explosions caused countless pyroclastic flows restricted to the north flank of the volcano (fig. 2C). After a pause in eruptive activity from February 10 to March 3, the effusive phase, from March 3 to

March 16, generated blocky, dark-gray to black, low-silica andesite lava flows north and northeast of the summit and generated block-and-ash flows on steep flanks of the upper edifice (fig. 2D). After effusion ceased on March 16, the lava flows continued to shed rockfall and block-and-ash flows until at least late May. In October 2006, remobilization of pinkish-gray ash deposits during rainy weather resulted in water-rich lahar deposits, primarily on the north flank of the volcano (Coombs and others, this volume).

Methods

Field Methods

We conducted limited geologic fieldwork on Augustine Island (fig. 1) during the eruption and continued with more detailed investigations during 3 weeks in August 2006 and 1 week in July 2008. We noted pyroclastic-current, mixed-avalanche, and lahar deposits at more than 500 sites and collected 72 representative bulk samples for grain-size and lithologic analyses (table 2).⁴ Where recognizable, distinct layers or facies present within each flow deposit were also sampled, and samples were taken at multiple sites along a longitudinal section of single flow units of at least two pyroclastic-flow deposits. As described below, all units contained clasts of multiple, distinct rock types, identifiable on the basis of color, morphology, and vesicularity. At 20 sites we performed “clast counts” to determine the proportions of various rock types within a given deposit. We conducted clast counts by picking a patch of ground at each site that contained at least 50 to 100 clasts, and counting the clasts that were 10 to 30 cm in diameter.

Methods for Analyzing Grain-Size Distributions

A total of 60 samples were submitted for grain-size analysis to the sediment-processing laboratory at the Cascades Volcano Observatory (table 3). All samples were sieved, using the visual-accumulation method, in one- ϕ intervals, from -6ϕ (32 mm diam) to 4ϕ (≥ 0.063 mm diam). Of the 60 samples, 17 samples had the fine-ash (<0.063 mm diam) portion analyzed on a Sedigraph to calculate the weight percentage of each size class between 5ϕ and 10ϕ (0.063 and 0.001 mm diam, respectively). Standard statistics for grain-size distributions were calculated for each bulk sample (table 4).

Methods for Analyzing Flow Components

Preliminary clast counts in the field were refined after grain-size analysis by performing lithologic analysis on representative size classes from explosive- and continuous-phase samples. Lithologic categories were initially defined in the

⁴Note that tables 2, 3, 4, 6 and 8 are grouped at the back of this chapter, after References Cited.

Table 1. Summary of 2006 eruption and resulting deposits at Augustine Volcano, Alaska.

[Phases, event dates and times, and unit names from Coombs and others (this volume). Seismic duration from McNutt and others (this volume). Plume height from Wallace and others (this volume). Units are defined in figure 2]

| Phase | Event | Date (2006) | Time of onset (AST) | Seismic duration (mm:ss) | Plume height (km) | Units emplaced | | Comments |
|--|-------|----------------|------------------------------|--------------------------------|-------------------------|-------------------------|--|--|
| | | | | | | Lava flows and domes | Flowage deposits | |
| Explosive January 11–28 | 1 | 1/11 | 4:44 | 1:18 | 6.5 | | Mixed avalanches (Exma). | Mixed avalanches of rock and snow were observed after these initial explosions, but were later covered. No lahars were observed. |
| | 2 | 1/11 | 5:12 | 3:18 | 10.2 | | | |
| | | 1/12 | | | | Ephemeral dome | | |
| | 3 | 1/13 | 4:24 | 11:00 | 10.2 | | Pyroclastic flows and currents (Expct); mixed avalanches (Exma) and lahars (Exlh). | Most widespread pyroclastic currents (Expct); mixed avalanches (Exma) and lahars (Exlh) in the east sector occurred during this interval. |
| | 4 | 1/13 | 8:47 | 4:17 | 10–16 | | | |
| | 5 | 1/13 | 11:22 | 3:24 | 10–16 | | Pyroclastic flows (Expf); mixed avalanche (Exma); lahar (Exlh). | Widespread pyroclastic flows (Expf); mixed avalanches (Exma) and lahars (Exlh) in the northern sector occurred during this interval. Thick pyroclastic flows with coarse levees (Expf) were common to the east and north. |
| | 6 | 1/13 | 16:40 | 4:00 | 9–11 | | | |
| | 7 | 1/13 | 18:58 | 3:00 | 13.5 | | Pyroclastic flows (Expf); mixed avalanche (Exma); lahar (Exlh). | Widespread pyroclastic flows (Expf); mixed avalanches (Exma) and lahars (Exlh) in the south sector occurred during this interval. Thick pyroclastic flows with coarse levees (Expf) were likely on all flanks. |
| | 8 | 1/14 | 0:14 | 3:00 | 10.2 | | | |
| | | | | | | Dome (Exd1) | | |
| | 9 | 1/17 | 7:58 | 4:11 | 13.5 | | Pyroclastic flows (Expf) | A pyroclastic flow (Expf) emplaced to the southwest, possibly other pyroclastic flows elsewhere. |
| | | | | | | Dome (Exd2) | | |
| | 10 | 1/27 | 20:24 | 9:00 | 10.5 | | Pyroclastic current (Expcc); Rocky Point pyroclastic flow (RPpf). | A pyroclastic current and the voluminous Rocky Point pyroclastic flow were emplaced to the north during this event. Transitional composition between other explosive-phase deposits (rich in scoriaceous low-silica andesite) and continuous-phase deposits (rich in high-silica andesite). |
| | 11 | 1/27 | 23:37 | 1:02 | 3.8 | | | Seismic signal indicates that this event was gas rich and mass poor. |
| Continuous January 28– February 10 | 12 | 1/28 | 2:04 | 2:06 | 7.2 | | | No observations of deposits from these events, but seismic signals suggest pyroclastic flows (McNutt and others, this volume). |
| | 13 | 1/28 | 7:32 | 3:00 | 7–11 | | | |
| | 14 | 1/28 | 14:31 | -- | 8–9 | | | |
| | -- | 1/29 | 11:17 | -- | -- | | Pyroclastic flows and currents (Cpf, Cpc, Cpfw). | Thick, voluminous pyroclastic flows (Cpf, Cpfw, Cpc) were emplaced on the north flanks. High-silica andesite was predominant in deposits; scoriaceous low-silica andesite was rare. No lahar or mixed-avalanche deposits were emplaced. Lava flows began to effuse at the end of the continuous phase. |
| | -- | 2/3 | -- | -- | -- | | | |
| Effusive March 3–16 | -- | 3/3 | | | | | | |
| | -- | | | | | | | |
| | -- | | | | | | | |
| | -- | 3/16 | | | | | | |
| Hiatus | | | | | | | | |
| Effusive March 3–16 | -- | 3/3 | | | | | | |
| | -- | | | | | | | |
| | -- | | | | | | | |
| | -- | 3/16 | | | | | | |

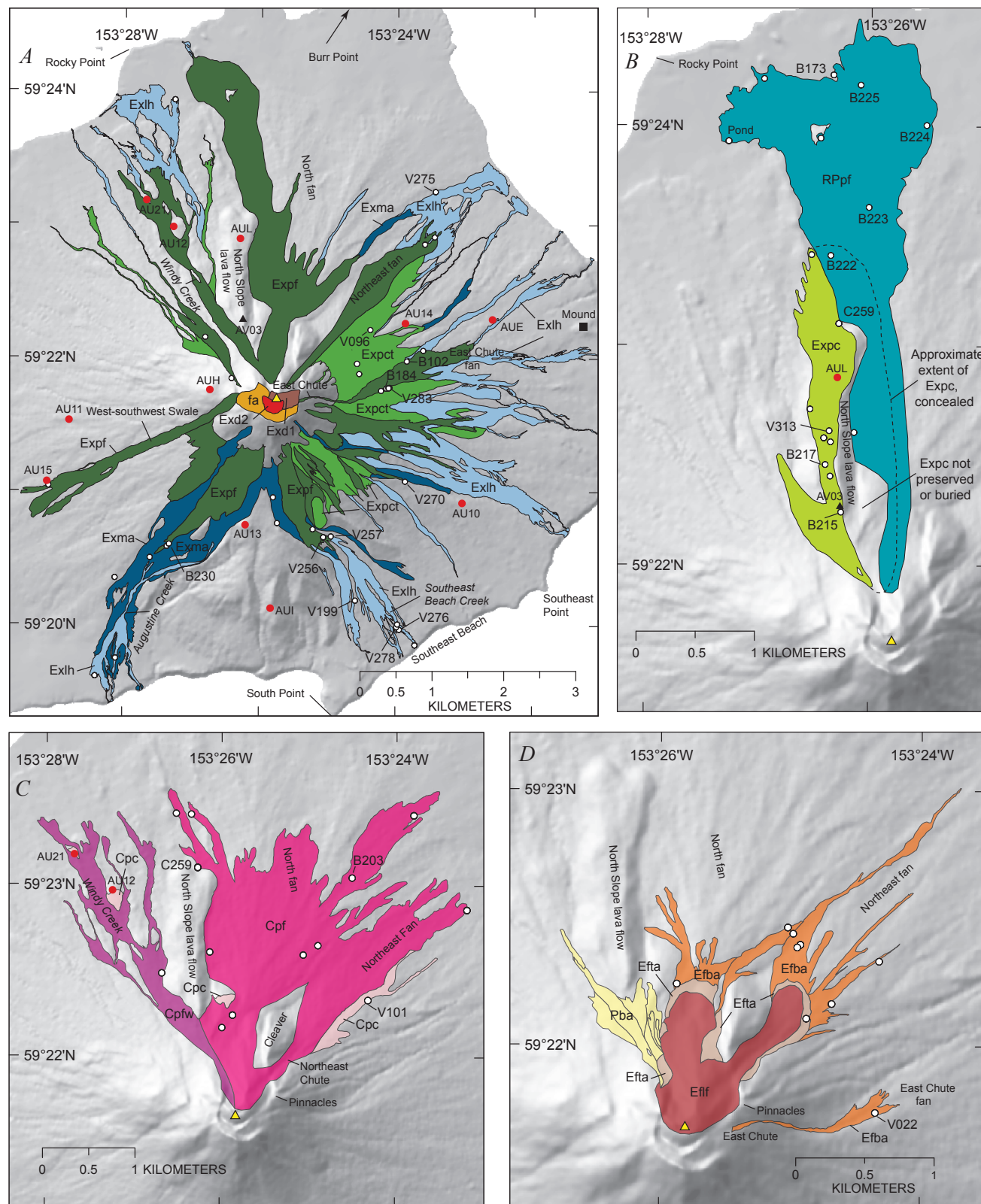




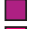
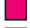

















Figure 2. Time sequence of geologic maps of Augustine Volcano showing distribution of 2006 Augustine deposits and select sample locations (after Coombs and others, this volume). *A*, Explosive-phase deposits of events 1 through 9. *B*, Explosive-phase deposits of event 10. *C*, Continuous-phase deposits. *D*, Effusive-phase deposits. All place names associated with Augustine Volcano are informal except Augustine Creek, Augustine Island, and Burr Point.

| EXPLANATION | | | | | |
|---|-----------------|------------------------------|---|---|--|
| Unit | Name | Phase and event | Dates (2006) | Origin | |
|  | Pba | Block-and-ash flow | Post-eruption | April and May | Collapse of lava flow, lines within indicate individual flow margins |
| | | Effusive phase | March 3–16 | | |
|  | Efta | Talus from lava flow | | | Rockfall |
|  | Eflf | Lava flow | | | Effusion of lava |
|  | Efba | Block-and-ash flow | | | Collapse of lava flow |
| | | Hiatus | Feb. 10–March 3 | | |
| | | Continuous phase | Jan. 28–Feb. 10 | | |
|  | Cpfw | Windy Creek pyroclastic flow | January 30 | | Dome collapse |
|  | Cpf | Pyroclastic flow | January 28–30 | | Dome collapse |
|  | Cpc | Pyroclastic current, thin | January 28–30 | | Dome collapse |
| | | Explosive phase | January 11–27 | | |
|  | fa | Fall deposits | Undifferentiated | January 13–27 | Tephra and ballistic fallout |
|  | RPpf | Rocky Point pyroclastic flow | Event 10 | January 27 | Dome collapse, depressurization |
|  | Expc | Pyroclastic current | Event 10 | January 27 | Dome collapse, depressurization |
|  | Exd2 | Lava dome 2 | Event 9 to 10 | January 17–27 | Effusion of lava |
|  | Exd1 | Lava dome 1 | Event 8 to 9 | January 14–17 | Effusion of lava |
|  | Expf | Pyroclastic flow, coarse | Events 5–9 | January 13–17 | Column collapse |
|  | Exlh | Lahar | Events 3–8 | January 13–14 | Pyroclastic currents across snow |
|  | Exma | Mixed avalanche | Events 3–8 | January 13–14 | Pyroclastic currents across snow |
|  | Expct | Pyroclastic current, thin | Events 3–4 | January 13–14 | Column collapse |
|  | Sample site | | |  | Remote-camera station |
|  | Seismic station | |  | GPS station | |
| | | | |  | Summit, Augustine Volcano |

field and later modified slightly after whole-rock compositional analysis and petrography (fig. 3; table 5). For a few samples, each size fraction was sorted into lithologic categories, and then clast populations for each rock type were counted and weighed (table 6). For most samples, however, we limited the lithologic analysis to the 4- and 8-mm size fractions.

2006 Flows and Flowage Deposits

Our results include emplacement chronology and detailed descriptions of the 2006 Augustine flowage deposits. We also summarize the detailed geologic mapping by Coombs and others (this volume). We use deposit characteristics, distribution, and timing to interpret emplacement and eruption mechanisms during each of the three eruptive phases.

Explosive-phase deposits include pyroclastic currents, lahars, and mixed avalanches on all flanks of the volcano. Pyroclastic deposits range from widely distributed, thin surge deposits to thick, lobate, flow deposits confined to drainages. In contrast, numerous pyroclastic flows of the continuous

phase formed a thick fan restricted to the north side of the volcano and no lahars or mixed avalanches. Effusive-phase lava flows on steep slopes collapsed to form block-and-ash-flow deposits of limited extent north and east of the vent.

Explosive-Phase Deposits, January 11–28

The explosive phase comprised 13 discrete explosions, each lasting 1–11 minutes (table 1). Each explosion produced tephra plumes, and most explosions produced flowage deposits that together draped all flanks of the volcano. Flowage deposits included those emplaced by pyroclastic currents, lahars, and mixed avalanches.

Events 1 and 2, January 11: Vulcanian Explosions and Mixed Avalanches

Two explosions on January 11 cleared the vent, released plumes 6 to 9 km asl, deposited ash on the volcano's flanks, and produced small flowage deposits on the upper flanks of the volcano (table 1) (Schneider and others, 2006; Bailey and



others, this volume). Seismicity suggests that the first short explosion was primarily a gas-release, vent-clearing event (McNutt and others, this volume). The second explosion probably produced the flowage deposits. After these explosions and before those of January 13, an ephemeral lava dome grew (table 1).

Alaska Volcano Observatory geologists on an overflight, plus Web- and fixed-camera images, documented mixed avalanches of rock and snow on the flanks of the volcano the afternoon after these explosions. Lobate deposits of the flows underlay upper drainages around the volcano (Coombs and others, this volume). The lobes were 50 to 300 m wide, confined to gullies, extended from 1 to 2 km down the flanks of the volcano from 300 to 700 m asl, and were at least several meters thick. Close examination of aerial photographs showed that the flows contained abundant snow, as well as rock debris. We observed little evidence of melting in the photographs; surface water was not released beyond the lobe fronts, although water rivulets formed on the flow surface. As a result, we infer that the flows were not particularly hot. These deposits were subsequently covered or destroyed by later events and so were not visited or sampled. Samples of the January 11 ash deposits contained altered, dense clasts and no juvenile material (Wallace and others, this volume). We therefore infer that these mixed-avalanche deposits contained little or no juvenile rock either.

Events 3 through 9, January 13–17: Widespread Pyroclastic Currents, Lahars, and Mixed-Avalanches

Seven explosions, five on January 13, one on January 14, and one on January 17, lasted 3–11 minutes. The explosions produced widespread pyroclastic currents, mixed avalanches, lahars, and tephra falls, and all deposits contained juvenile material (table 1, fig. 2A). The short duration of these events, their pyroclastic nature, and their seismic characteristics indicate that they were vulcanian. McNutt and others (this volume) infer that the short duration and the dominantly emergent characteristics of events 3–9 (table 1) indicate a moderately uniform distribution of gas within the magma as it exited the vent. The high proportions of vesicular, high- and low-silica andesite within pyroclastic products of the eruption are consistent with short-term, explosive release of gas-rich magma (fig. 4).

Figure 3. Photographs of clastic rock types ejected during 2006 eruption of Augustine Volcano, Alaska. *A*, Low-silica andesite scoria. *B*, Dense low-silica andesite. *C*, High-silica andesite, friable and vesicular with a cinderblock-like texture. *D*, Dense intermediate-silica andesite. *E*, Banded scoria with end members of high-silica andesite (HSA) and low-silica andesite scoria (LSAS).

Table 5. Rock types in flow deposits from the 2006 eruption of Augustine Volcano, Alaska.

| Lithology (acronym) | Description | Vesicularity ¹ |
|---|--|---------------------------|
| Low-silica andesite scoria (LSAS) | Reddish-brown to black vesicular porphyritic andesite with distinctive, pale- to olive-green rinds. Smaller lapilli are wholly olive green. Clasts commonly are cauliform. Abundant phenocrysts of plagioclase and less abundant pyroxene visible in hand specimen. | 33±5 |
| Dense low-silica andesite (DLSA) | Dark-gray to black, poorly vesicular andesite. Some groundmass is glassy, and clasts are commonly angular. Phenocrysts include plagioclase, clinopyroxene, and orthopyroxene. Some lapilli and blocks have breadcrust rinds. | 20±4 |
| High-silica andesite (HSA) | Light- to medium-gray, moderately vesicular, crystal-rich high-silica andesite. Phenocrysts include plagioclase, pyroxene, and amphibole. Clasts are lower in density than DLSA and commonly rounded owing to friable, cinderblock-like texture. Clast interiors may be variably oxidized. | 37±8 |
| High-silica andesite pumice (HSAP) | White to cream-colored porphyritic andesite, moderately to highly vesicular. Phenocrysts include plagioclase, pyroxene, and amphibole. | ~42 |
| Dense intermediate-silica andesite (DIA) | Light- to medium-gray, poorly vesicular porphyritic andesite. Some groundmass is glassy, and clasts are commonly angular. | 22±3 |
| Banded | Banded clasts; any combination of lithologies above. | 39±9 |
| Oxidized | Red, pink, orange, and yellow tinted clasts. Includes glassy, dense, vesicular clasts and crystals. May not all be juvenile. | Not determined |
| Crystals | Crystals, singly or in clots (with little to no groundmass attached; crystals more abundant than groundmass). Consistently present in the 2-mm and smaller size classes, increasing in proportion with decreasing size class. | Not applicable |
| High-silica inclusions ² | Lavender patches and veinlets within HSA clasts in continuous-phase pyroclastic-flow deposits. In thin section, the patches are monocrystalline and polycrystalline masses in a groundmass of quartz, feldspar, clear glass, and vesicles. Masses are predominantly plagioclase (mostly sieve textured) but also include orthopyroxene and biotite. Micrographic textures are relatively common. | Not determined |
| Fine-grained gabbroic inclusions ² | Salt-and-pepper, equigranular blocks or inclusions within dense low-silica andesite blocks of effusive-phase deposits. Crystals are ≤2 mm-diameter skeletal plagioclase, amphibole, and two-pyroxene. | Not determined |

¹ As determined by point count by Larsen and others (this volume); errors are plus and minus 1σ.

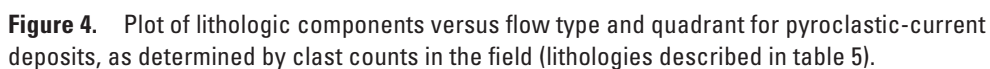
² Lithology recognized in the field but not observed in the laboratory.

Explosive-Phase Pyroclastic Currents

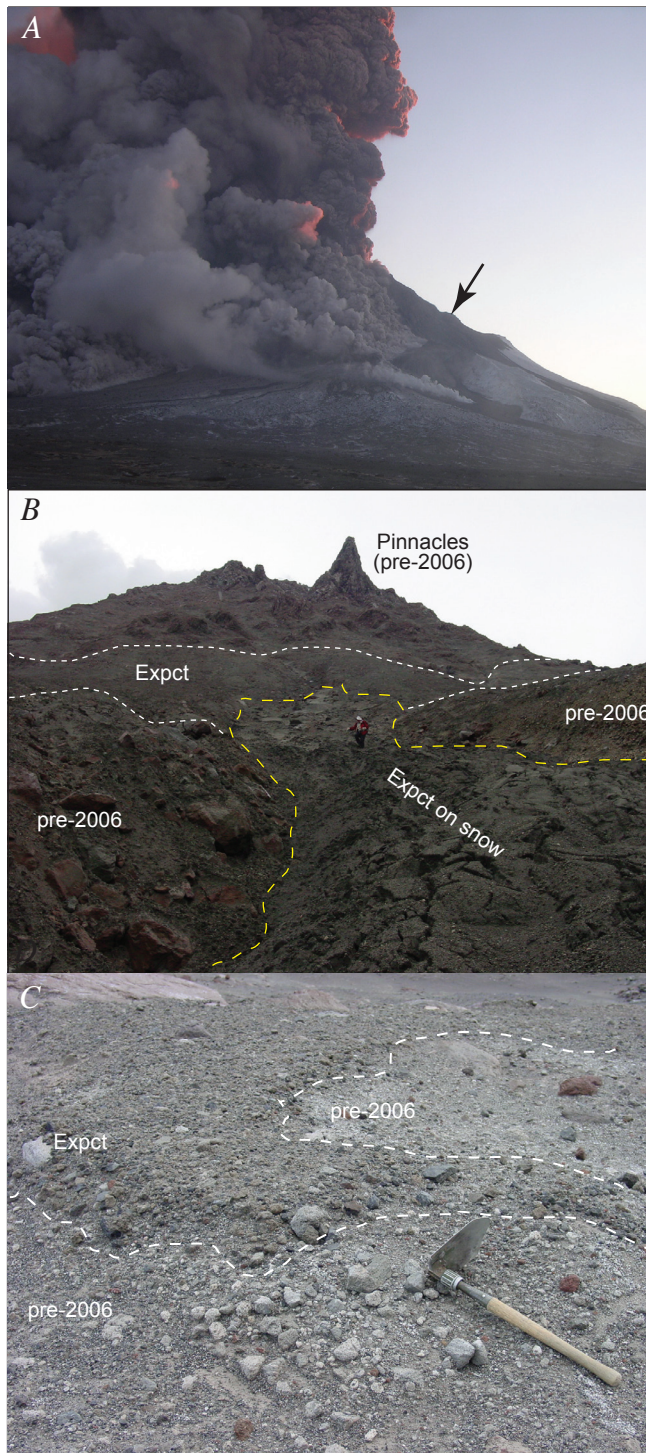
Aerial reconnaissance on January 12, 16, and 18, time-lapse photographs, and seismic data constrain the emplacement of pyroclastic currents during the sequence of events 3 through 9 (table 1). Seismic signals from stations downslope of flows or beside flowpaths include 10–30-minute-long, cigar-shaped codas and increases in amplitude on temporary broadband stations 10–20 minutes after each explosion. Such distinctive signals on instruments below or next to flows, and their absence in other quadrants, delineate flowpaths (McNutt and others, this volume). Comparison of signals from instruments on all flanks of Augustine suggests that the longest-lasting flow occurred in a time-staggered sequence around the volcano. Signals indicating

large flows were first recorded on east-side seismometers during events 3 through 5, on north-side seismometers during events 5 and 7, and on south-side seismometers during event 8 (Coombs and others, this volume; McNutt and others, this volume). Smaller flows occurred during the other events (table 1). Coombs and others (this volume), using time-lapse images from stations north and east of the volcano, report pyroclastic currents on the east and northeast flanks during events 4 and 5 and on the north flank during event 5 and smaller flows on the east and north flanks of the volcano after event 5. Aerial reconnaissance on January 16 indicated pyroclastic flowage deposits on all flanks of the volcano. An aerial survey revealed that an explosion on January 17 produced a pyroclastic flow on the Southwest flank, and seismicity suggests flows on the Northwest flank as well.

Deposits of the first pyroclastic currents (unit Expt) commonly are poorly sorted, massive, and ungraded; however, near distal margins the deposits overlie graded and crudely bedded facies rich in dense clasts, as large as 1 m across. (fig. 6). Typical deposits have a bimodal size distribution with modes in lapilli- and ash-size and very fine ash components



ranging from 8 to 15 percent (figs. 6, 7). In contrast, basal stratified facies have stunted or absent lapilli-size modes and very fine ash components of less than 5 percent. Bedding within the fines-deficient facies nearly parallels bedding planes or dips at low angles toward source, and grading, if present, is inverse and coarse tailed (fig. 6). The stratified basal facies grades upward to the more common massive facies above within 1 or 2 cm.



After the initial widespread pyroclastic currents, multiple lobate pyroclastic flows (unit Expf, fig. 2A) funneled into valleys on all flanks of the volcano and produced deposits with archetypal morphology, including blocky, lobate margins and levees (fig. 8). The coarse pyroclastic-flow deposit (unit Expf) invariably overlies thin pyroclastic deposits (unit Expct) and thus postdates events 3 and 4 in drainages to the east and north and event 7 to the south and southwest. The largest flows moved as far as 3 to 4 km from source and typically moved farther along narrower valley axes than did initial widespread flows. The complex digitate margins of these distal flows thus now overlie pre-2006 surfaces (fig. 8). Deposit lobes are 5 to 30 m across and 1 to 2 m thick at distal or levee margins, although some thin toward their interiors and upslope to as little as 20 cm (fig. 9).

Coarse pyroclastic-flow lobes form overlapping sequences that indicate multiple episodes of deposition (fig. 9). Longitudinal cross sections of overlapping flow lobes indicate that subsequent flows plowed up and incorporated sediment from previous lobes even on gentle slopes. In adjacent areas, such lobes conformably overlie pre-2006 substrate with little evidence of erosion. Erosion of older 2006 pyroclastic-flow deposits by younger ones and an absence of such erosion on pre-2006 surfaces suggest that the older deposits remained somewhat fluid when subsequent flows inundated them.

The coarse pyroclastic-flow deposit (unit Expf, fig. 2) is poorly sorted, massive, and ungraded to inversely graded (fig. 9). Typical deposits have a bimodal size distribution, with lapilli and medium-to-coarse-ash modes (figs. 7, 9). Fine-grained basal layers may lack lapilli and blocks and have large fine-ash components. Inverse coarse-tail grading is common where blocks and large lapilli concentrate near the surface behind flow-lobe margins (fig. 9).

Figure 5. Photographs of thin explosive-phase pyroclastic-current deposit (unit Expct). *A*, Time-lapse photograph taken at 1645 AKST January 13, 2006, from Burr Point showing a pyroclastic current of event 6 moving down north slope of volcano toward camera. Arrow denotes blanket of debris already in place across the upper flanks, inferred to be unit Expct. *B*, Unit Expct deposit on east slope of volcano below Pinnacles (~1 km northeast of vent). Deposit is absent on steep, pre-2006 outcrops, including Pinnacles in background. In foreground, deposits in a gully were emplaced on snow. Later melting of snow caused deposits to become cracked and lumpy. *C*, Initial explosive-phase pyroclastic deposits (unit Expct) emplaced on pre-2006 moss- and lichen-covered surface, which was probably windswept of snow at time of deposition. Leading edge of 2006 flow is in middle of photograph. Flow drapes pre-2006 surface in a way typical of this deposit.

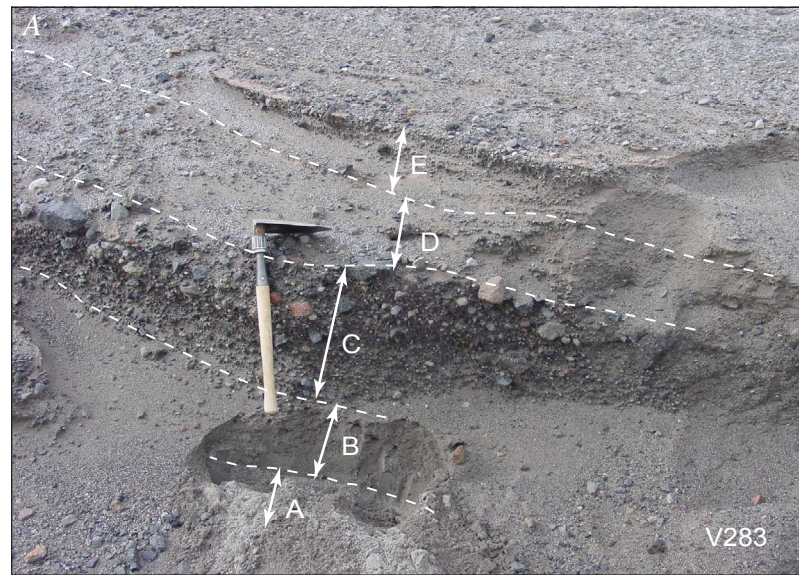
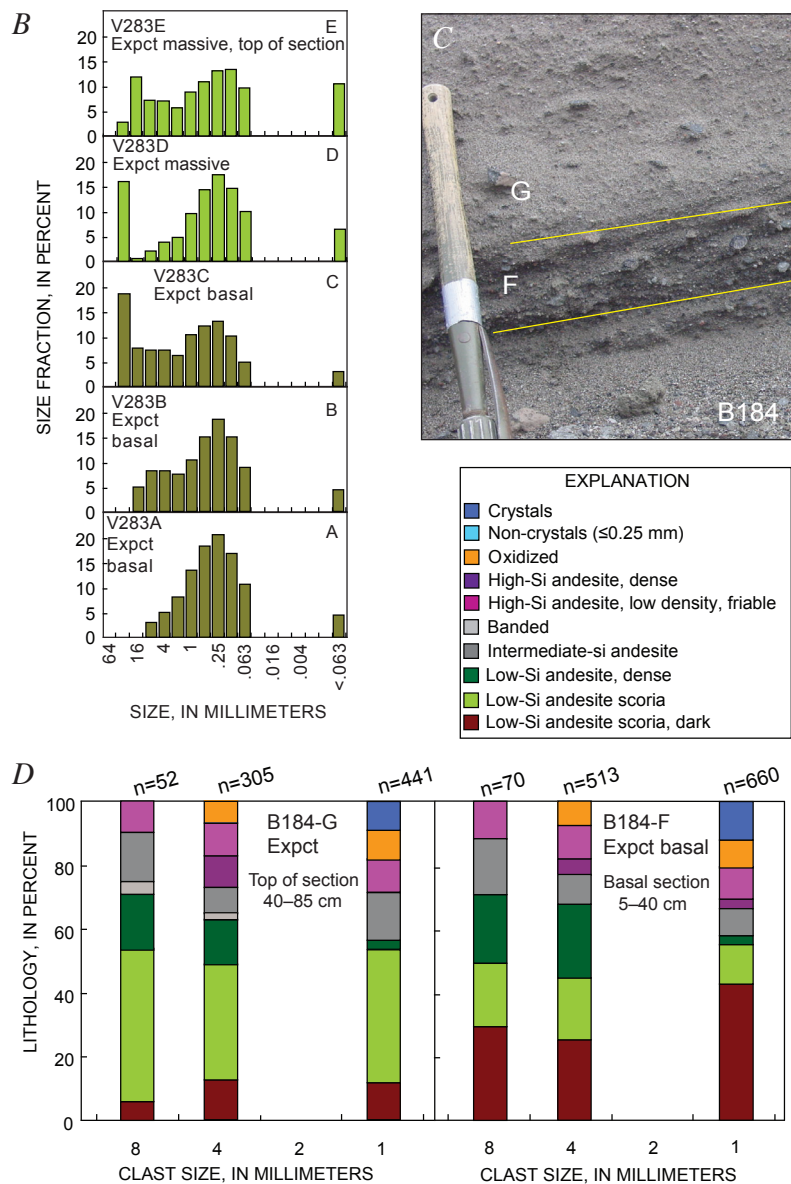


Figure 6. Basal stratified facies of thin explosive-phase pyroclastic-current deposit (unit Expct) on east flank of Augustine Volcano at station V283 (fig. 2A; table 3). *A*, Photograph of inversely graded, faintly stratified facies (layers A–C) overlain by ubiquitous, massive blanketing facies of deposit (layers D, E). Shovel is 50 cm long. *B*, Grain-size histograms of layers designated in figure 6A. *C*, Photograph of outcrop at station B184, approximately 50 m upslope of that shown in figure 6A, showing two 2006 layers on top of pre-2006 surface. Layer F is faintly crossbedded, and, like layers A through C at station V283, is friable. Layer G is typical blanketing facies of deposit. *D*, Plots of lithologic components of sample B184-F of basal facies and typical sample B184-G of deposit. Basal facies contains greater proportions of dark scoria and dense clasts than overlying deposit and other explosive-phase pyroclastic deposits. Sample locations are shown in figure 2A and table 2.



All pyroclastic deposits of the early explosive phase (events 3–9) contain similar proportions of lithologic components (figs. 4, 10; table 7). Low-silica andesite is the dominant rock type, and scoria is more common than dense rock (fig. 10). Subordinate rock types include high-silica andesite and dense, intermediate-silica andesite. Size- and density-segregation processes selectively sorted numerous blocks and lapilli of greenish-gray low-silica andesite scoria to the surface of pyroclastic flows as they slowed, lending deposits

an easily distinguishable greenish gray hue. In fine-grained fractions, the three key constituents become more difficult to recognize, and we identify increasing proportions of phenocrysts (fig. 10).

Explosive-Phase Mixed Avalanches and Lahars

Mixed avalanches and lahars were generated by the first widespread pyroclastic currents (generally unit Expct) that moved across winter snowpack during events 3 through 8 on January 13 and 14; no such flows occurred thereafter. Aerial reconnaissance on January 12 and 16 constrains the emplacement of these flows. Flowline patterns along drainages are visible in oblique aerial photographs of January 16 but not in those of January 12. Scoured slopes and vegetation, as well as striations along northward-, eastward-, and southward-oriented streampaths, caused the patterns. These features were most conspicuous downslope of fresh pyroclastic-current deposits, and farther downstream in several drainages as far as the coast. Later observations showed that mixed-avalanche and lahar tracks caused the patterns (fig. 2A).

We infer that one or more of the six events on January 13–14 generated both mixed avalanches and lahars and, more specifically, that the first widespread pyroclastic currents to descend any particular valley during January 13–14 generated these flowage deposits (fig. 2A). Time-lapse photographs taken from the Mound camera (fig. 2A) suggest that east-side lahars had moved into several drainages downstream of the informally named East Chute during event 3 or 4 (Coombs and others, this volume, fig. 4C). Time-lapse photographs taken from Burr Point show fresh coarse pyroclastic-flow deposits (unit Expf) that descended the Northeast fan (fig. 2A; Coombs and others, this volume, figs. 5C, 5D). These pyroclastic-flow deposits overlap lahar deposits and one mixed-avalanche deposit, downstream along Northeast fan, suggesting that the

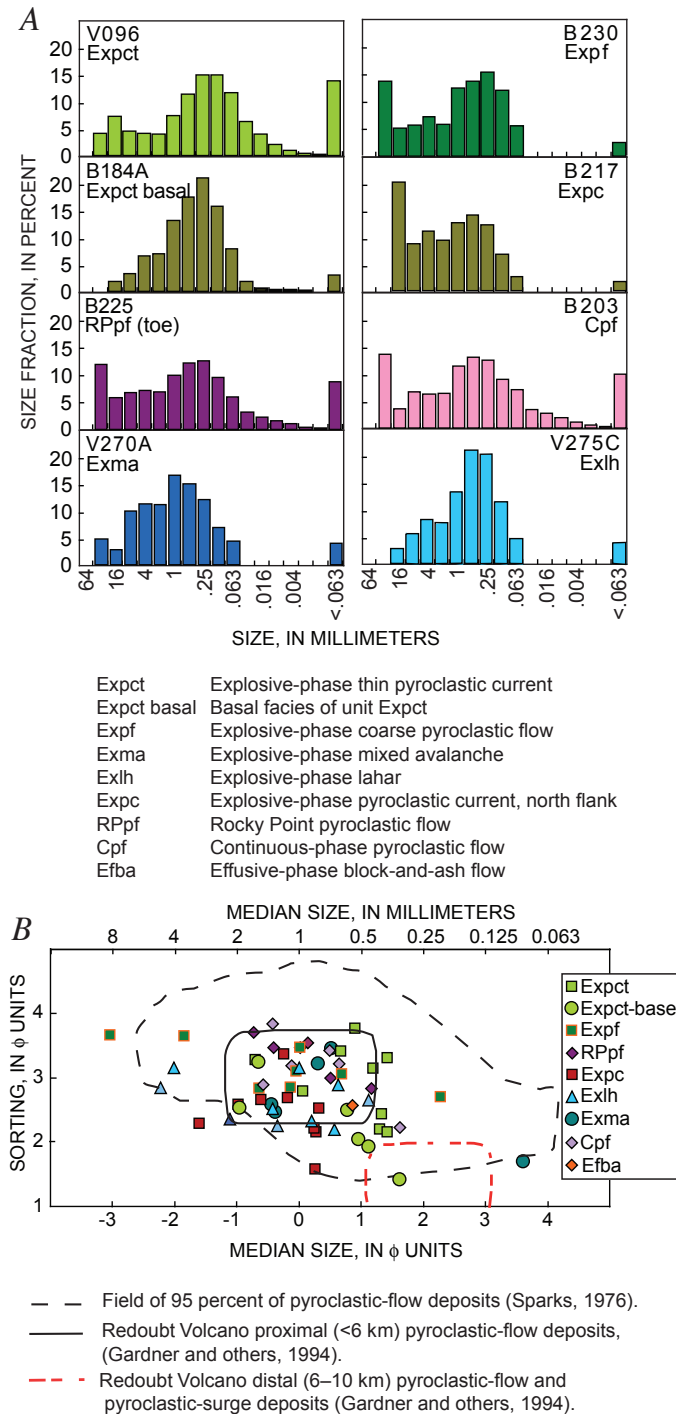


Figure 7. Summary of results from grain-size analyses of 2006 flowage deposits at Augustine Volcano. **A**, Histograms showing grain-size distribution of each clastic-flow type. Pyroclastic deposits with high fines content include deposits from initial thin, and subsequent coarse, explosive-phase pyroclastic deposits, the Rocky Point pyroclastic-flow deposit, and most continuous-phase pyroclastic-flow deposits. Some explosive-phase pyroclastic deposits are fines deficient. Bimodality with modes in lapilli and coarse-ash fractions, though present in some samples, is not conspicuous. **B**, Sorting versus median grain size for 2006 pyroclastic-flow deposits. Most samples fall within region of worldwide pyroclastic-flow deposits (dashed line; after Sparks, 1976) and 1989–90 proximal pyroclastic-flow deposits of Redoubt Volcano (solid line; after Gardner and others, 1994). Sample locations are shown in figure 2 and table 2; grain-size data are listed in tables 3 and 4.

lahar and mixed-avalanche deposits were emplaced during events 3 through 5. Seismic signals provide further clues about the timing of lahar and mixed-avalanche emplacement (in this volume: Coombs and others; McNutt and others). Seismic stations adjacent to flowpaths recorded high-frequency, cigar-shaped codas following explosions, whereas other stations far from flowpaths recorded only explosion signals (McNutt and others, this volume). Broadband stations downstream of flows also showed increased seismicity as long as 20 minutes after initial explosion signals. The postexplosion timing and characteristics of these seismic signals suggest that they were

produced by pyroclastic flows, mixed avalanches, and lahars that flowed toward the stations (Coombs and others, this volume). For example, station AUE, located between East Chute and Mound (fig. 2A) within about 100 m of a lahar path, recorded dominant, long-duration flowage signals, the longest of which lasted more than 30 minutes during event 3 and was partly caused by lahars passing near the station, rather than by pyroclastic flows upslope (McNutt and others, this volume). Stations AUE and AU14 also recorded signals consistent with flowage phenomena during events 4 and 5. The signal during event 5, in particular, could plausibly include lahars. Stations AUL and AU12 both recorded

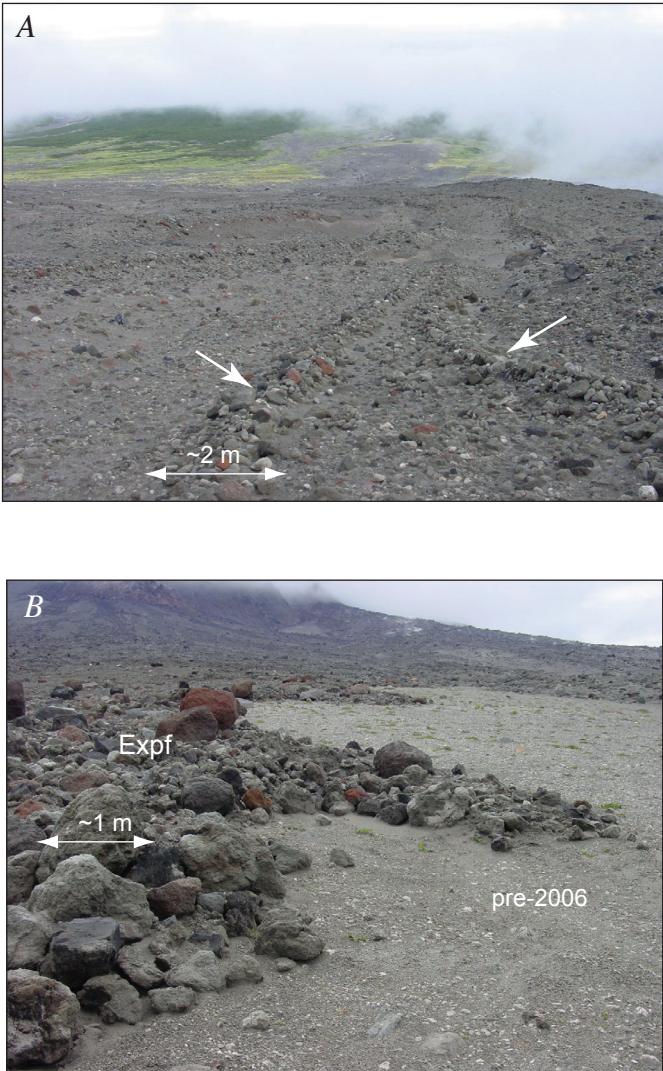


Figure 8. Photographs of coarse explosive-phase pyroclastic-flow deposits (unit Expf). *A*, Medial levees (arrows), approximately 50 cm high concentrate large lapilli and blocks and define margins of lobate deposits. *B*, Digitate, distal margin of coarse pyroclastic-flow deposit.

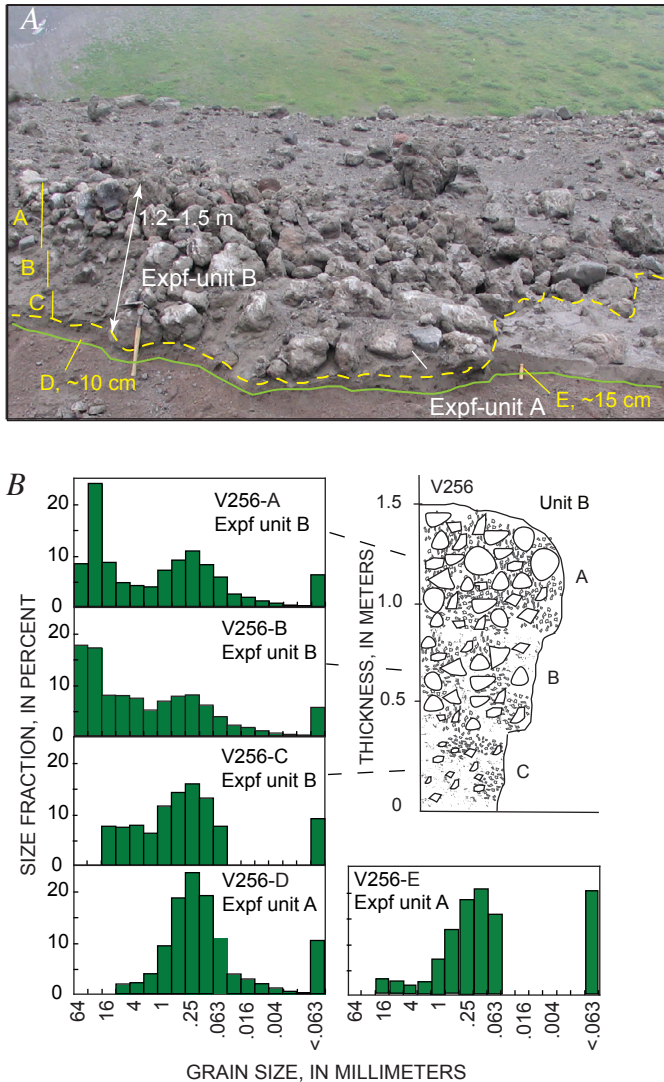


Figure 9. Overlapping explosive-phase pyroclastic-flow deposits (unit Expf) at station V256 (fig. 2A). *A*, Photograph showing distal margin of pyroclastic-flow unit B where it has overrun and partially eroded pyroclastic-flow unit A. Sampling sites are denoted in yellow as A through E. *B*, Unit B is inversely graded, as shown by histograms of grain-size distribution and by graphic log to right. Sample locations are shown in figure 2A and table 2.

flows during event 5 but not during earlier events. These deposits, which were the first widespread pyroclastic flows of the 2006 eruption, probably generated the lahars that moved downstream of North Fan and within Windy Creek drainage to the coast (fig. 2A). On the basis of the protracted seismic signals recorded at stations AU15, AU13, and AUI (fig. 2A), to the southwest and south of the volcano, pyroclastic flows and the mixed avalanches and lahars that they generated in Augustine Creek and Southeast Beach Creek probably occurred during event 8.

Mixed-Avalanche Deposits

Mixed-avalanche deposits (unit Exma) crop out south and east of the volcano, from upper slopes downstream as far as the coast, and extend from near the margins of some thin explosive-phase pyroclastic-flow deposits (fig. 2A). Mixed-avalanche deposits are most widespread in drainages on the southwest to southeast flanks of the volcano (fig. 2A). In the upper parts of Augustine Creek drainage, mixed-avalanche

deposits occupy wide swaths of the valley, interrupted only by younger coarse pyroclastic-flow lobes (fig. 2A). In medial and distal reaches of valley systems, such as Augustine Creek, mixed-avalanche deposits crop out next to lahars (figs. 11–13). In areas where mixed-avalanche and lahar deposits mingle, the mixed-avalanche deposits occupy flow margins and commonly form islands surrounded by lahar deposits (fig. 13). On the east side of Augustine Island, mixed-avalanche deposits of more limited extent commonly are confined to upper-slope gullies and span a few minor drainages downslope (fig. 2A).

Mixed-avalanche deposits have distinctive irregular surfaces crisscrossed with cracks. These cracks cut through the soft sediment that forms the deposits, and in August 2006, several months after the eruption, the cracks locally exposed snow. In protected, proximal reaches during August 2006, we observed that some deposits contained snow, some overlay snow, and others had distinctive, extremely uneven, lumpy surfaces due to the melting of both underlying and contained snow (figs. 11, 12). Along vegetated slopes at lower elevations, deposit surfaces were littered with uncharred alder and willow branches that had been broken to pieces and denuded small stems and twigs. Nearby such littered surfaces, deposit remnants were also scattered on top of large boulders and throughout patches of alder and willow whose upper branches were commonly denuded and broken but not charred. Apparently, the brush in mixed-avalanche paths was commonly buried and protected under snowpack when snow and debris mixtures slid across it. As a result, the vegetation, whose tops were generally clipped and destroyed, were irregularly draped with debris. Deposit margins, which are broadly lobate and do not form levees themselves, are common as levees of axial lahar flows (fig. 12).

The thickness of explosive-phase mixed-avalanche deposits ranges from 0.2 to 3 m and averages about 0.5 m. Poorly sorted, ungraded deposits typically have modes in gravel- and sand-size ranges (fig. 11). The deposits contain proportions of juvenile rock types similar to those of explosive-phase pyroclastic-flow debris. Locally, the lumpy surfaces are rich in fines (<0.063 mm diam) and cracked where snowmelt had pooled, collected the fines, and subsequently dried (fig. 11).

Lahar Deposits

Explosive-phase lahar deposits (unit Exlh) underlie the middle to lower parts of most drainages around the volcano, except those to the west (fig. 2A). Generally, lahar deposits are downstream of pyroclastic-flow deposits and adjacent to, or downstream of, mixed-avalanche deposits (figs. 2A, 13). Watery lahars and floods reached the coast on most flanks of the volcano (fig. 2A).

The variation in the areal extent of lahar inundation suggests a variation in water content among lahars. The most widespread lahar deposits are also those with characteristics most suggestive of high water content. The deposits

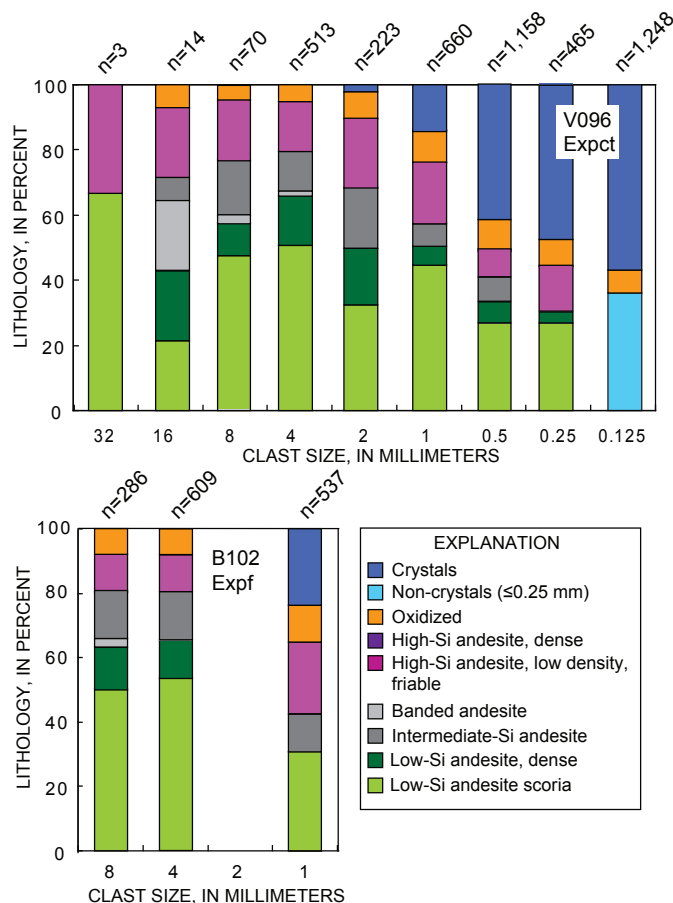


Figure 10. Plots showing lithologic components versus clast size for pyroclastic deposits of explosive-phase events 3 through 9. Above, initial explosive-phase pyroclastic deposit (unit Expt) and below, subsequent explosive-phase pyroclastic-flow deposit (unit Expf). Sample locations are shown in figure 2A and table 2.

Table 7. Overview of lithologic components in key deposits of the three phases of the 2006 eruption of Augustine Volcano, Alaska.

[Phases, events, and units (after Coombs and others, this volume). Component values are 8-mm data averaged from table 6 and recalculated to 100 percent. Components are low-silica andesite scoria (LSAS), dense low-silica andesite (DLSA), dense intermediate-silica andesite (DIA), high-silica andesite (HSA), and mixtures (banded), defined in table 5. Units are defined in figure 2. Mixed-avalanche (Exma) and lahar (Exlh) data are not included in "Average for unit" column]

[illegible]¹Oxidized + pumice.
$$^2\text{LSA} = \text{LSAS} + \text{DLSA}.$$
$$^3\text{IA} = \text{DIA} + \text{banded}.$$

downvalley of East Chute are the best examples of these water-rich flows (figs. 12*B*, 14*A*). On the east flank of the volcano, between about 500 and 100 m asl, long linear lahar levees, 2 to 10 m wide and about 20 cm high, consist of cobble and boulder accumulations littered with sand and silt. The levees trace along vegetated terraces and mossy surfaces upstream of the youngest explosive-phase coarse pyroclastic-flow deposit (unit Expf), toward their apparent source, the older, thin pyroclastic-current deposit (unit Expct; figs. 2*A*, 12). In between levees, large lahars were water rich and erosional. Boulders as large as 3 m in diameter, commonly of low-silica andesite scoria, dot eroded and scoured surfaces. In this scoured regime, willows and alders are commonly battered on their upstream sides, denuded,

and bent downslope into bayonet-stick forms (fig. 14*A*). Downstream, levees lead into channels where the water-rich debris mixture flowed and deposited 30- to 100-cm-thick channel facies (fig. 14*B*). In outcrop, the channel facies has characteristics typical of transitional or hyperconcentrated-flow deposits, such as intermediate sorting, crude bedding, and both inverse and normal grading (fig. 14*B*). Where exposed, inversely graded strata underlie crudely stratified, normally graded sediment. In distal reaches, levees range in size and character from linear trains of scattered cobbles and boulders to boulder-cobble-rich accumulations, as thick as 50 cm.

Areally extensive lahar deposits commonly have margins bordered by mixed-avalanche deposits, suggesting

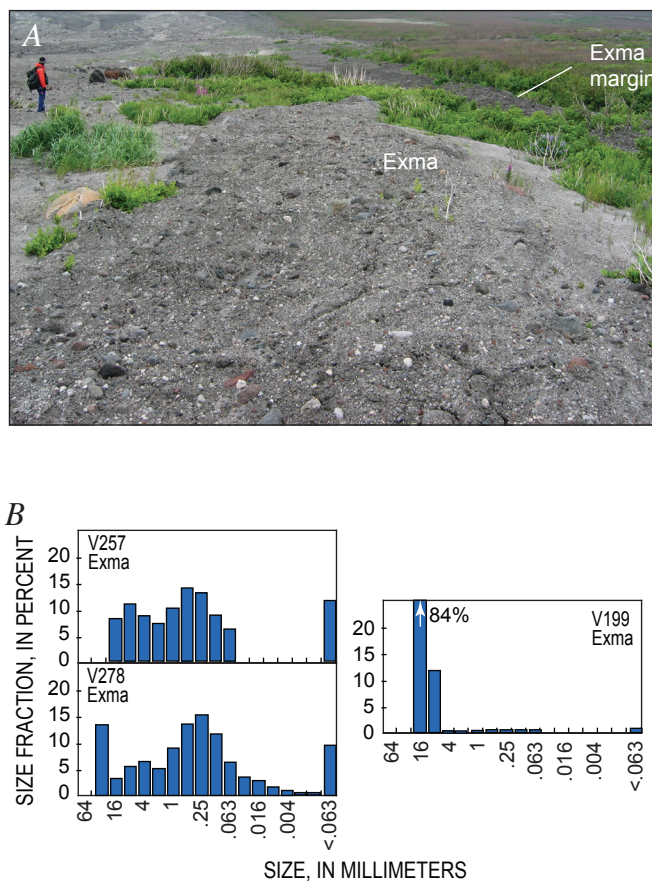


Figure 11. Photograph and grain-size plots of explosive-phase mixed-avalanche deposits (unit Exma). *A*, View downstream of mixed-avalanche deposit showing irregular, lumpy surface texture. Cracks formed after incorporated snow had melted, and wet, compacted fines had dried and contracted. Margin of deposit, cutting across upper right of photo, drapes vegetation. Apparently, much debris in this area was emplaced on top of snow that covered and protected vegetation, then melted into place, partly burying small alder trees. *B*, Histograms of grain-size distribution of mixed-avalanche deposits, illustrating variability of size distribution. Sample locations are shown in figure 2*A* and table 2.

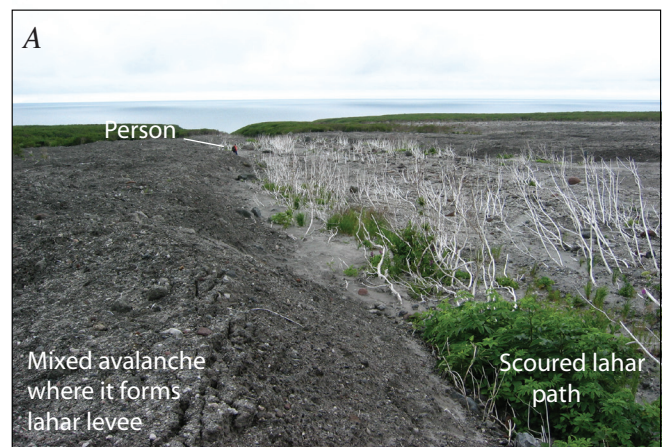


Figure 12. Photographs of lahar levees; view downstream. *A*, Boulders, cobbles, and sparse matrix that have accumulated along right margin of lahar. *B*, Mixed avalanche deposit (unit Exma) forms left-marginal levee-terrace, 2 m high, of lahar flow to right. Lahars denude alders and willows, forming bayonetlike stems that are battered and bent downstream. Green vegetation was protected from flow by burial under snow.



Figure 13. Photographs of explosive-phase lahar deposits. *A*, Aerial view down Augustine Creek on lower south-southwest flank of volcano, showing lahar deposit (unit Exlh; light-blue dashed outline and flow-direction arrows). Mixed-avalanche deposit (unit Exma) forms terraces lateral to, and islands within, lahar deposit. Lahar channels are scoured. *B*, Photograph of small-scale (~5 m across) lahar deposits. Lahar deposits in foreground (dashed lines) were generated by explosive-phase pyroclastic-flow deposit (unit Expf; solid lines) that came to rest on snow. *C*, Aerial view of bouldery mixed-avalanche and lahar deposits in Augustine Creek, bordering scoured lahar channels that cut seacliff. Lahar transport formed bouldery delta as far as 100 m offshore.

a genetic relation between these two types of deposit. South-southwest of the volcano, mixed-avalanche deposits are situated in intermediate valley reaches between source pyroclastic-flow deposits and lahars. Farther downstream, along intermediate to distal reaches of Augustine Creek, terraces of lumpy-surfaced mixed-avalanche deposits border lahar deposits rather than boulder-cobble levees (fig. 12*B*). In between these mixed-avalanche terraces are scoured lahar surfaces with scattered boulders, much like the scoured surfaces of the large lahars described above (fig. 12*A*). Downstream of the marginal mixed-avalanche deposits, boulder-cobble levees become evident. Near the coastline in Augustine Creek, bouldery mixed-avalanche and lahar deposits are situated on either side of a scoured channel incised in a low seacliff (fig. 13*C*). Lahars carried boulders as large as 1 m in diameter through the channel, and carried other boulders as far as 100 m into the ocean. We observed similar relations between mixed avalanches and lahars that moved to the coast along drainages on the south and south-east sides of the island.

The smallest-volume lahar deposits appear to have originated at the coarse margins of explosive-phase the pyroclastic-flow deposit (unit Expf, fig. 13*B*); fluid breakaways are visible at the toes and margins of some of the younger coarse pyroclastic-flow-deposit lobes. The lahar deposits, which are typically only few meters wide and no more than a few tens of meters long, have cobble-rich margins that become progressively less distinct with distance downslope (fig. 13*B*). These deposits are present where the pyroclastic flow deposit (unit Expf) evidently came to rest on top of snowpack.

The lithologic composition of lahar deposits (unit Exlh) is similar to that of explosive-phase pyroclastic currents (units Expt, Expf) and virtually identical to that of mixed-avalanche deposits (unit Exma). The greenish-gray, low-silica andesite scoria that is common in all explosive-phase deposits is also diagnostic in lahar deposits (tables 6, 7). A combination of size and density segregation has concentrated greater than 50 percent scoria in lahar-levee deposits. The channel facies of lahar deposits contain scoria proportions typical of other explosive-phase deposits, but also oxidized lithic clasts and pumice from pre-2006 deposits (table 6). These rock types are present in the lahars owing to progressive entrainment of sediment along the flowpath. At Augustine, lahar flowpaths rarely exceed 2 km in length, and so bulking factors in deposits are rarely much greater than 10 percent.

Grain-size characteristics of Augustine lahar deposits are similar to those of the transitional to hyperconcentrated flows documented at other volcanoes (Scott, 1988; Vallance, 2000). The sorting index ranges from 2.2 to 3.2, typical of transitional flows (table 2; Scott, 1988). The upper, crudely bedded deposits are moderately well sorted, have the finest mean grain size, and have grain-size distributions with a mode of about 0.5 mm (figs. 14*A*, 14*B*). Underlying, more massive deposits have the greatest proportions of coarse particles, the poorest sorting, and grain-size distributions with a weak bimodality (figs. 14*A*, 14*B*).

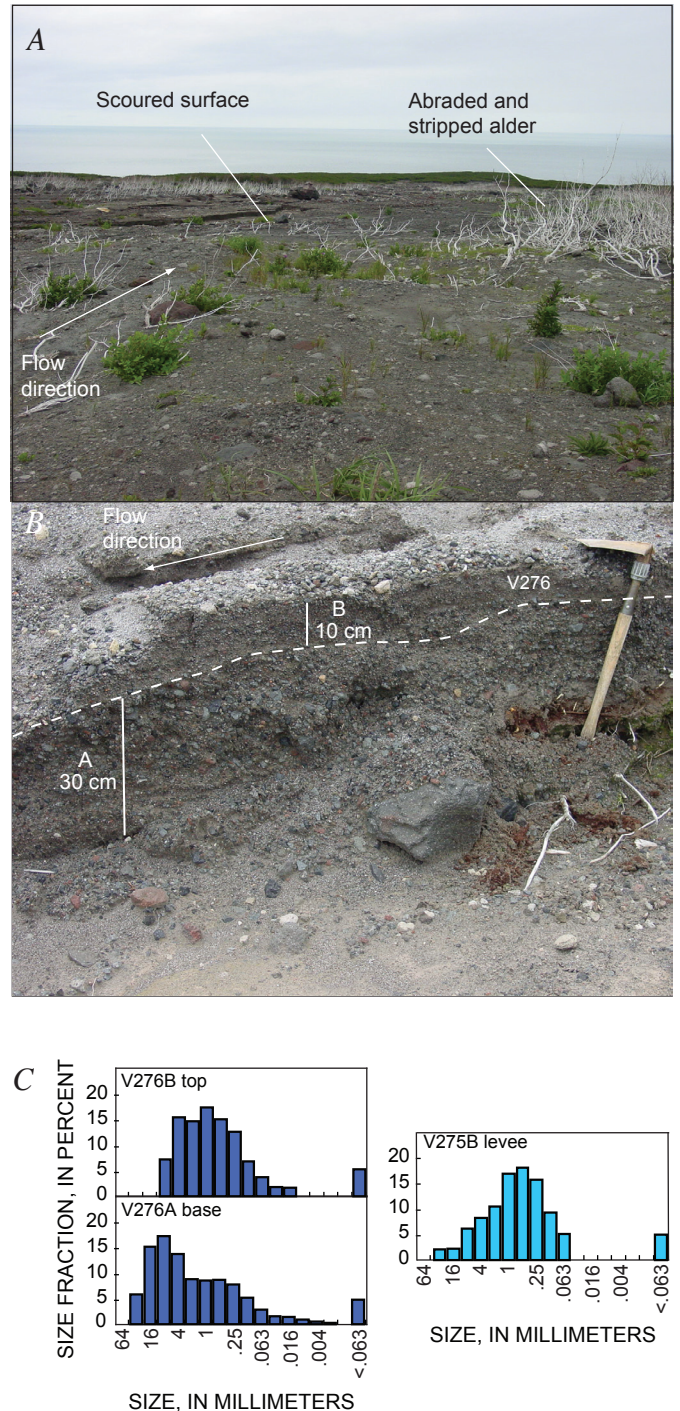


Figure 14. Photographs of scoured lahar surface (*A*) and nearby vertical section (*B*) at sample location V276, with histograms of deposit grain-size characteristics (*C*). *A*, Lahar surface is not only scoured but also displays willows and alders stripped of vegetation and bent in flow direction to form bayonetlike sticks. *B*, Normally graded lahar deposit where it funneled into distal channel and began to deposit its sediment load. Layer B is faintly stratified. Shovel is 50 cm long. *C*, Basal layer A contains a larger proportion of large clasts and also more fines than layer B. Nearby levee deposit (sample V275B) is relatively fines poor. Sample locations are shown in figure 2*A* and table 2.

Events 10 through 13, January 28–29: Pyroclastic Flows to the North and the Transition to the Continuous Phase

The 9-minute-long explosion of event 10 produced the largest-volume pyroclastic output of the explosive phase and sent pyroclastic currents northward. Events 11 through 13 either generated no pyroclastic currents or produced no deposits distinguishable from those of the subsequent continuous phase. Two distinctive pyroclastic currents occurred in rapid succession during event 10 (McNutt and others, this volume; Coombs and others, this volume). The first deposit contains large proportions of dense, nonvesicular andesite (unit Expc, fig. 2*B*). The second more widespread deposit, named the “Rocky Point pyroclastic flow,” overlies the first deposit and covers an area of about 3 km² from the volcano’s summit northward toward Rocky Point (unit RPpf, fig. 2*B*).

Stratigraphy, the destruction of monitoring devices, and the characteristics of seismic signals constrain the timing of the two large pyroclastic flows on the north flank to event 10. At 2024 AKST January 27, 2006 (0524 UTC, Jan. 28, 2006), a forceful blast destroyed seismic station AUL and GPS station AV03, both then located on the prehistoric North Slope lava flow (fig. 2*B*). Lithologically distinct pyroclastic deposits at these sites and battered fragments of the stations within deposits downstream (fig. 15*A*) shows that the initial flow (unit Expc) destroyed the stations. The Rocky Point pyroclastic flow overlies this pyroclastic-current deposit and underlies pyroclastic-flow deposits correlated to the continuous phase (unit Cpf; figs. 15*B*, 15*C*), suggesting that the flows occurred between 2024 AKST January 27 (event 10) and aerial observations midday on January 29 during the early part of the continuous phase. Coombs and others (this volume) infer that the Rocky Point flow occurred during event 10, on the basis of deposit size (largest of the 2006 eruption), the extent of the postexplosion seismic signal (~30 minutes), the relative size of the ash signal on radar (largest of the 2006 sequence, Schneider and others, 2006), and the number of lightning strikes (most recorded strikes during the 2006 eruption; Thomas and others, this volume). We accept their interpretation that the largest flow should correspond to an event with a long seismic coda, an ash-rich plume, and numerous lightning strikes. Event 10 is the only likely eruptive pulse during the time interval in question with these characteristics.

Explosive-Phase Pyroclastic-Current Deposit

The pyroclastic-current deposit (unit Expc) drapes the conspicuous North Slope lava flow (Waitt and Begét, 2009) and spills onto gentler slopes, a distance of 3.3 km northward from its source at the summit to its distal margin (fig. 2*B*). The limited distribution of this flowage deposit along the top of a ridge 50–100 m high is likely an artifact of the deposit’s unknown extent: eastward, beneath pyroclastic-flow deposits

of Rocky Point and the continuous phase; and westward, beneath younger deposits of the adjacent, upper-eastern Windy Creek drainage (figs. 2*B*, 2*C*). The thickness of the deposit varies. Along the steep eastern margin of the prominent lava flow, it is 20 to 150 cm thick; on the lava flow’s western edge, it thins irregularly to zero, revealing patches of pre-2006 deposits. Under varying thicknesses of continuous-phase pyroclastic flow deposits (unit Cpf) and the Rocky Point pyroclastic-flow deposit (unit RPpf), it is 5 to 50 cm thick to the east (fig. 15). North to north-northwest of the North Slope lava flow, it thins to a few centimeters and extends downslope as irregular patches within tracts of alder. In this area, the alders are singed and stripped of leaves above 1 to 2 m above ground and unaffected below, suggesting that margins of the flow were gas rich and contained insufficient heat either to melt underlying snowpack fully or to burn vegetation. Snow melting during spring and summer thaw subsequently emplaced the patches.

Outcrops of the pyroclastic-current deposit commonly are inversely graded, massive to faintly bedded, and loose or friable (figs. 15, 16). Some parts appear to be ungraded, especially those overlain by and, possibly eroded by younger pyroclastic flows. Grain size ranges from fine ash to lapilli, has a mode in the coarse-ash-size fraction and, where coarser overall, has another faint mode in the lapilli-size fraction (fig. 16*C*).

The pyroclastic-current deposit is lithic rich and varies somewhat in the proportions of lithologic components intermediate between those of previous explosive-phase deposits and those of subsequent continuous-phase deposits (fig. 16*D*). Like previous pyroclastic deposits of the explosive phase, angular, dense, low- and intermediate-silica andesite clasts make up 25 to 50 percent of the rock types in the deposit. In contrast, however, the pyroclastic-current deposit contains greater proportions of high-silica andesite than all previous explosive-phase deposits (fig. 16; tables 6, 7).

The pyroclastic-current (unit Expc) and the Rocky Point (unit RPpf) deposits originated during the same 9-minute event, and so we considered their possible genetic relation but rejected that hypothesis for the following reasons. First, the pyroclastic-current deposit crops out in extensive areas where evidence of the Rocky Point pyroclastic flow is absent. Second, where the two deposits crop out together their contact is abrupt, sharp, and commonly erosionally unconformable. Third, grain-size characteristics of the two deposits differ where they overlap; for example, thin, fine-ash edges of the Rocky Point deposit overlie much coarser ash and lapilli deposits of the pyroclastic-current deposit (fig. 15*B*). These observations are inconsistent with a cogenetic origin, and so we conclude that these two units followed one another successively within a few minutes during event 10.

Explosive-Phase Rocky Point Pyroclastic Flow

The most voluminous and widespread pyroclastic flow of the 2006 eruption also occurred during event 10. The Rocky Point pyroclastic flow originated near the summit of the

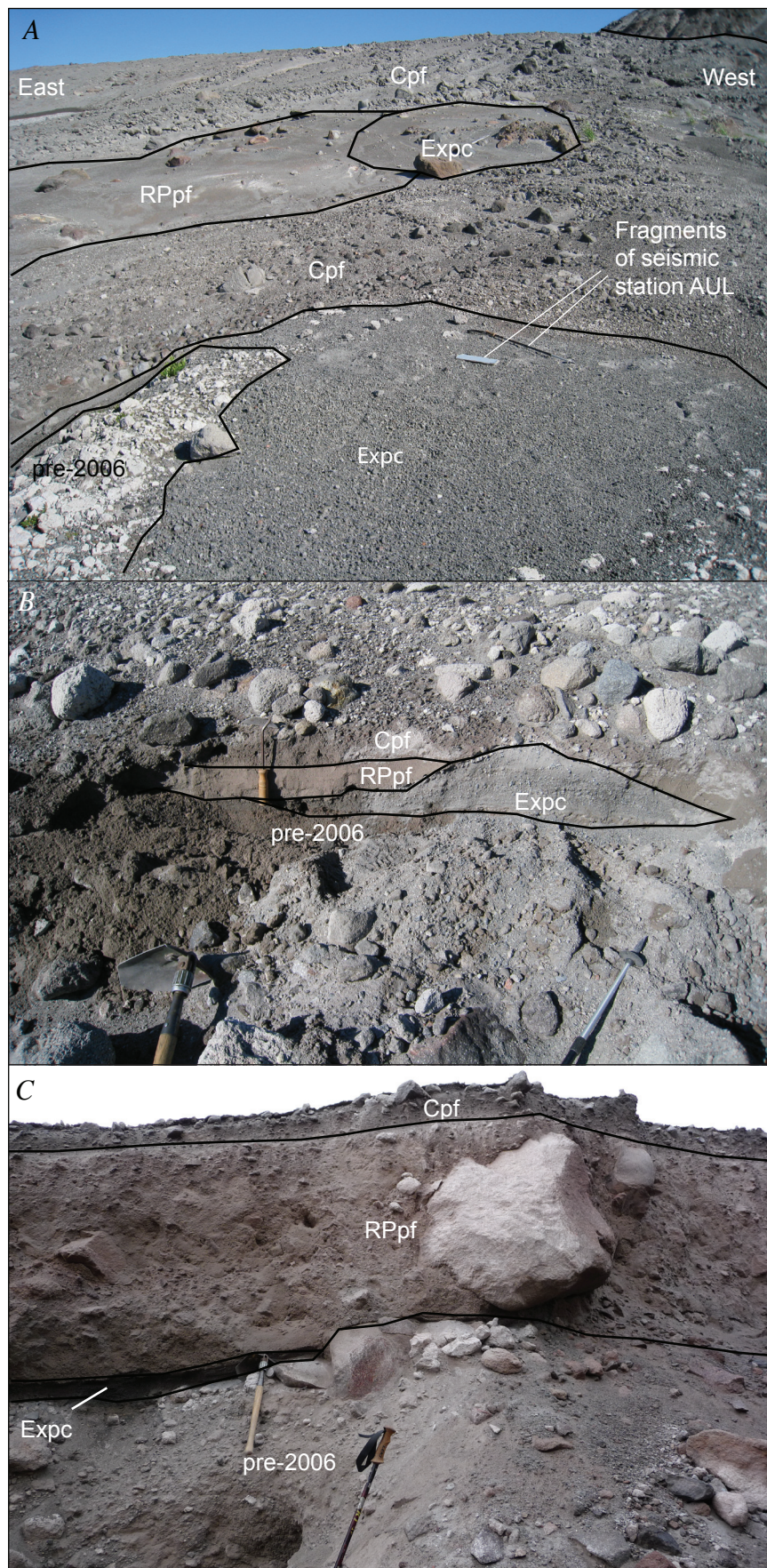
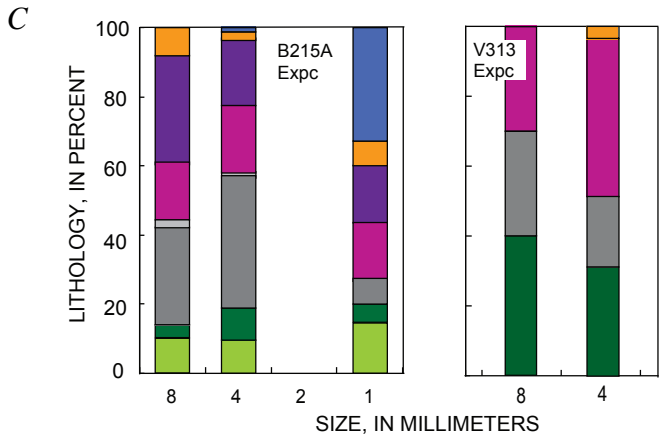
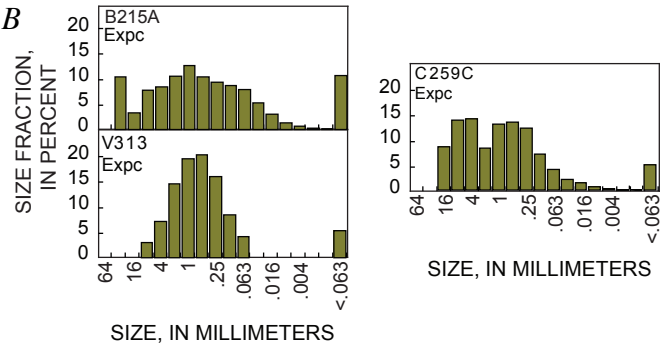
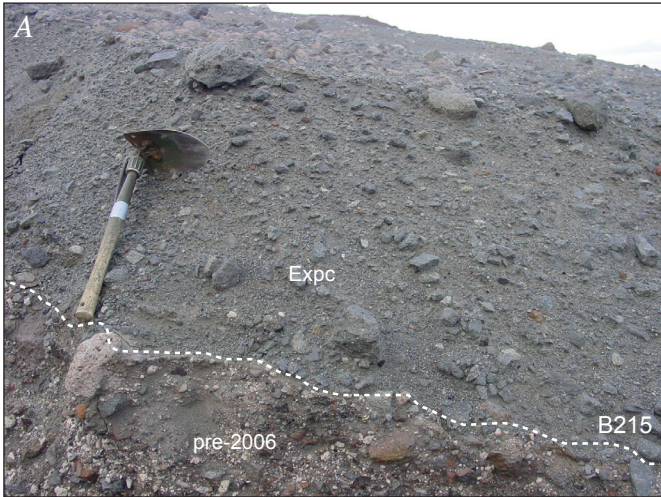


Figure 15. Photographs illustrating relations between 2006 explosive- and continuous-phase pyroclastic deposits on north flank of Augustine Volcano. *A*, Surface of pyroclastic-current deposit (unit Expc), oldest of 2006 deposits at this locality, with scattered fiberglass fragments, 40 and 90 cm long, from upslope seismic station AUL and GPS station AV03. Rocky Point pyroclastic-flow deposit (unit RPpf) thins from left to right (east to west) and disappears, whereas younger, continuous-phase pyroclastic-flow deposit (unit Cpf) drapes over and around gentle slopes. *B*, Thin, fine-grained Rocky Point deposit (unit RPpf) underlies continuous-phase pyroclastic-flow deposit (unit Cpf) and overlies friable, light-gray deposit (unit Expc). *C*, Rocky Point deposit (unit RPpf), 1 m thick, is in same stratigraphic position as in figure 15B.

volcano; traveled northward about 4 km, where a low ridge system, capped by a 50-m-high hill, divided the flow into two large and one small parts; and, finally, spread out to form several lobes across a nearly flat surface (figs. 2*B*, 17*C*). The flow moved just more than 5 km from its source and stopped less than 1 km from the shoreline near Rocky Point.



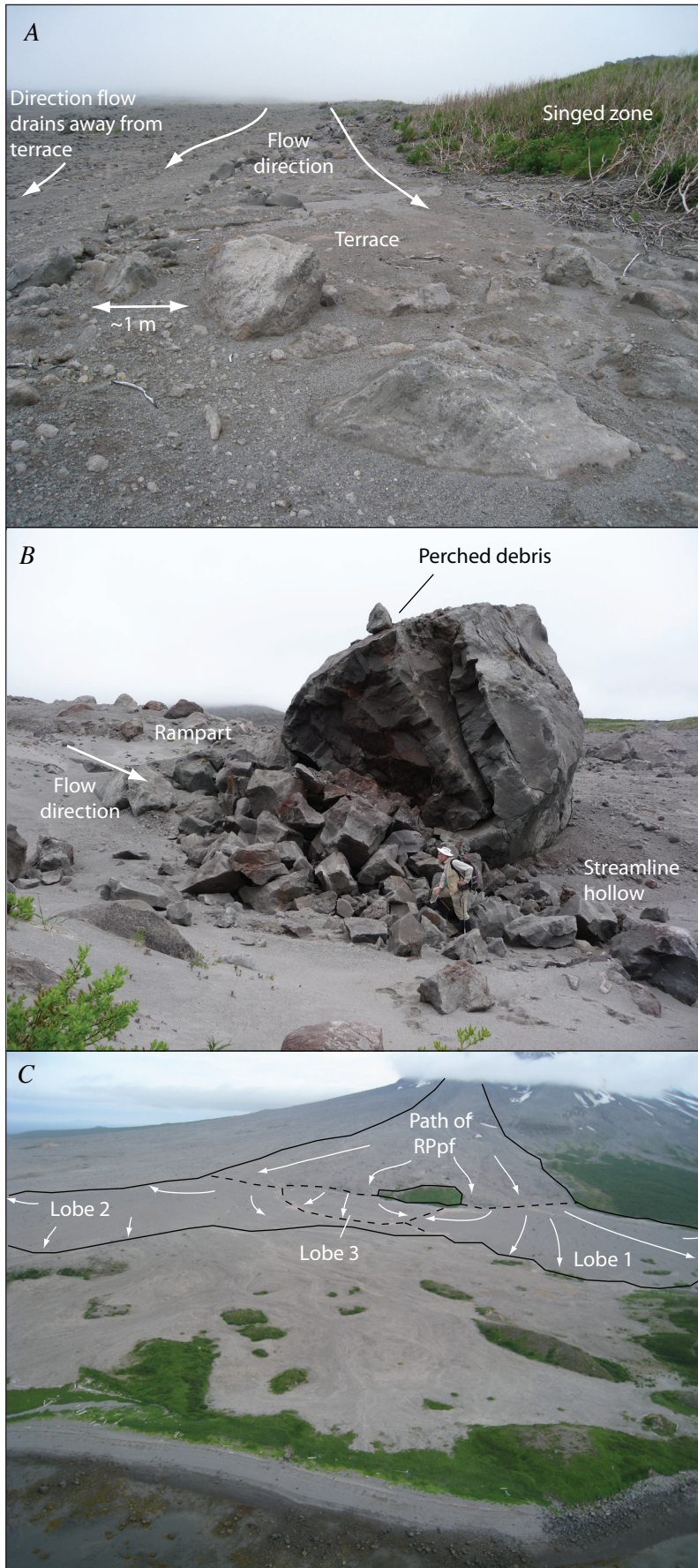
| EXPLANATION | | | |
|------------------------|------------------|-----------------------|--------------------------|
| Crystals | Oxidized | Banded | Intermediate-Si andesite |
| Dense high-Si andesite | High-Si andesite | Dense low-Si andesite | Low-Si andesite scoria |

The Rocky Point pyroclastic-flow deposit (unit RPpf; fig. 2*B*) is distinctive, not only because of its size and distribution north of the volcano but also because of its physical characteristics. The deposit widens from about 0.3 to 1.8 km from south to north, averages 5 to 6 m in thickness, has maximum thicknesses of 10 to 15 m, and has a volume of about $1.6 \times 10^7 \text{ m}^3$ (Coombs and others, this volume). Continuous-phase pyroclastic-flow lobes overlie proximal parts of the deposit (compare figs. 2*B*, 2*C*). Axial parts of the deposit thicken to as much as 15 m but thin to less than 1 m where the flow moved across steep slopes, locally revealing pre-2006 deposits on especially steep scarps. Narrow, blocky marginal terraces are present where a ridge to the west and a 50-m-high hill to the east funneled part of the flow (fig. 17*A*). The terraces, which apparently formed at ephemeral levels during the receding stage of the passing flow, are thus marginal relics of a fluid flow whose mass largely drained away and accreted downslope. Dozens of large blocks, 3 to 10 m in diameter, dot the axial medial surfaces but are absent near lateral or distal deposit margins. Such blocks commonly have pyroclastic-debris aprons that ramp up on their stoss sides and stream-line hollows on their lee sides (fig. 17*B*). Many blocks have patches of fine material, centimeters to a few tens of centimeters thick, with scattered lapilli and blocks perched on their tops (fig. 17*B*).

Along its eastern margin, the Rocky Point pyroclastic-flow deposit thins to a few centimeters and divides into numerous small tongues. These features were distinguishable in August 2006 from the subdued features of pre-2006 deposits only by the absence of moss and lichens. The western margin of the deposit is more readily delineated because there the flow lapped up on a prominent ridge, leaving behind not only deposits a few centimeters thick but also a fringe of scorched, broken, and denuded alders (fig. 17*A*).

Three distinct lobes of the Rocky Point pyroclastic-flow deposit fan across a flat surface north of an east-west ridgeline (fig. 17*C*). These lobes, which are about 10 m thick where flows debouched onto the plain, and thin to a few centimeters

Figure 16. Explosive-phase pyroclastic-current deposit (unit Expc) on north-slope lava flow (fig. 2*A*). *A*, Photograph of cross section, 80 cm thick, from the site of samples V303 and B215 near GPS station AV03, destroyed during event 10. Shovel is 50 cm long. *B*, Grain-size distribution plots of deposits at site illustrated in figure 16*A* and at two other sites. Relatively high fines content of sample B215A is unlike that of other samples from this deposit. *C*, Plots of lithologic components of fines-poor deposit. Deposit is more like those of continuous phase than those of explosive phase and proportion of dense clasts is greater than in other deposits, suggesting a lithologic transition from explosive-phase to continuous-phase magma composition. Sample locations are shown in figure 2*A* and table 2.



near margins, coalesce to form nearly continuous deposit along about 1.8 km of the plain from east to west (fig. 17C). Lobes exhibit radiating systems of low ridges and swales. Like those Cole and others (2002) describe in large dome-collapse pyroclastic flows at Montserrat, these linear features parallel flow directions. In cross section, ridges have gentle slopes and broad axes spaced 5 to 20 m apart transverse to flow directions. Swales anastomose in the downflow direction, such that individual ridgelines are rarely traceable more than a few tens of meters. The large blocks that protrude 2 to 5 m above the surface are concentrated within thick axial parts of the lobes and poke through both ridges and swales described previously. These large blocks are absent where deposits thin and thus rarely appear within 100 m of lobe margins. Like the axial blocks upslope, such large blocks commonly preserve accumulations of fine matrix and lapilli, 5 to 20 cm thick, on their tops. Lobe margins thin to a few centimeters and commonly concentrate broken and slightly singed alder branches (figs. 18A, 18B).

As the westernmost lobe spread westward, it buried a shallow pond, resulting in several openwork depressions surrounded by accumulations of fine ash on the surface of the deposit where the pond had been. The interaction of hot pyroclastic debris and underlying water must have generated steam that migrated through the deposits, winnowing fine ash to form elutriation pipes. The openwork depressions are the surface manifestation of these elutriation pipes, which are not exposed in cross section.

Figure 17. Photographs illustrating features of the Rocky Point pyroclastic-flow deposit (unit RPpf). *A*, Terrace formed shortly after peak flow, with subsequent channel drainaway during waning flow. *B*, Perched debris, debris rampart, and streamline hollow on this 8-m-high block suggest the following sequence: (1) flow was thick and energetic enough to move block 3 km into place; (2) subsequent flow was high enough over top of large block to leave debris; (3) waning flow formed a debris rampart and streamline hollow around block; and (4) highly fluid, waning flow drained downstream away from steep slopes, leaving thin deposits, locally less than 1 m thick. *C*, Flowpath illustrates approximate overall streamlines and three depositional lobes on low-lying apron north of volcano.

Thick fill deposits did not crop out by July 2008, intermediate ones have characteristics typical of pyroclastic flows, and thin ones have characteristics of surgelike flows. Deposits from about 0.3 to more than 1 m thick are predominantly massive, though faintly inversely graded within their basal few centimeters (fig. 15C). Deposits not only thin toward lateral and distal margins but also fine (figs. 15B, 18C). Coarse deposits have modes in the coarse-ash to lapilli range, and fine marginal deposits have modes in the coarse-ash range (fig. 18C). Overall, the Rocky Point pyroclastic-flow deposit is relatively fines rich, containing 7 to 13 percent very fine ash, with the most fines rich parts at distal margins (fig. 18C).

The Rocky Point pyroclastic-flow deposit shows even more striking lithologic variations compared with earlier explosive-phase flows (units Expt and Expf) than does the coeval deposit (unit Expc). Friable high-silica andesite constitutes as much as 80 percent of clasts (excluding crystals) in most size classes, and low-silica andesite scoria generally less than 10 percent of the total (fig. 18D). White, high-silica andesite pumice is also a significant constituent, constituting as much as 20 percent of coarse to very coarse ash. Lapilli include significant proportions of both dense and scoriaceous low- to intermediate-silica andesite (fig. 18D).

Large blocks, 3 to 10 m in diameter, differ markedly in composition from lapilli and blocks smaller than about 1 m in diameter scattered on the surface of the deposit. The larger blocks that we examined consisted of uniform, intermediate-silica andesite or banded andesite. In contrast, in many areas, especially on distal fans, lapilli and smaller blocks at the surface consist predominantly of high-silica andesite. The huge blocks are probably too large to have been ejected from the vent during event 10, suggesting that this rock type originated by disruption of a dome that had grown between events 9 and 10. Smaller clasts carried on the surface to distal margins would have been emplaced last and therefore indicate the composition of the rock ejected from the vent during the last stages of event 10, after the capping domerock had been removed explosively. If these arguments are valid, event 10 disrupted a dome composed predominately of intermediate silica andesite, then tapped progressively deeper in the conduit and magma chamber to erupt high silica andesite, typical of late-stage event 10 and of the continuous-phase events that followed.

Continuous-Phase Deposits, January 28–February 10

The continuous phase began January 28 and lasted until February 10 (table 1). The first half of this phase, until about February 3, was marked by continuous emission of ash to heights below 4 km asl, punctuated by explosions that injected ash to 5 to 8 km asl (Schneider and others, 2006; Wallace and others, this volume). Direct observations of the volcano were hindered during this interval by poor weather and ashy haze, especially on the north flank (Coombs and others, this

volume). Seismicity was dominated by flowage signals, which recorded the movement of pyroclastic flows down the north flanks (Power and Lalla, this volume). Fine, light-gray, massive ash deposits on the island likely represent elutriation from pyroclastic flows generated during this interval (Wallace and others, this volume). These observations, coupled with volume estimates (Coombs and others, this volume), suggest that rapid effusion of lava and dome collapse leading to numerous block-and-ash-flows dominated the early part of the continuous phase. From February 3 to 10, magma-flux rate waned, and a coherent lava flow and summit lava dome grew (Coombs and others, this volume).

The early part of the continuous phase generated pyroclastic-flow deposits (units Cpf and Cpfw) and thin pyroclastic-current deposits (unit Cpc, fig. 2C). Secondary flowage deposits, such as avalanches and lahars, were not identified. Lava effusion during the second half of the continuous phase probably generated small block-and-ash flows, but these were likely covered by, and indistinguishable from, subsequent effusive-phase block-and-ash flows.

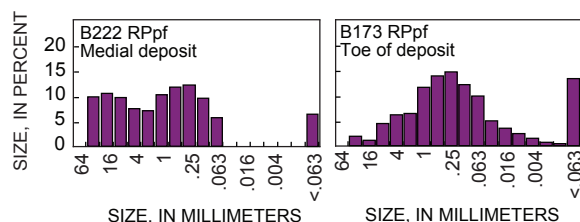
Flow Morphology and General Characteristics

All pyroclastic-flow deposits of the continuous phase have similar composition, grain-size distribution, and outcrop characteristics but differ in morphology. Continuous-phase pyroclastic flows constitute thick, composite fans to the northeast and north of the summit (unit Cpf, fig. 2C). The Windy Creek pyroclastic-flow deposit (unit Cpfw, fig. 2C), however, is an anastomosing deposit on the northwest flank, which, on the basis of the timing of destruction of a seismometer on that flank (Coombs and others, this volume, fig. 15), we surmise was emplaced during a particularly large single-flow event. The continuous-phase pyroclastic current (unit Cpc) is a thin marginal facies emplaced coevally with the two pyroclastic-flow deposits described above. Unlike explosive-phase flows, continuous-phase flows were all restricted to the north quadrant of the volcano (fig. 2C).

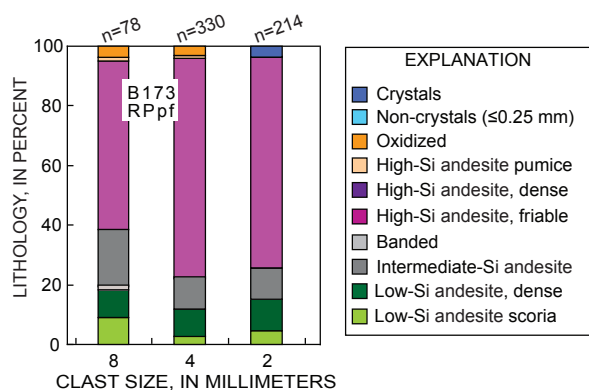
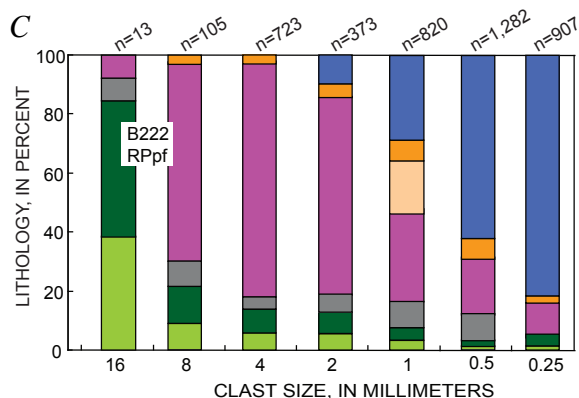
The north and northeast fans of continuous-phase pyroclastic flows reach from the summit to about 100 m asl. Flows in the north fan traveled downslope between a cleaver and a prehistoric lava-dome remnant, and those in the northeast fan flowed down the Northeast Chute (fig. 2C). Prominent lateral-flow levees, rich in large blocks, define dozens of overlapping flow lobes, especially in the upper reaches of the fans (fig. 19A). The lower halves of these two fans spread out and overlap downslope of the cleaver. The lower edges consist predominantly of multiple, lobate fingers, as far as 4 km from the summit. Subdued levees define some flow margins, but elsewhere the distal lobes fan out with indistinct edges (fig. 19B). Although most flows traveled over unvegetated terrain, some lobes struck and singed alders near their termini. Comparison of digital terrain models of the volcano's edifice from before and after the continuous phase suggests that the two fans are as much as 20 m thick in their



B



C



upper reaches (Coombs and others, this volume), whereas individual lobes are generally only as much as 2 m thick.

The Windy Creek pyroclastic flow (unit Cpfw, fig. 2C) was the only continuous-phase flow to travel northwestward; it fanned out over the northwest flank in a series of channels as it followed topographic lows over the somewhat-hummocky topography (fig. 19C), finally stopping about 50 m asl. The destruction of seismic station AU12 (fig. 2C) within its pathway pinpoints its emplacement at 03:24 AKST January 30 (Coombs and others, this volume). The deposit contains abundant blocks, as large as several meters across, that commonly form lateral levees alongside wide, flat-bottomed channels.

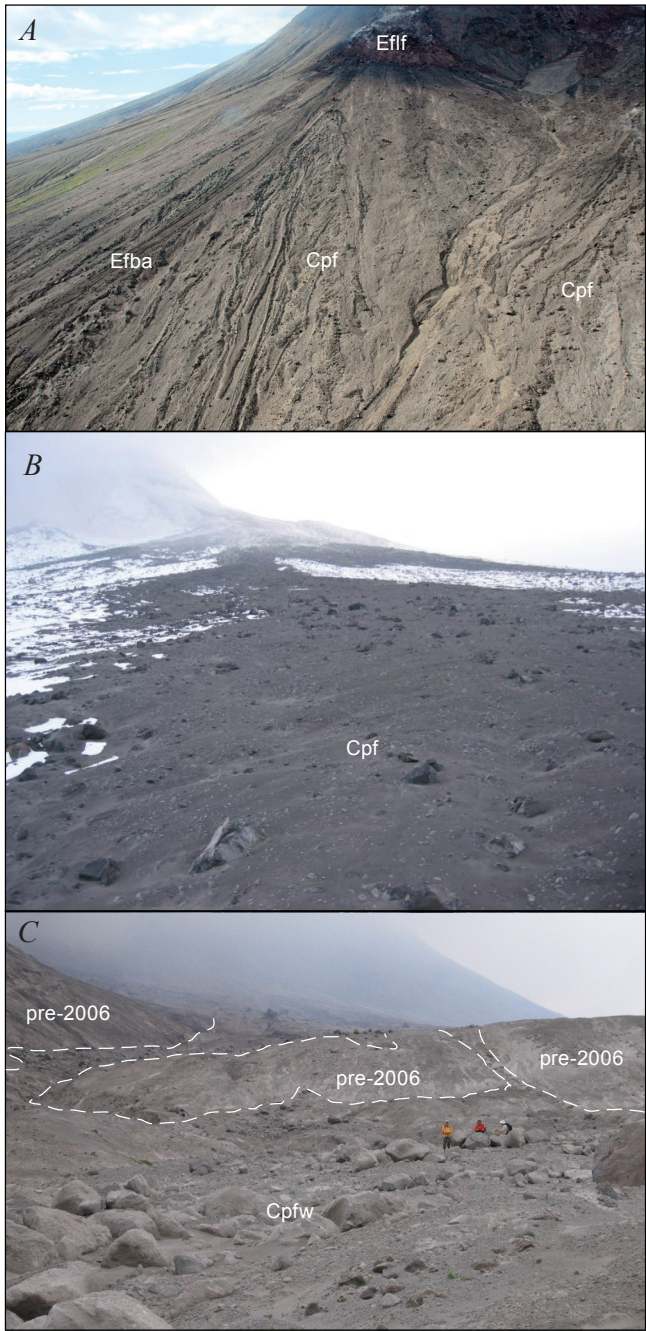
The thin pyroclastic-current deposit (unit Cpc, fig. 2C) is mapped in several locations as a feathered edge facies of continuous-phase flows alongside margins of thicker flows, or where continuous-phase flows lap onto topographic highs. The deposit is generally less than 0.2 m thick and in some places consists only of scattered clasts of friable high-silica andesite atop the pre-2006 surface (Coombs and others, this volume, fig. 15).

Grain-size distributions in continuous-phase pyroclastic-flow deposits are similar to those in earlier pyroclastic-flow deposits, particularly the coarse explosive-phase deposits. Grain-size distribution in continuous-phase flow deposits is moderately bimodal, with modes in lapilli and medium-ash size classes (fig. 7A).

Continuous-Phase Compositions

The shift in eruptive style that began during event 10 continued during the continuous phase and corresponds with a shift in lithologic composition. As revealed in pebble counts and lithologic analysis, continuous-phase composition vary somewhat among individual deposits but generally the deposits are rich in high-silica andesite, dense intermediate-silica andesite, and banded clasts, with slightly less dense low-silica andesite and basically no low-silica andesite scoria (figs. 4, 19D; tables 6, 7).

Figure 18. Rocky Point pyroclastic-flow deposit (unit RPpf), with grain-size characteristics and lithologic components. *A*, Photograph of distal-lobe margins marked by scorched willow branches and large lapilli (sample location B173). Arrow denotes the flow direction. Shovel is 50 cm long. *B*, Histograms of grain-size distribution of medial and distal deposit. Toe of deposit, which was not overlain by lobes of later flow pulses, is finer than more proximal deposits. *C*, Plots of lithologic components of the Rocky Point pyroclastic-flow deposit. Deposit contains abundant friable, high-silica andesite, a rock type also characteristic of subsequent continuous-phase deposits. Sample locations are shown in figure 2B and table 2.



The appearance of continuous-phase deposits shows the shift toward more silicic clast compositions: the deposits are characteristically pale brownish-pink to gray, lighter colored than the explosive- and effusive-phase deposits.

Effusive-Phase Deposits, March 3–16

The effusive phase began after an eruptive hiatus from about February 10 to March 3 (table 1). Whereas effusion of coherent lava lobes northward and northeastward began at the summit near the end of the continuous phase in early February, these lobes were enlarged during the effusive phase, and block-and-ash-flow deposits from February were buried by the products of March activity.

Effusion ultimately produced low-silica andesite in the form of a summit lava dome and two lava flows, descending northward and northeastward from the vent. As the lava emerged and became unstable, blocky material dislodged to form talus deposits, and caused rockfalls and gas release. The release of gas from the fragmenting lava generated block-and-ash flows that traveled down the north, northeast, and east flanks of the volcano (fig. 2D).

Talus Deposits

Aprons of rockfall deposits skirt the front of the northern and northeastern lava flows (unit Efta, fig. 2D). The deposits are highly oxidized, blocky, and unstable, and extend approximately 75 to 100 m beyond the lava flows (figs. 20A, 20B). These deposits were not sampled, owing to their instability and proximity to the oversteepened lava-flow fronts. We estimate the thickness of these talus aprons at 5 to 20 m.

Block-And-Ash-Flow Deposits

Block-and-ash flows were initiated from four areas: (1) the effusive-phase lava dome, (2) the front of the northern lava flow, (3) the front of the northeastern lava flow, and (4)

Figure 19. Photographs and lithologic components of continuous-phase pyroclastic-flow deposits (units Cpf and Cpfw). *A*, Continuous-phase deposit (unit Cpf) below effusive-phase lava flow (unit Eflf) on northeast flank of volcano. Thin, dark fingers of effusive-phase block-and-ash-flow deposit (unit Efba) sit atop overlapping, leveed lobes that compose deposit (unit Cpf). *B*, Distal toe of farthest-reaching part of deposit (unit Cpf) on north fan. Some distal parts of deposit lack levees and instead have feathered edges. *C*, Windy Creek pyroclastic-flow deposit (unit Cpfw). Flow swept around and over topographic highs on northwest flank, with little deposition on steep lee slopes. *D*, Plot of lithologic components of deposit. Sample locations are shown in figure 2C and table 2.

the top and margin of the northeastern lava flow, which then traveled down East Chute (fig. 2D). The block-and-ash flows formed distinctive black, blocky, narrow tongues that are visible beyond the apron of varying and jumbled talus blocks (unit Efba, figs. 2D, 20C, 20D). The long, lobate deposits commonly have blocky levees. The northeastern block-and-ash-flow deposit is estimated to average 6 m in thickness, whereas the others average less than 3 m. Grain-size characteristics of this block-and-ash-flow deposit suggest concentrations of coarse lapilli and coarse ash and an absence of fine ash (fig. 2E).

Lithologic analyses indicate that effusive-phase pyroclastic-flow deposits contain significantly more low-silica andesite clasts than do either explosive- or continuous-phase deposits (figs. 4, 20F). Very few of these low-silica andesites are scoriaceous. The effusive-phase deposits also contain small to modest proportions of intermediate- and high-silica andesite (figs. 4, 20F). Hydrothermally altered and oxidized clasts are more common in effusive-phase block-and-ash-flow deposits than in the pyroclastic-flow deposits of other phases. Huge blocks of oxidized material, as large as several meters across, are common in outcrop.

Discussion

Lithologic Composition and the Three Eruptive Phases

Our field observations in August 2006 quickly revealed that the three eruptive phases were unique, not only in terms of style of volcanism, including associated seismicity, geodetic response, and ash emissions, but also in terms of the types and morphologies of deposits that were produced and, in particular, of their lithologic composition (fig. 4). Two important characteristics were revealed through lithologic analysis of the 2006 flowage deposits: (1) each lithology is present in the deposits of each eruptive phase and in each flow type, and (2) the lithologic proportions are unique to and consistent in the deposits of each eruptive phase.

Lithologic analysis reveals systematic changes in magma composition and clast texture during the 2006 Augustine eruption. Deposits of the three eruptive phases varied in composition and clast type, although a single rock type or group of rock types dominated each phase (figs. 4, 21, table 7). Thus, the explosive phase predominantly produced low-silica andesite, mostly as scoria, but also as 10–20 percent dense clasts; the continuous phase predominantly produced high-silica andesite and lesser intermediate-silica andesite and banded clasts, with clasts of all compositions varying in vesicularity; and the effusive phase produced an even higher proportion of low-silica andesite than the explosive phase, mostly as non-vesicular to sparsely vesicular clasts. Most clasts larger than 1 cm in diameter in effusive-phase block-and-ash flows are low-silica andesite (fig. 21).

Lithologic transitions coincided generally, but not exactly, with shifts in style of volcanism as marked by the three eruptive phases. Explosive-phase deposits of events 3 through 9 (Jan. 13–17) are lithologically similar, whereas event 10 (Jan. 28) yielded two flows whose lithologic composition differed from that of flows erupted earlier. The 9-minute explosion generated the pyroclastic-current that draped the north-slope lava flow and the voluminous Rocky Point pyroclastic flow, marking not only a transition from intermittent vulcanian explosions to continual dome collapses, but also a compositional transition within pyroclastic deposits from primarily scoriaceous, low-silica andesite to primarily friable, high-silica andesite (table 5). This compositional shift began the transition from the explosive to the continuous phase.

Disruption of two lava domes that had grown before event 10 (between Jan. 13 and 27) probably influenced the compositional shift, particularly in dense rock types, within event 10 pyroclastic deposits, but the tapping of a deeper, more silicic magma caused the most striking lithologic shift (figs. 4, 21, table 7; Larsen and others, this volume). The older dome (unit Exd1, fig. 2A), emplaced January 14–17, and shallow residual magma in the conduit are two possible sources of the dense, low-silica andesite clasts within the event-10 deposits, the pyroclastic current (unit Expc) and Rocky Point pyroclastic-flow (unit RPPf). A younger, explosive-phase lava dome (unit Exd2, figs. 2A, 21), composed of intermediate- to high-silica andesite and banded andesite, was extruded between events 9 and 10 (Jan. 17 and 27). Disruption of this younger dome may have generated the huge intermediate-silica andesite blocks within the Rocky Point pyroclastic flow and partly caused the increases in dense high-silica andesite within the deposits of both event 10 pyroclastic deposits. We conclude that pulverization of the domes caused increases in nonvesicular magma, resulting in inclusion of dense clasts in event 10 ejecta. Concentrations of more vesicular high-silica andesite within the Rocky Point pyroclastic-flow deposit, especially in distal areas and on the deposit surfaces, originated from the vent last and indicate the tapping of a deeper, more silicic magma body during event 10 that continued during the continuous phase (Larsen and others, this volume).

The proportions of low- to intermediate- to high-silica andesite in clastic deposits changed abruptly during event 10, at the start of the continuous phase, and again after the hiatus that preceded the effusive phase (figs. 4, 21). These trends heralded changes in eruption rate, magma composition, and gas content. During the explosive phase before event 10, proportions were about 70:15:15. During event 10 proportions showed a rapid change to 38:27:35 and then to 20:15:65. Subsequently, pyroclastic-flow deposits emplaced during the continuous phase contained no scoria, but enough dense low-silica andesite to change proportions to approximately 25:35:40. Probably, the magma had become sufficiently gas poor and had extruded slowly enough that no vesicular low-silica andesite ejecta formed, and fewer than a third of the ejecta were composed of dense, low-silica andesite. During

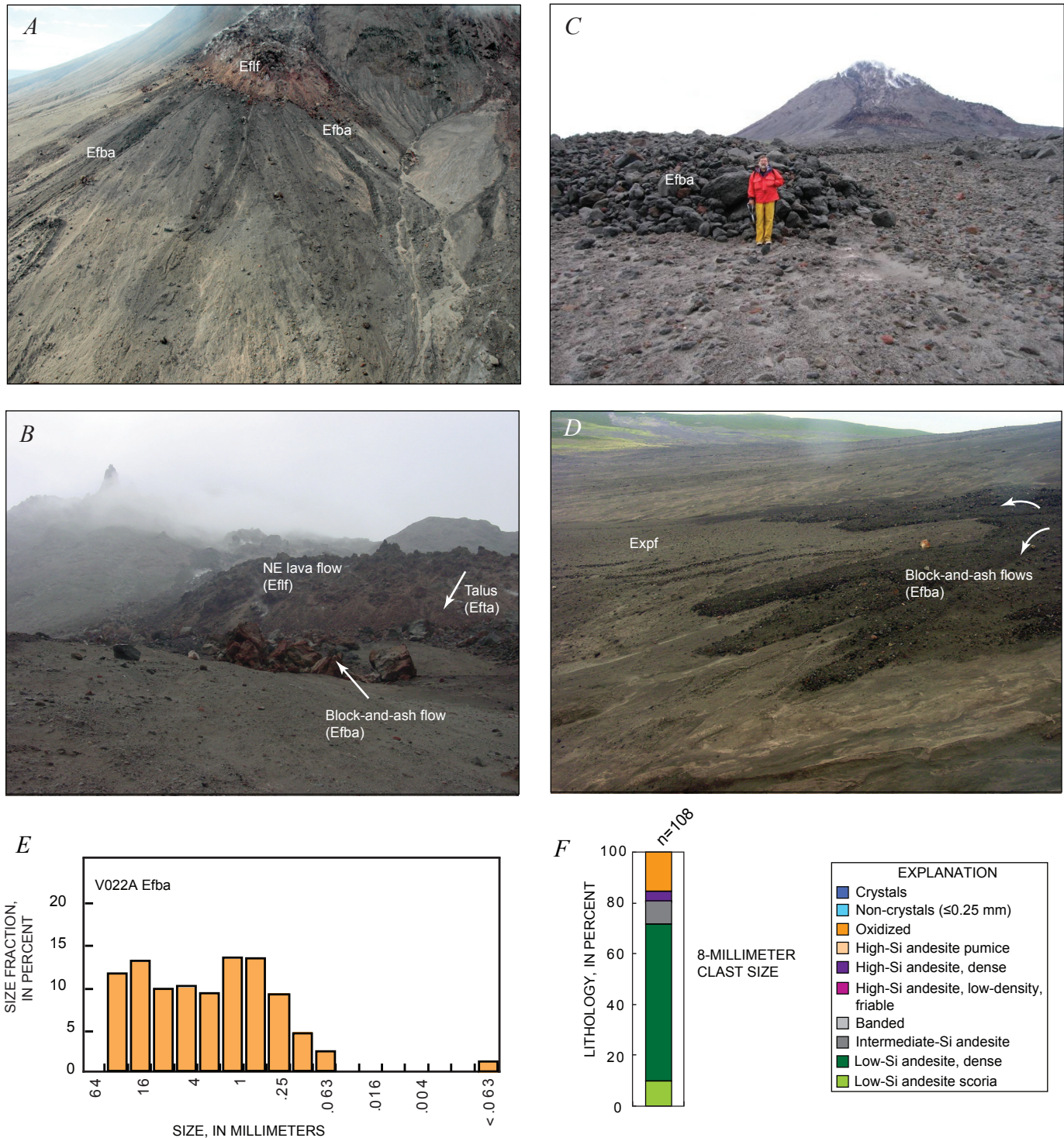


Figure 20. Photographs, plot of grain-size distribution, and lithologic components of effusive-phase block-and-ash-flow deposit (unit Efba). *A*, Aerial view south towards effusive-phase block-and-ash-flow deposit (unit Efba) and lava flow (unit Eflf). *B*, View of the northeast lava flow (unit Eflf), rockfall talus apron (unit Efta) below lava, and short block-and-ash-flow deposit (unit Efba). *C*, Distal margin of block-and-ash-flow deposits (unit Efba). *D*, Oblique aerial view of distinctive black block-and-ash-flow deposits in East Chute area. These deposits resulted from fracturing and collapse of parts of new lava flow. *E*, Grain-size distribution of block-and-ash-flow deposits. *F*, Plot of lithologic components of block-and-ash-flow deposit. Sample locations are shown in figure 2D and table 2.

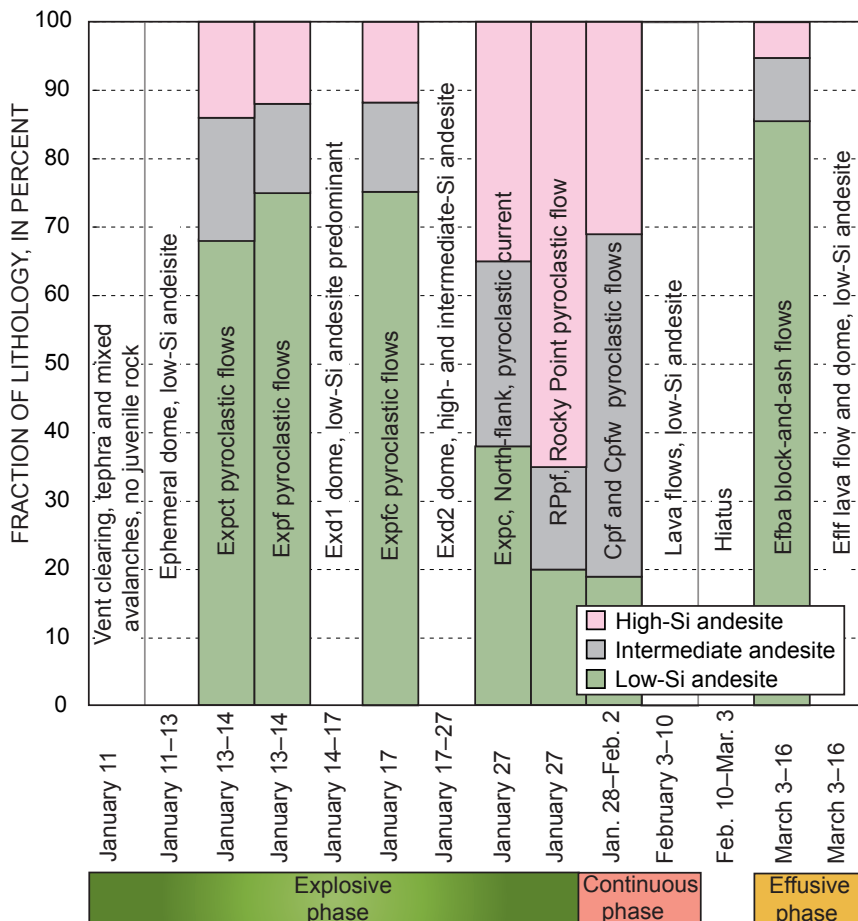


Figure 21. Plot summarizing chronologic changes in chief lithologic components in deposits of 2006 eruption of Augustine Volcano. Proportion of low-silica andesite, initially high, diminished at end of explosive phase and during continuous phase as proportion of intermediate- and high-silica andesite increased. These trends reverse from continuous phase to effusive phase. Low-silica andesite increased during the effusive phase and changed from being predominantly scoriaceous during the explosive phase, to predominantly dense during the effusive phase.

the continuous phase, proportions of both intermediate- and high-silica andesite increased significantly.

Banded clasts, which include any combination of compositions, most commonly compose bands of high- and low-silica andesite (table 4; Larsen and others, this volume). The proportions of banded clasts in the deposits varied widely but were largest in continuous-phase deposits (fig. 4), suggesting that mixing of low- and high-silica andesite magmas was common throughout the eruption but probably greatest during the continuous phase. Larsen and others (this volume), interpret the intermediate-silica andesite to be the product of complete mixing between high- and low-silica andesitic magmas.

Effusion of low-silica andesite lava began before the end of the continuous phase and continued during the effusive phase, producing block-and-ash flows predominantly composed of dense, low-silica andesite, sparse scoria, and about 13 percent high-silica andesite (figs. 4, 21, table 7). Larsen and others (this volume) suggest that the waning stages of the continuous and the effusive phase extruded the last dregs of eruptible high-silica andesite magma along with low-silica andesite lavas. High-silica andesite clasts in block-and-ash flows derive from inclusions of such material within the lava flow itself or from erosion and incorporation from underlying, continuous-phase pyroclastic-flow deposits.

Origin and Downslope Behavior of Pyroclastic Currents and Flows

During the 2006 eruption of Augustine Volcano, the chief factors that influenced pyroclastic-flow behavior and the nature of their deposits were genesis, grain size, and the characteristics of the surface over which they flowed. Column collapse from short-lived vulcanian blasts, dome collapse, and the collapse of viscous lavas on steep slopes caused the pyroclastic currents documented in this study.

Column-collapse flows during the explosive phase spread widely and probably were dilute and laterally mobile where they overran snowpack. Subsequent flows had similar fines content but were confined to drainages. This change in flow morphology occurred once previous pyroclastic flows had either melted the snowpack or coated the snow with layers of pyroclastic debris sufficiently thick to insulate new flows from the underlying snow. In contrast, the dome-collapse Rocky Point pyroclastic flow and the continuous-phase flows involved neither column collapse nor the influence of underlying snow. Only the Rocky Point pyroclastic flow, possibly because it was more voluminous and finer grained than subsequent flows, showed evidence of appreciable dilution as it moved. The dome failure that generated the large-volume

Rocky Point pyroclastic flow may have been deeper seated than subsequent dome-collapse flows, thereby unloading incompletely degassed lava that decompressed explosively to inflate the initial pyroclastic mass. The subsequent continuous-phase flows behaved as partially fluidized granular flows. In contrast, effusive-phase block-and-ash flows were caused exclusively by collapses of andesite lava-flow margins. These block-and-ash flows, though hot, were sufficiently coarse and permeable that gas escaped rapidly and lapilli and blocks were mostly supported by particle-to-particle contacts. These flows behaved basically as rock avalanches because their ash-and-gas mixture provided little fluidization to ameliorate their frictional-granular characteristics.

Formation of Levees and Digitate Margins During Pyroclastic-Flow Emplacement

Scoria-rich column-collapse flows of the explosive phase, dome-collapse flows of the continuous phase, and block-and-ash flows of the effusive phase all behaved similarly, regardless of their diverse origins, to produce deposits with coarse blocky levees and digitate distal margins, a morphology indicative of partially fluidized, granular flows with high solids fractions (fig. 22). Some of these pyroclastic flows may have been highly energetic on steep slopes near their source, but as they descended the volcano's slopes, hot particle and gas mixtures settled to form granular basal flows that moved across intermediate and gentler slopes of the volcano's apron. Overriding, elutriate ash clouds (fig. 5A) would have obscured basal granular flows. Once the pyroclastic flows began to decelerate, large, low-density particles began to migrate to the surfaces of the basal granular flows (figs. 9, 22A). The surface velocities of such granular flows are greater than those of propagating flow fronts; thus, particles at the surface migrate toward distal and lateral margins, where they accrete particle by particle, and then lag behind the moving flow to form levees (fig. 22B; for example, Lube and others, 2007). Fines-poor aggregations of outsize low-density particles that accrete at active flow fronts influence the behavior of the granular flow in two ways. First, because the largest particles in natural grainflows are commonly more angular than smaller ones, the coarse mixture at the front of flows may develop a greater Coulomb friction than in the finer following flows (Pouliquen and others, 1997). Second, coarse mixtures that form at flow margins are generally more permeable than finer interior flows. Because fluid, in this case gas, can more readily escape from the coarse and, therefore, permeable flow fronts than from the relatively less permeable ash-rich flows that follow, flows evolve Coulomb-friction-dominated perimeters that encompass fluidized or partially fluidized interiors, for example, in debris-flow systems (Iverson, 1997). More mobile debris that pushes a perimeter of less mobile debris results in unstable flow and the formation of large-particle-rich clefts and lobes at propagating flow fronts (Pouliquen and Vallance, 1999). When such partially fluidized, granular pyroclastic flows come to rest, they preserve clefts, lobes, and

finger-shaped bifurcations as digitate deposit margins that are relics of granular-flow instabilities (fig. 22A).

A similar segregation process can occur with low-density particles and cause cleft-and-lobe structures. Vallance and Savage (2000) show that density segregation, though dependent on a different sorting mechanism than size segregation, is highly efficient in the upper parts of granular flows. Thus, if a flow contains large, low-density particles, such as pumice or scoria, these particles will migrate to the surface, where velocities are highest, and then move toward flow margins. If the perimeter thus formed is more frictional than the interior flow, a flow instability results, and the flow breaks into clefts and lobes. Again, the mechanism depends on the granular character of the flow; however, optimal density segregation occurs in more energetic granular flow than does optimal size segregation (Vallance, 1994; Vallance and Savage, 2000).

In such natural phenomena as pyroclastic flows, the granular material traps gas, which, if it cannot readily escape, partially supports the weight of the particles. The medium is then partially fluidized and thus flows more easily downslope. Pouliquen and Vallance (1999) modeled such flows in the laboratory by pouring aerated 500°C ash or sand down an inclined surface. The granular, sediment-rich basal avalanches control the behavior of these flows. Segregation of large, low-density particles that initially move upward and then toward flow fronts, as well as elutriation of small particles at flow fronts, ultimately forms coarse, permeable perimeters that are dominated by Coulomb friction (Pouliquen and Vallance, 1999). Consolidation of solids and entrapment of gas generate fines-rich flow interiors that are partially fluidized (Pouliquen and Vallance, 1999, fig. 7). As the flows slow and eventually come to rest, frictional contrasts with the bed—large at the flow perimeter and small in the fluid flow interior—cause flow instabilities that commonly result in digitate deposits similar to the flow fingers observed at Augustine Volcano in 2006 (fig. 22).

Behavior of Energetic Pyroclastic Currents—Implications for the Generation of Their Deposits

The initial pyroclastic-flow deposits of the explosive phase, and those from a vigorous dome collapse during event 10, share characteristics which indicate that they were energetic and diluted by gas ingestion as they moved. Such features include widespread, but thin, deposits; gradual thinning of deposits at lateral and distal margins and an absence of lateral or distal levees; the presence of large blocks in thick axial deposits and the absence of such blocks near margins; the presence of deposits on topographically high areas; evidence of vigorous elutriation, such as fines-deficient “lag” deposits and cogenetic fine marginal deposits; and temperatures insufficient to burn vegetation or completely melt underlying snow. On the basis of the deposits that these dilute, energetic flows produced, the most important processes are settling of large and dense blocks into thick, fluid axial parts

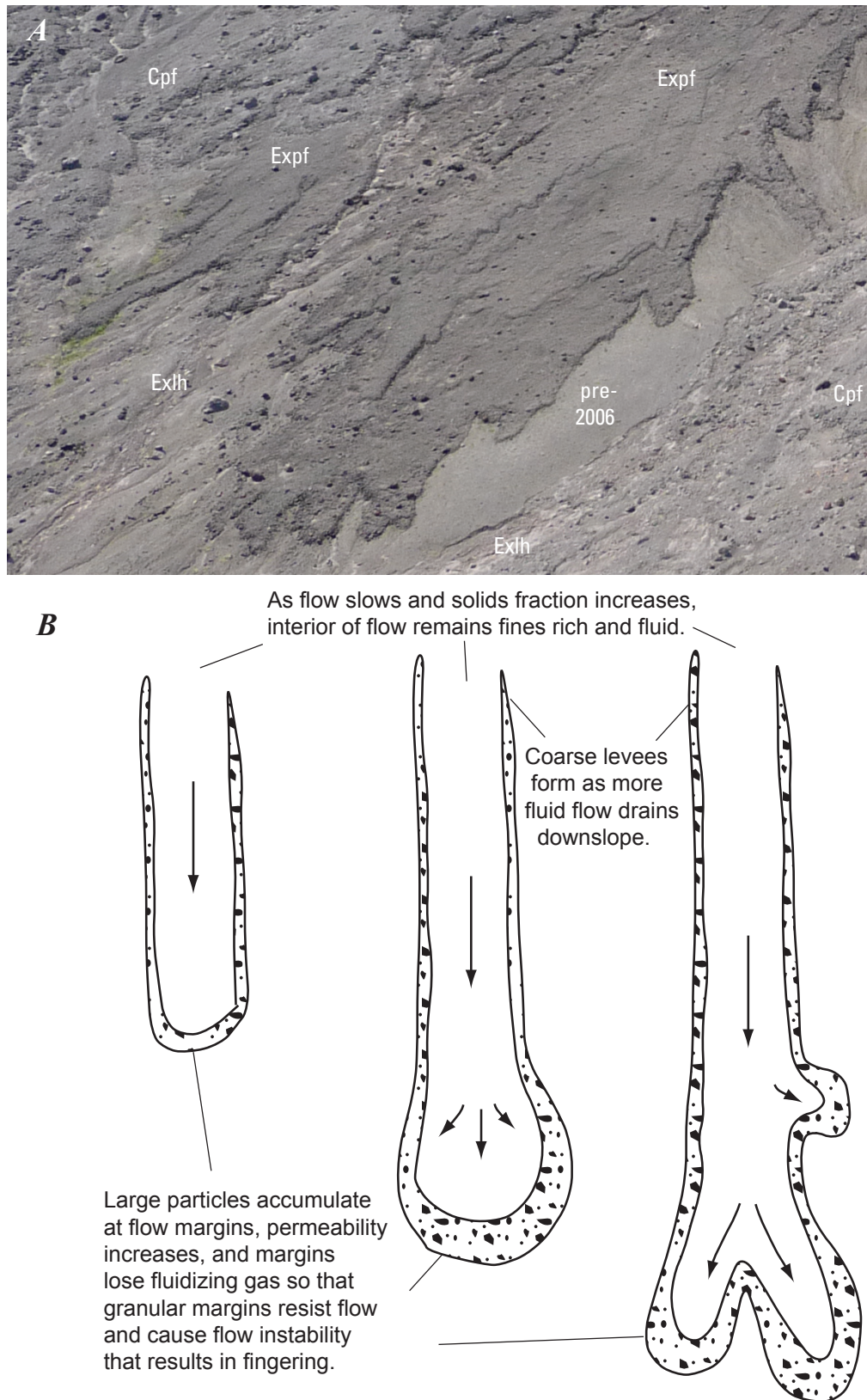


Figure 22. *A*, Oblique aerial photograph of part of northeast fan, showing coarse blocky digitate margins of explosive- and continuous-phase pyroclastic-flow deposits (units Expf and Cpf). *B*, Line drawing illustrating evolution of fingering in moving pyroclastic flow.

of the flow; elutriation of fine ash to form proximal lag facies and marginal fine surges, and a propensity to spread laterally, especially across snow-covered slopes. Each of the three types of explosive-phase deposit documented in this study exhibit some, but not all, of these features.

The Rocky Point pyroclastic flow originated as a large dome collapse that probably caused a sudden depressurization of deep-seated lava; it then evacuated the entire conduit and must have tapped into a magma “chamber” at 4- to 6-km depth. The collapse and decompressively vesiculated conduit magma generated a surge-like flow whose deposits fine and taper to thin margins, despite the enormous blocks contained in axial zones. The deposit shows notable drainaway features, such as stranded terraces (fig. 17A), matrix debris perched on blocks whose tops reach 8 m above the deposit surface (fig. 17B), and pre-2006 scarp surfaces that protrude through axial, meters-thick deposits lying on gentler slopes in adjacent areas. Cole and others (2002) described voluminous pyroclastic-flow deposits at Montserrat that originated from dome collapse and share many characteristics with the Rocky Point pyroclastic-flow deposit. For example, the Montserrat deposits also contain large blocks with matrix debris perched on their tops, indicating flow depths greater than local deposit thicknesses. Similarly, ridge-and-swale features, concentrations of low-density clasts, and tree fragments characterize distal zones. In the Rocky Point pyroclastic-flow deposit, we additionally noticed pyroclastic debris ramparts piled up on the stoss sides, and streamline hollows on the lee sides, of large blocks that had been grounded on steep slopes early in the depositional sequence (fig. 17B). Cole and others (2002, fig. 22) inferred that as these sheetlike flows decelerated, the upper parts of the flow drained downslope to form tapering, distal deposits with concentrations of low-density particles at their surface. On gently sloping fans, swales (inappropriately called furrows by Cole and others) are radially oriented parallel to flow but exhibit subordinate anastomosing patterns that divide and truncate the gently sloping ridges paralleling them. The large blocks are distributed 100 to 500 m inboard of the deposit margins situated both on ridges and in swales. We infer that the complex anastomosing swale patterns were paths followed by the most fluid pyroclastic debris as it drained away from material slightly more resistant to flow along ridges, while simultaneously following predominantly radial flow directions. On the basis of their characteristics, we concur with Cole and others (2002) that large dome-collapse pyroclastic flows like those at Montserrat and Rocky Point moved as a sheetlike body that drained away downslope, stranding huge blocks along slopes and fan apices. When it reached low-gradient slopes, the flow accreted incrementally at fan apices to form ~10-m-thick accumulations, and the overriding flow pushed downslope to produce fines-rich deposits, rich in low-density particles, that thin gradually toward distal margins.

The distribution and characteristics of the pyroclastic-current deposit (unit Expct, fig. 2B) suggest that it was the energetic product of laterally directed explosions at the beginning of event 10. Its deposit is similar to initial

explosive-phase pyroclastic currents (unit Expct), but differs notably in its ubiquitous friability, mostly lacking fine matrix particles, and its distribution across the axis of a 50- to 100-m-high ridge. Even though it flowed across snowy slopes, the pyroclastic current did not generate lahars. The deposit at distal margins fines and tapers to thin edges. We infer that this deposit was emplaced by a surge-like flow because of its distribution on a high ridge and its lack of fine particles. Explosions directed northward at the beginning of event 10 probably initiated the pyroclastic current.

Initial pyroclastic flows of the explosive phase (unit Expct, fig. 2A) invariably flowed across snowpack, scoured it, and commonly came to rest on snow; thus, this underlying snow, rather than conditions at the vent, chiefly controlled both flow behavior and deposit characteristics (fig. 23). Deposits preserved on top of snow suggest that flows had cooled significantly to near-ambient temperatures during transit. This observation implies considerable heat transfer because pyroclasts exited the vent at temperatures in excess of the solidus temperature (Larsen and others, this volume). We infer that ingestion and vaporization of snow fluidized the flows so that the resulting deposits are widespread, commonly thin, and thin toward their lateral margins but do not fine there. Unlike the Rocky Point pyroclastic-flow deposit, these deposits rarely are more than 1 m and commonly only 10 to 20 cm thick (fig. 5B). Because the flows originated by column collapse of short-lived vulcanian plumes rather than by dome collapse, they did not carry outside blocks. Blocks smaller than 1 m across are scattered across deposit surfaces, even near margins (fig. 5C). Where emplaced on windswept snow-free terrain, the deposits are smooth surfaced and thin toward margins. These deposits' distal margins rarely are preserved because distal parts of the deposits generated lahars and mixed avalanches. The evolution and behavior of these flows across snow are discussed in more detail below.

Behavior of Pyroclastic Flows Across Snow and the Evolution of Mixed Avalanches and Lahars

Theoretical analysis and experimental results by Walder (2000a,b) suggest a mechanism whereby initial pyroclastic flows can spread across snowpack and generate mixed avalanches and lahars. Pyroclastic flows can erode substrates formed of snow or ice through a combination of mechanical and thermal processes at the bed. Walder shows both theoretically (2000a) and experimentally (2000b) that thermal scour can effectively incorporate snow at the base of a pyroclastic flow. The fundamental cause of thermal scour is unstable fluidization of the pyroclast layer by a brief, intense burst of vapor at the instant when hot grains contact snow that involves vapor bubbling and particle convection which disrupt the snow surface (Walder, 2000b). The analysis shows that an upward flux of water vapor immediately upon pyroclastic-flow contact with snow can be great enough to fluidize the pyroclastic layer efficiently under the proper conditions. Those conditions are

a function of emplacement temperature, overburden pressure or pyroclastic-flow thickness, and grain size, as illustrated in figures 24A and 24B. If vaporization is sufficient, hot pyroclastic material is efficiently mixed with underlying snow, and melting is enhanced. The tendency toward fluidization at the interface can enhance both the mobility of a pyroclastic flow and its ability to form slurries of snow, water, and pyroclastic material that may later coalesce and flow downstream. Increase in temperature and decrease in grain size favor

fluidization at the interface, but the relation to overburden pressure is more complex. Overburden pressure at the interface enhances fluidization to a point where total load is too great and then suppresses the process (fig. 24A).

We can approximately constrain the overburden pressure P for Augustine flows by using deposit thickness, solids fraction, and rock density as proxies in calculating values for the actual flow, such that $P = v\rho_{\text{rock}}gh$, where the solids fraction v of the deposit is about 0.4 to 0.5, the density of the rock ρ_{rock}

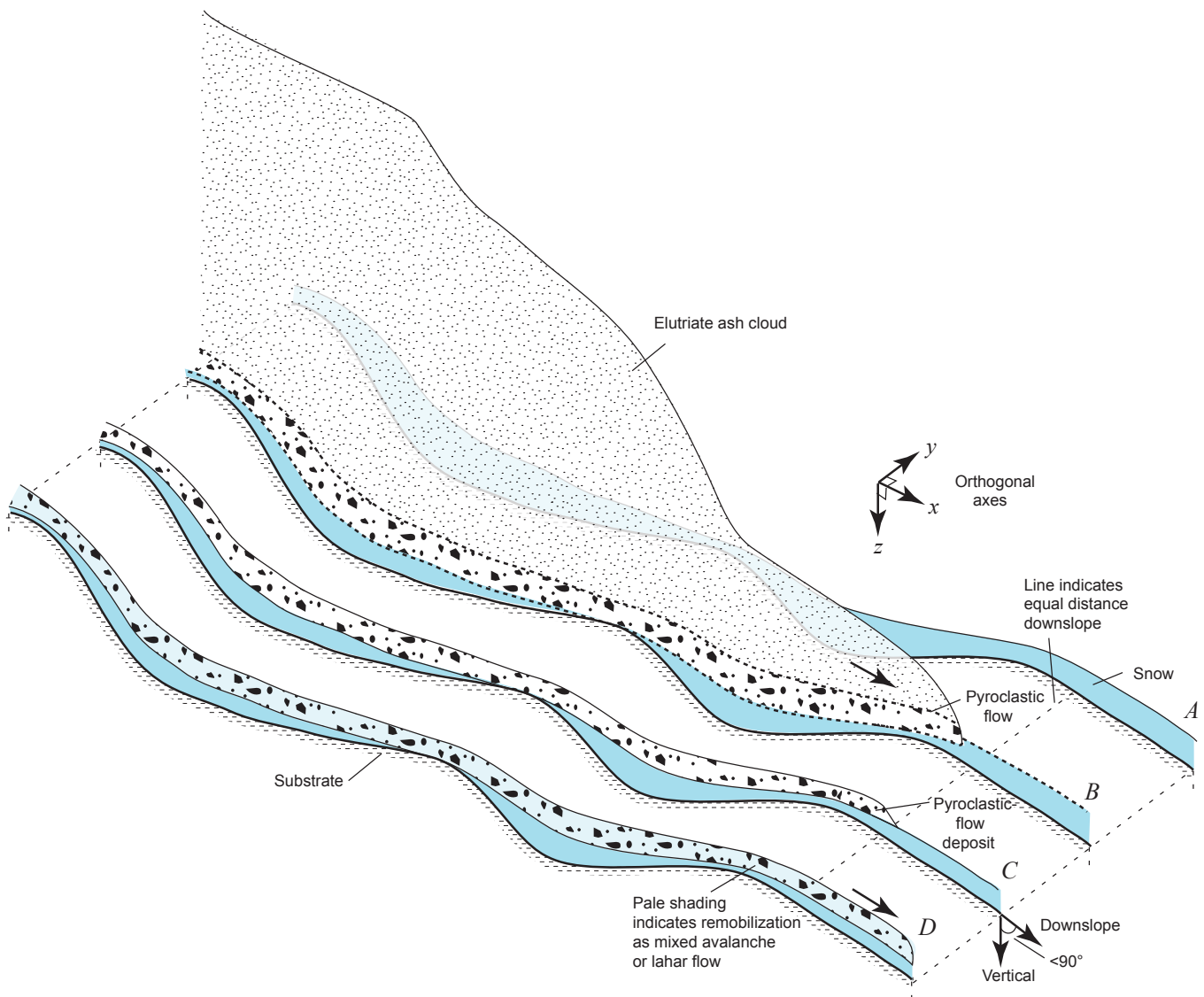


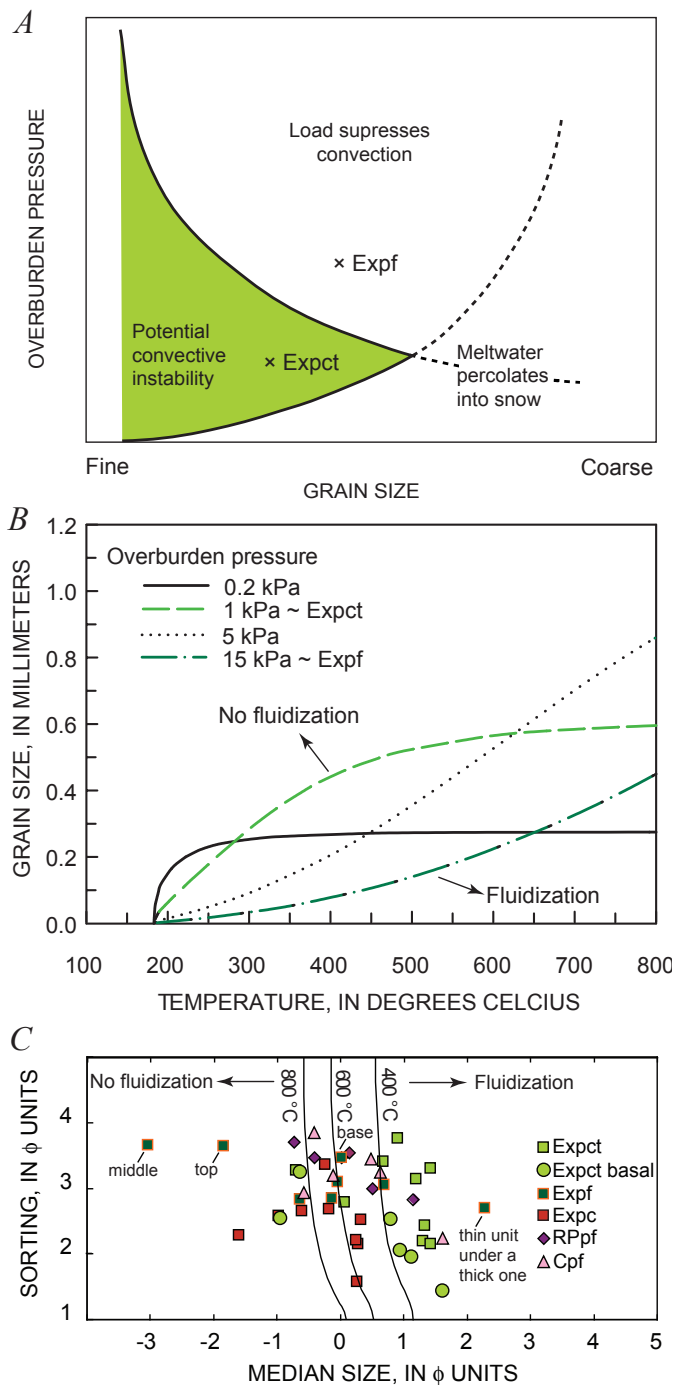
Figure 23. Schematic sketches of successive stages in the interaction of a pyroclastic flow with snow. *A*, Initial snow-covered slope. *B*, How a pyroclastic flow might move across snow, partially eroding and incorporating it. *C*, The pyroclastic flow stops briefly or decelerates almost to a stop. *D*, Finally, a mixture of snow, water, and pyroclastic debris begins to move and forms mixed avalanches (or lahars). Field evidence supports either sequence *A–B–D* or *A–B–C–D* but cannot distinguish whether pyroclastic flows come to a complete stop before initiating mixed avalanches or merely decelerates. Once in motion, mixed flows likely contain hot or warm pyroclastic debris, especially large particles, which can continue to convert snow to water through heat exchange, allowing the mixture to become progressively wetter with distance downstream.

is 1,600 to 2,600 kg/m³, g is the gravitational constant, and h is the deposit thickness. Vaporization of snow dilutes moving flows, so that flow depth would have been greater than the thickness of deposits, but the solids fraction would probably have been correspondingly smaller, and so our simple calculation is not unreasonable. A further assumption is that the gas phase largely supports the pyroclasts, so that hydrostatic and total pressures are approximately equal. This assumption implies that the flow is fully fluidized—basal fluid pressure would diminish in the degree to which fluidization is partial. Our estimated P values for the initial thin pyroclastic current (unit Expct, fig. 2A) that initiated mixed-avalanche and lahar flows, using $h = 0.1$ – 0.2 m, are about a tenth (0.6–2.5 kPa) of those for subsequent flows; they appear to lie in the field where fluidization is favored (figs. 24A, 24B). The subsequent flows (unit Expf, fig. 2A) yield estimated overburden pressures that may fall in the field of suppressed fluidization where $P = 8$ – 20 kPa and $h = 1$ – 2 m (fig. 24B). Fine-grained pyroclastic flows are more apt to fluidize snow substrates than are coarse-grained flows—in fact, within reasonable, pyroclastic-flow temperature ranges of 300–800°C, grain size is a more important factor than temperature for inducing thermal scour (figs. 24A, 24C). Our grain-size data show that the initial thin pyroclastic current (unit Expct), which was generally finer grained than those that followed, falls in a field favorable to thermal scour of snow and coeval fluidization (fig. 24C). Lastly, we note that tephra-fall and pyroclastic debris from previous eruptions insulated underlying snow from subsequent flows (fig. 5A), greatly diminishing their facility for efficient thermal scour or fluidization.

Initial pyroclastic flows of the explosive phase invariably generated lahars and mixed avalanches, but some of these secondary flows were wetter and more laharic than others. Apparently, the resulting mixtures were sensitive to the available proportions of hot pyroclast material and snow. On the east side of the volcano, secondary flows were quite watery, and recognizable mixed-avalanche deposits are small or absent. In contrast, on the south side of the volcano, mixed-avalanche deposits predominate in medial reaches and form extensive marginal terraces and axial islands in distal reaches, as illustrated in Augustine Creek (figs. 2A, 13).

On the basis of field observations, our conception of how pyroclastic flows moving over snow generate slurries of snow, water, and pyroclastic material and how these mixtures behave downstream is illustrated in figures 23 and 25. Once a pyroclastic flow is in motion, it scours substrate snow thermally and mechanically, converting some snow to vapor and some to water. Our field data cannot constrain whether slurry mixtures begin to move while pyroclastic flows remain in motion (sequence A–B–D, fig. 23) or whether pyroclastic flows come to a complete stop, and then the wettest parts of slurries break away (sequence A–B–C–D, fig. 23)—each scenario is possible, given local conditions. We envision that moving slurries contain hot pyroclastic blocks and lapilli that transfer their heat more slowly than smaller particles and continue to melt remaining snow in slurries as they move. Thus, slurries that

contain significant amounts of snow are likely to become progressively more water-rich downstream. The wettest parts of the slurries will be the most mobile, and such parts will coalesce where drainages join downstream. Flows that contain little snow will behave like lahars, segregating both large and low-density particles to their surfaces and margins and forming bouldery levees as they flow downstream (fig. 12A); however, those flows that contain significant amounts of snow will also segregate low-density snow toward their margins (fig. 25). By this process, mixtures that contain substantial



amounts of snow and move significant distances downstream can generate both snow-rich, marginal flows that slide across surfaces protected by snowpack, and water-rich axial flows that scour channels and are mainly lahars (fig. 25). The sliding marginal flows, like those in Augustine Creek (fig. 13A), preserve vegetation under snowpack, destroy exposed vegetation, and form marginal mixed-avalanche deposits that become draped over vegetation and are littered with shattered branches (figs. 11A, 12A). The cogenetic, water-rich axial flows scour their beds and leave trails of stripped vegetation and scattered boulders in their wakes (fig. 12A).

Relation Between Volume and Planimetric Area for Pyroclastic Flows and Surges—Implications Concerning Mobility

On the basis of simple dimensional analysis, we expect that planimetric area, A , will scale with deposit volume, V , to the two-thirds power for granular mass flows of similar origin with sudden onset. We see that $V = h_{\text{ave}} A$, where h_{ave} is

the average deposit thickness. For lahars Iverson and others (1998) argued that $h_{\text{ave}} \approx \varepsilon A^{1/2}$, where ε is a constant and the deposits are dominantly tabular and thin relative to their lateral dimensions (that is, ε is a small constant). Substituting this approximation into the first equation gives the desired relation, $A = cV^{2/3}$, where c is a hypothetical constant, such that $c = \varepsilon^{2/3}$ (Iverson and others, 1998). Iverson and others demonstrated the validity of this relation statistically by calibrating c with data from lahars. Dade and Huppert (1998) showed a similar relation to be true for debris avalanches, and Griswold and Iverson (2007) demonstrated such relations for nonvolcanic debris flows and rock avalanches. Finally, Calder and others (1999) and Widiwijayanti and others (2009) suggested such a relation for pyroclastic flows from the recent eruptions of Montserrat and Merapi.

We hypothesize here that log-log plots of planimetric area versus volume for pyroclastic-current deposits with similar origins and characteristics will fall along linear trends, such that $A = cV^{2/3}$, where c is a constant for similar groups of flows. To test and calibrate this relation, we analyzed trends in pyroclastic-current inundation data from Soufrière Hills Volcano, Montserrat (Calder and others, 1999; Druitt and others, 2002a), Mount St. Helens in 1980 (Rowley and others, 1981), Merapi Volcano, Indonesia, in 2006 (Charbonnier and Gertisser, 2008), and Augustine Volcano in 2006 from this study (fig. 26A). We find considerable scatter among the data for pyroclastic-current deposits relative to those for lahars, rockfall avalanches, and volcanic debris avalanches (fig. 26B). Pyroclastic currents generally yield more widely varying data because such currents have diverse origins and behavior. Some currents, such as surges (Druitt and others, 2002a; Loughlin and others, 2002), are dilute and more mobile than others that are granular. Some currents have highly energetic origins at the vent, and others begin as simple gravitational collapses of domes and lava flows (Druitt and others, 2002b). Finally, some currents have a sudden onset, and others erupt continuously over significant time periods. In our analysis, we consider only currents that have a sudden onset, because the condition of continuous pyroclastic-current production violates the assumptions in the model presented here (Iverson and others, 1998). Our plot (fig. 26A) suggests grouping pyroclastic-currents into three flow types on the basis of mobility and, coincidentally, origin: (1) dome-collapse flows, (2) column-collapse flows, and (3) energetic surge-like flows. We obtain regression-line and two-thirds-slope correlations with large coefficients of determination, meaning positive correlations between planimetric area and deposit volume, for each flow types; however, we consider the correlation for the third type to be quite tentative because it includes only four data pairs (table 8). We tested whether best-fit regressions differ significantly from specified two-thirds-slope fits and observed that they do not differ significantly (table 8). In contrast, best-fit regressions do differ significantly from zero-slope fits for all three types, implying that the null hypothesis of no correlation between planimetric area and deposit volume must be rejected. Our statistical analyses of data for dome-collapse and column-collapse flows support our hypothesis that planimetric area A

Figure 24. Plots that show how overburden pressure, temperature, and grain size influence potential for convective instability that favors erosion and entrainment of snow by pyroclastic flows moving across snowpack (from Walder, 2000b). **A**, Schematic plot of overburden pressure versus grain size, showing how decrease in grain size favors convective instability. Relation of overburden pressure to such instabilities is more complex. Increasing pressure increases likelihood of snow entrainment until load becomes too great and instability is suppressed. **B**, Isobaric plots of grain size versus temperature, showing field of snow fluidization and suppressed fluidization. We estimated likely overburden pressures of 2006 Augustine pyroclastic flows on their substrate by using explosive-phase-deposit parameters as proxies. Thus, pressure $P \approx \nu \rho gh$, where ν is solids fraction of deposit, ρ is rock density, g is gravitational constant, and h is deposit thickness. Such a calculation assumes that fluidizing gas supports weight of particles. Incomplete fluidization would diminish actual overburden pressure. Our estimated P values for initial thin pyroclastic-current deposit (unit Expct) that initiated mixed-avalanche and lahar flows are about a tenth of those for subsequent pyroclastic-flow deposits (unit Expf) and appear to lie in field where fluidization is favored. Subsequent flows yield estimated overburden pressures that may suppress fluidization. **C**, Isothermic boundaries between fluidization and its inverse on our sorting-versus-median- ϕ -size data for 2006 Augustine pyroclastic flows. Grain-size characteristics of initial flows (unit Expct) plot in field where fluidization is more likely than for those of subsequent flows.

varies with $V^{2/3}$. We tentatively advance a similar relation for energetic surgelike flows but suggest that such a relation needs further testing with data.

The ratio $A/V^{2/3} = c$ gives a dimensionless measure of mobility calibrated for similar types of pyroclastic currents, and such calibrated mobility factors have a potential use in volcanic hazard assessments. Genesis, energy, and grain-size

characteristics, all of which influence mobility among pyroclastic-currents, vary too widely for all flows to fall along similar trends (fig. 26A). As we might expect, surgelike flows are highly mobile and have a mobility factor of $c \approx 520$ that is greater than that of lahars, with $c \approx 200$ (fig. 26B; Iverson and others, 1998). The column-collapse flows studied here have a moderate mobility factor of $c \approx 150$, only slightly less than that

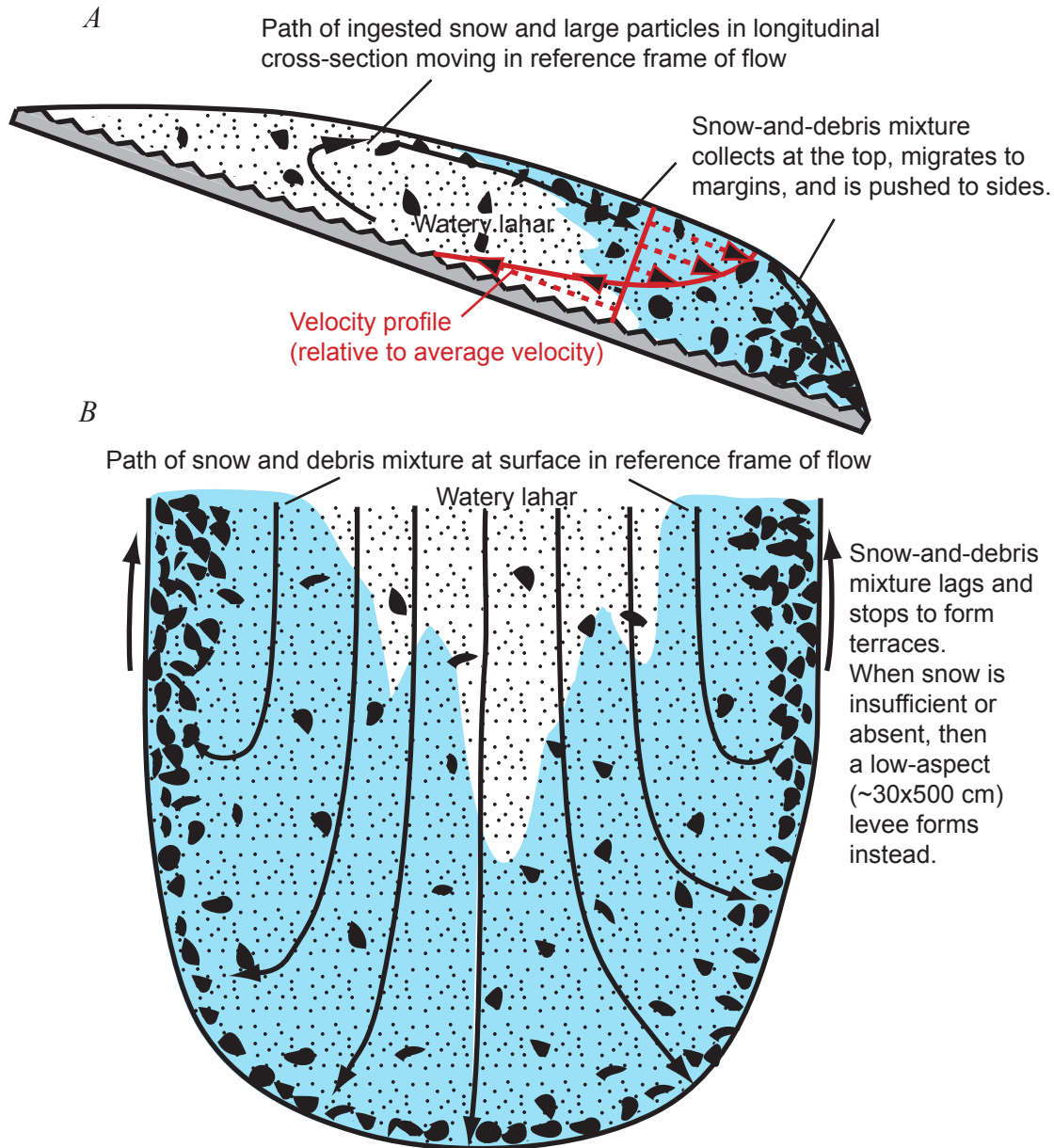


Figure 25. Schematic diagrams showing how simultaneous segregation of low-density snow and entrained coarse particles to surface of a mixed flow (simultaneous mixed avalanche and lahar) results in segregation of both snow and debris mixture to front (A) and margins (B) of flow. Whether such flows produce boulder-cobble levees or marginal mixed-avalanche deposits depends on amount of snow entrained at any particular time and place downstream while flow is in motion. Frame of reference advects downstream at average speed of flow (that is, at propagation velocity of flow front).

for lahars. Dome-collapse flows have a mobility factor of $c \approx 37$, a result similar to that of Widiwijayanti and others (2009), suggesting that they are no more mobile than volcanic debris avalanches and only slightly more mobile than nonvolcanic rockfall avalanches (fig. 26B). Mobilities of similar types of pyroclastic currents, as measured with our ratio $A/V^{2/3}$, yield more consistent results than H/L ratios, where H is the fall height and L is the runout distance (for example, Hayashi and Self, 1992; Calder and others, 1999). However, appropriate data are sparse, and our mobility relations could benefit by testing with additional data. Widiwijayanti and others (2009) present data illustrating the relation of cross-sectional area versus volume for dome-collapse flows and obtain the result: cross-sectional area = $0.05\text{--}0.1V^{2/3}$. Their data allow hazard zones for dome-collapse flows to be drawn in a consistent, repeatable way at any volcano, using the LAHARZ procedure of Iverson and others (1998). Cross-sectional areas for more energetic and dilute pyroclastic currents have proved difficult to measure, and data are needed to assess and calibrate the utility of the LAHARZ method for such flows. Indeed, mobile pyroclastic surges commonly accompany even the least mobile types of pyroclastic flow, such as those generated by the collapse of lava domes and flows.

Conclusions

The 2006 eruption of Augustine Volcano provided an opportunity to observe explosions, map and characterize pyroclastic and other flowage deposits, and test hypotheses concerning the origins and behavior of these flows. In particular, this study provided us with an unusual opportunity to observe the interaction of pyroclastic currents with winter snowpack. We summarize below our chief conclusions drawn from our data, and the methodologies that generated it.

1. Each of the three phases of the 2006 eruption had a distinctive style of volcanism and distinctive flowage deposits. The explosive phase comprised short vulcanian explosions that punctuated dome growth and produced pyroclastic currents on all flanks of the volcano. Initial pyroclastic currents spread widely across winter snowpack and generated slurries that coalesced to form mixed avalanches and lahars, whereas the final pyroclastic currents of the explosive phase involved explosive disruption and decompression of a lava dome. Continuous-phase activity consisted of rapid lava-dome growth and frequent dome-collapse pyroclastic flows restricted to the north sector of the volcano, followed by an andesite lava flow. After a 3-week pause, activity resumed with the extrusion of lava and a dome, accompanied by periodic block-and-ash flows, during the final, effusive phase of the eruption.
2. The three eruptive phases were unique—not just in terms of style of volcanism, including its associated seismicity, geodetic response, and ash emissions—but also in terms of the types and morphologies of deposits that were produced, and, in particular, of their basic lithologic components—low-, intermediate-, and high-silica andesite. Overall, during the three phases, lithologic compositions trended from low-silica andesite to high-silica andesite and back to low-silica andesite. However, each rock type is present in the deposits of each eruptive phase and each flow type.
3. The chief factors that influenced pyroclastic-current behavior and the morphology of their deposits were genesis, grain size, and the characteristics of the surfaces over which they flowed. Column collapse from short-lived vulcanian blasts, dome collapse, and the collapse of viscous lavas on steep slopes caused the pyroclastic flows documented in this study. Column-collapse flows during the explosive phase spread widely where they overran snowpack. Subsequent, similar flows were confined to drainages because previous pyroclastic currents had melted the snowpack, or coated it with ash or debris sufficient to insulate the later flows from the underlying snow. In contrast, later dome-collapse flows involved neither column collapse nor the influence of underlying snow. Because it was voluminous, the dome failure that generated the Rocky Point pyroclastic flow may have been sufficiently deep seated that unloading of incompletely degassed lava caused explosive decompression which initiated an energetic flow. High proportions of juvenile high-silica andesite within the deposits suggest that the Rocky Point explosion opened the conduit to the magma chamber and made way for continuous output of magma during the next phase. The subsequent, continuous-phase flows behaved as partially fluidized granular flows. Effusive-phase block-and-ash flows were caused exclusively by collapses of andesite lava flows.
4. Pyroclastic flows can erode and incorporate substrates formed of snow or ice through a combination of mechanical and thermal processes at the bed. Conversion of snow to vapor by hot pyroclast material fluidized such flows and thus enhanced their spread across snowpack and the resulting production of mixed avalanches and lahars. Walder's hypothesis (2000a,b) that thermal scour can effectively incorporate snow into a pyroclastic current, given proper pressure, temperature, and grain-size conditions at the pyroclastic layer's interface with substrate snow, is consistent with field observations during this study. Grain-size characteristics of initial pyroclastic flows, and estimates of overburden pressure at their base, are conditions that are favorable to thermal scour of snow and coeval fluidization. These flows scoured substrate snow and generated secondary slurry flows, whereas subsequent flows did not.
5. Initial pyroclastic flows of the explosive phase invariably generated lahars and mixed avalanches, but some of these secondary flows were wetter and more laharic than others. Where secondary flows were quite watery, mixed-avalanche

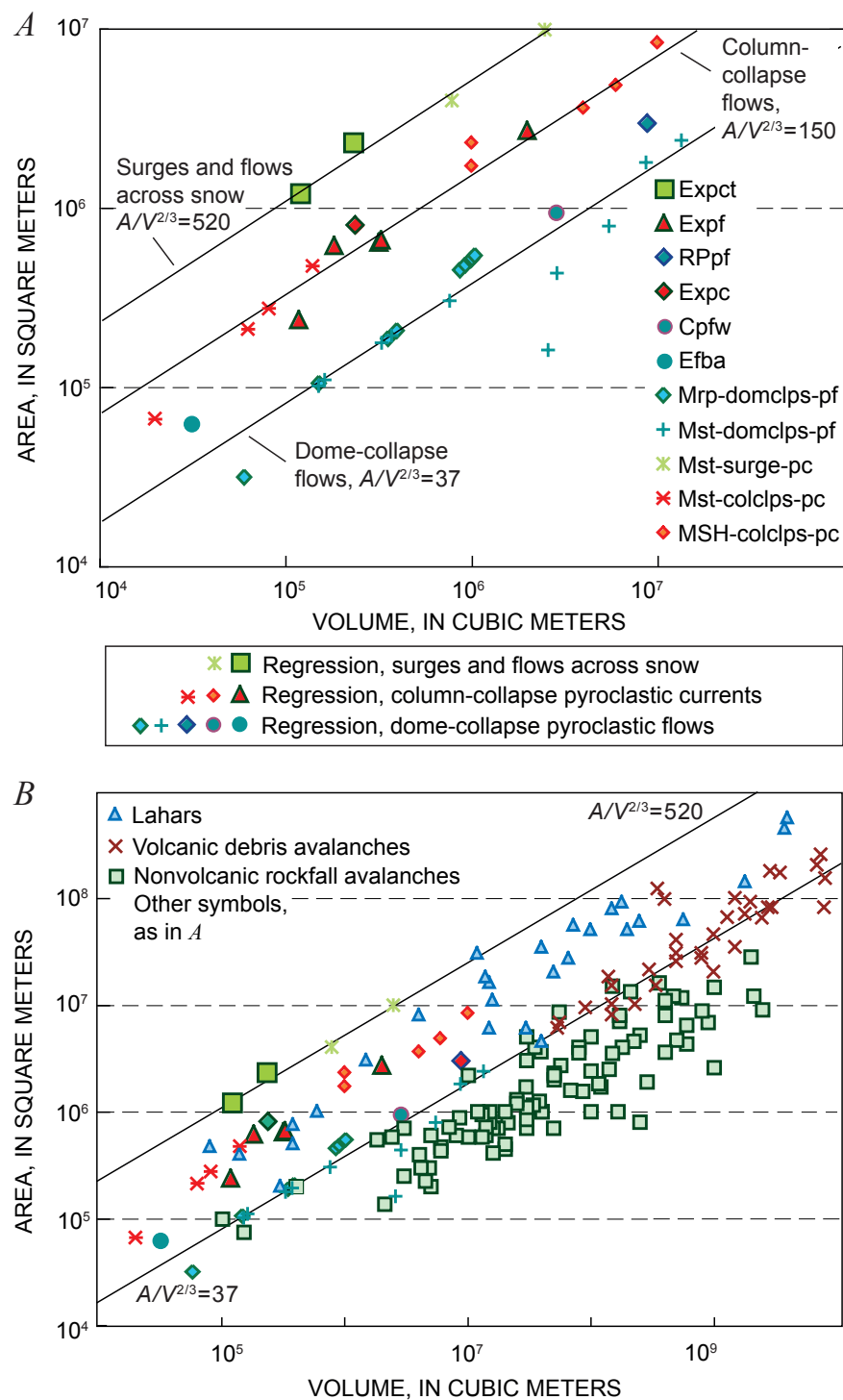


Figure 26. Plots of planimetric area versus volume for pyroclastic-current deposits of the 2006 eruption of Augustine Volcano relative to other pyroclastic currents, lahars, and debris avalanches. *A*, Augustine pyroclastic currents plotted with data of Charbonnier and Gertisser (2008) for Merapi pyroclastic currents (Mrp), of Calder and others (1999) for Montserrat currents (Mst), and of Rowley and others (1981) for Mount St. Helens currents (MSH). *B*, Area versus volume for worldwide occurrences of lahars (Iverson and others, 1998) and nonvolcanic debris flows and rock avalanches (Griswold and Iverson, 2007). Best fits to data of specified two-thirds-slope models are plotted in figure 26A for 21 dome-collapse flows, 14 column-collapse flows, and 4 surgelike flows. Same abbreviations for Augustine units as in figure 2; domclps-pf, dome-collapse pyroclastic flows; colclps-pc, column-collapse pyroclastic currents; and surge-pc, surgelike flows. Parameters and analysis of variance statistics for these models and for best-fit regression-line models are listed in table 8.

deposits were small or insignificant. Mixed-avalanche deposits that contained substantial snow blanketed medial reaches of valleys and had associated extensive marginal terraces and axial islands in distal reaches. Flows that incorporated significant amounts of snow formed cogenetic mixed avalanches that slid across surfaces protected by snowpack and water-rich axial lahars that scoured channels.

6. Plots of planimetric area (A) versus volume (V) for pyroclastic currents with similar origins and characteristics exhibit linear trends, such that $A = cV^{2/3}$ where c is a constant for similar types of flow. This relation was tested and calibrated for dome-collapse, column-collapse, and surgelike flows, using inundation-volume data from Montserrat (Calder and others, 1999), Mount St. Helens in 1980 (Rowley and others, 1981) and Augustine in 2006. The ratio $A/V^{2/3} = c$ gives a dimensionless measure of mobility, calibrated here for each of the three types of pyroclastic current. Energetic flows like surges are highly mobile and have an apparent dimensionless mobility factor of $c \approx 520$; column-collapse flows have a moderate mobility factor of $c \approx 150$; and dome-collapse flows have an approximate mobility factor of $c \approx 35$, suggesting that these flows are not much more mobile than rock avalanches. Such calibrated mobility factors have a potential use in volcanic hazard assessments.

Acknowledgments

The entire staff of Alaska Volcano Observatory generously shared observations, ideas, and data that greatly helped us improve and refine this study. Numerous people set up and maintained the field camp during summer of 2006, without which this study would have been difficult or impossible. We especially thank Game McGimsey, Tina Neal, Evan Thoms, Cheryl Cameron, and Dan Jones for logistical field support. Our helicopter pilot, Rick Farrish transported us safely around the island, often in difficult conditions. Tim Druitt and Kristi Wallace provided careful reviews that helped us improve many defects in the manuscript.

References Cited

- Bailey, J.E., Dean, K.G., Dehn, J., and Webley, P.W., 2010, Integrated satellite observations of the 2006 eruption of Augustine Volcano, *in* Power, J.A., Coombs, M.L., and Freymueller, J.T., eds., *The 2006 eruption of Augustine Volcano, Alaska*: U.S. Geological Survey Professional Paper 1769 (this volume).
- Begét, J.E., and Kienle, J., 1992, Cyclic formation of debris avalanches at Mount St. Augustine volcano: *Nature*, v. 356, no. 6371, p. 701–704.
- Begét, J.E., and Kowalik, Z., 2006, Confirmation and calibration of computer modeling of tsunamis produced by Augustine Volcano, Alaska: *Science of Tsunami Hazards*, v. 24, no. 4, p. 257–267.
- Calder, E. S., Cole, P.D., Dade, W.B., Druitt, T.H., Hoblitt, R.P., Huppert, H.E., Ritchie, L., Sparks, R.S.J., and Young, S.R., 1999, Mobility of pyroclastic flows and surges at the Soufrière Hills Volcano, Montserrat: *Geophysical Research Letters*, v. 26, p. 537–540.
- Cervelli, P.F., Fournier, T., Freymueller, J.T., and Power, J.A., 2006, Ground deformation associated with the precursory unrest and early phases of the January 2006 eruption of Augustine Volcano, Alaska: *Geophysical Research Letters*, v. 33, no. L18304, doi:10.1029/2006GL027219, p. 1–5.
- Cervelli, P.F., Fournier, T.J., Freymueller, J.T., Power, J.A., Lisowski, M., and Pauk, B.A., 2010, Geodetic constraints on magma movement and withdrawal during the 2006 eruption of Augustine Volcano, Alaska, *in* Power, J.A., Coombs, M.L., and Freymueller, J.T., eds., *The 2006 eruption of Augustine Volcano, Alaska*: U.S. Geological Survey Professional Paper 1769 (this volume).
- Charbonnier, S.J., and Gertisser, R., 2008, Field observations and surface characteristics of pristine block-and-ash flow deposits from the 2006 eruption of Merapi Volcano, Java, Indonesia: *Journal of Volcanology and Geothermal Research*, v. 177, p. 971–982.
- Coats, R.R., 1950, Volcanic activity in the Aleutian Arc: *U.S. Geological Survey Bulletin* 974-B, p. 35–49.
- Cole, P.D., Calder, E.S., Sparks, R.J.S., Clarke, A.B., Druitt, T.H., Young, S.R., Herd, R.A., Harford, C.L., and Norton, G.E., 2002, Deposits from dome-collapse and fountain-collapse pyroclastic flows at Soufrière Hills Volcano, Montserrat, *in* Druitt, T.H., and Kokelaar, B.P., eds., *The eruption of Soufrière Hills Volcano, Montserrat, from 1995 to 1999*: *London Geological Society Memoirs*, p. 231–262.
- Coombs, M.L., Bull, K.F., Vallance, J.W., Schneider, D.J., Thoms, E.E., Wessels, R.L., and McGimsey, R.G., 2010, Timing, distribution, and volume of proximal products of the 2006 eruption of Augustine Volcano, Alaska, *in* Power, J.A., Coombs, M.L., and Freymueller, J.T., eds., *The 2006 eruption of Augustine Volcano, Alaska*: U.S. Geological Survey Professional Paper 1769 (this volume).
- Dade, W.B., and Huppert, H.E., 1998, Long runout rockfalls: *Geology*, v. 26, p. 803–806.
- Daley, E.E., 1986, Petrology, geochemistry, and the evolution of lavas at Augustine Volcano, Alaska: Fairbanks, University of Alaska, 106 p.
- Dettermen, R.L., and Reed, B.L., 1980, Stratigraphy, structure, and economic geology of the Iliamna Quadrangle, Alaska: *U.S. Geological Survey Bulletin* 1368-B, 86 p.

- Druitt, T.H., Calder, E.S., Cole, P.D., Hoblitt, R.P., Loughlin, S.C., Norton, G.E., Ritchie, L.J., Sparks, R.J.S., and Voight, B., 2002a, Small-volume, highly mobile pyroclastic flows formed by rapid sedimentation from pyroclastic surges at Soufrière Hills Volcano, Montserrat; an important hazard, *in* Druitt, T.H., and Kokelaar, B.P., eds., *The eruption of Soufrière Hills Volcano, Montserrat, from 1995 to 1999*: London Geological Society Memoirs, p. 263–279.
- Druitt, T.H., Young, S.R., Baptie, B., Bonadonna, C., Calder, E.S., Clarke, A.B., Cole, P.D., Harford, C.L., Herd, R.A., Luckett, R., Ryan, G., and Voight, B., 2002b, Episodes of cyclic Vulcanian explosive activity with fountain collapse at Soufrière Hills Volcano, Montserrat, *in* Druitt, T.H., and Kokelaar, B.P., eds., *The eruption of Soufrière Hills Volcano, Montserrat, from 1995 to 1999*: London Geological Society Memoirs, p. 281–306.
- Gardner, C.A., Neal, C.A., Waitt, R.B., and Janda, R.J., 1994, Proximal pyroclastic flow deposits from the 1989–1990 eruption of Redoubt Volcano, Alaska—stratigraphy, distribution, and physical characteristics: *Journal of Volcanology and Geothermal Research*, v. 62, p. 213–250.
- Griswold, J.P., and Iverson, R.M., 2007, Mobility statistics and automated hazard mapping for debris flows and rock avalanches: U.S. Geological Survey Scientific Investigations Report 2007–5276, 49 p.
- Harris, G.W., Swanson, S.E., and Nye, C.J., 1987, Comparative petrology and petrography of the 1976 and 1986 ejecta of Augustine Volcano [abs.]: *Geological Society of America Abstracts with Programs*, v. 19, p. 387.
- Hayashi, J.N., and Self, S., 1992, A comparison of pyroclastic flow and debris avalanche mobility: *Journal of Geophysical Research*, v. 97, p. 9063–9071.
- Iverson, R.M., 1997, The physics of debris flows: *Reviews in geophysics*, v. 35, p. 245–296.
- Iverson, R.M., Schilling, S.P., and Vallance, J.W., 1998, Objective delineation of lahar-inundation hazard zones: *Geological Society of America Bulletin*, v. 110, p. 972–984.
- Jacobs, K.M., and McNutt, S.R., 2010, Using seismic *b*-values to interpret seismicity rates and physical processes during the preeruptive earthquake swarm at Augustine Volcano 2005–2006, *in* Power, J.A., Coombs, M.L., and Freymueller, J.T., eds., *The 2006 eruption of Augustine Volcano, Alaska*: U.S. Geological Survey Professional Paper 1769 (this volume).
- Johnston, D.A., 1978, Volatiles, magma mixing and the mechanism of eruption of Augustine Volcano, Alaska: Seattle, University of Washington, Ph.D. thesis, 204 p.
- Kienle, J., and Forbes, R.B., 1977, Augustine—evolution of a volcano: Fairbanks, University of Alaska, Geophysical Institute Annual Report 1975–76, p. 26–48.
- Kienle, J., and Swanson, S.E., 1985, Volcanic hazards from future eruptions of Augustine Volcano, Alaska: Geophysical Institute, University of Alaska Fairbanks, Rep. UAG R-275, 2nd ed., 122 p.
- Larsen, J.F., Nye, C.J., Coombs, M.L., Tilman, M., Izbekov, P., and Cameron, C., 2010, Petrology and geochemistry of the 2006 eruption of Augustine Volcano, Alaska, *in* Power, J.A., Coombs, M.L., and Freymueller, J.T., eds., *The 2006 eruption of Augustine Volcano, Alaska*: U.S. Geological Survey Professional Paper 1769 (this volume).
- Loughlin, S.C., Calder, E.S., Clarke, A.B., Cole, P.D., Luckett, R., Mangan, M.T., Pyle, D.M., Sparks, R.J.S., Voight, B., and Watts, R.B., 2002, Pyroclastic flows and surges generated by the 25 June 1997 dome collapse, Soufrière Hills Volcano, Montserrat, *in* Druitt, T.H., and Kokelaar, B.P., eds., *The eruption of Soufrière Hills Volcano, Montserrat, from 1995 to 1999*: London Geological Society Memoirs, p. 191–210.
- Lube, G., Cronin, S.J., Platz, T., Freundt, A., Proctor, J., Henderson, C., and Sheridan, M.F., 2007, Flow and deposition of pyroclastic granular flows; a type example from the 1975 Ngauruhoe eruption, New Zealand: *Journal of Volcanology and Geothermal Research*, v. 161, p. 165–186.
- McNutt, S.R., Tytgat, G., Estes, S.A., and Stihler, S.D., 2010, A parametric study of the January 2006 explosive eruptions of Augustine Volcano, Alaska, *in* Power, J.A., Coombs, M.L., and Freymueller, J.T., eds., *The 2006 eruption of Augustine Volcano, Alaska*: U.S. Geological Survey Professional Paper 1769 (this volume).
- Miller, T.P., McGimsey, R.G., Richter, D.H., Riehle, J.R., Nye, C.J., Yount, M.E., and Dumoulin, J.A., 1998, Catalog of the historically active volcanoes of Alaska: U.S. Geological Survey Open-File Report 98-0582, 104 p.
- Pierson, T.C., 1994, Volcanic mixed avalanches; a distinct eruption-triggered mass-flow process at snow-clad volcanoes: *Geological Society of America Bulletin*, v. 106, p. 1351–1358.
- Pouliquen, O., Delour, J., and Savage, S.B., 1997, Fingering in granular flows: *Nature*, v. 386, p. 816–817.
- Pouliquen, O., and Vallance, J.W., 1999, Segregation induced instabilities of granular fronts: *Chaos*, v. 9, p. 621–630.
- Power, J.A., and Lalla, D.J., 2010, Seismic observations of Augustine Volcano, 1970–2007, *in* Power, J.A., Coombs, M.L., and Freymueller, J.T., eds., *The 2006 eruption of Augustine Volcano, Alaska*: U.S. Geological Survey Professional Paper 1769 (this volume).
- Power, J.A., Nye, C.J., Coombs, M.L., Wessels, R.L., Cervelli, P.F., Dehn, J., Wallace, K.L., Freymueller, J.T., and Doukas, M.P., 2006, The reawakening of Alaska's Augustine

- Volcano: Eos (American Geophysical Union Transactions), v. 87, no. 37, p. 373, 377.
- Rowley, P.D., Kuntz, M.A., and McCleod, N.S., 1981, Pyroclastic-flow deposits, *in* Lipman, P.W., and Mullineaux, D.R., eds. The 1980 eruptions of Mount St. Helens: U.S. Geological Survey Professional Paper 1250, p. 489–512.
- Schneider, D.J., Scott, C., Wood, J. and Hall, T., 2006, NEXRAD weather radar observation of the 2006 Augustine volcanic eruption clouds [abs.]: Eos (American Geophysical Union Transactions), v. 87, abstract V51C-1686.
- Scott, K.M., 1988, Origins, behavior, and sedimentology of lahars and lahar-runout flows in the Toutle-Cowlitz River system: U.S. Geological Survey Professional Paper 1447-A, 78 p.
- Siebert, L., Begét, J.E., and Glicken, H., 1995, The eruptive history of Augustine Volcano, Alaska: Journal of Volcanology and Geothermal Research, v. 66, no. 1, p. 367–395.
- Sparks, R.S.J., 1976, Grain-size variations in ignimbrites and implications for the transport of pyroclastic flows: Sedimentology, v. 23, p. 147–188.
- Swanson, S.E., and Kienle, J., 1988, The 1986 eruption of Mount St. Augustine; field test of a hazard evaluation: Journal of Geophysical Research, v. 93, no. 85, p. 4500–4520.
- Thomas, R.J., McNutt, S.R., Krehbiel, P.R., Rison, W., Aulich, G., Edens, H.E., Tytgat, G, and Clark, E., 2010, Lightning and electrical activity during the 2006 eruption of Augustine Volcano, *in* Power, J.A., Coombs, M.L., and Freymueller, J.T., eds., The 2006 eruption of Augustine Volcano, Alaska: U.S. Geological Survey Professional Paper 1769 (this volume).
- Vallance, J.W., 1994, Experimental and field studies related to the behavior of granular mass flows and the characteristic of their deposits: Houghton, Michigan Technological University, Ph.D.dissertation, 197 p.
- Vallance, J.W., 2000, Lahars, *in* Sigurdsson, H., Houghton, B.F., McNutt, S.R., Rymer, H., and Stix, J., eds., Encyclopedia of volcanoes: San Diego, Calif., Academic Press, p. 601–616.
- Vallance, J.W., and Savage, S.B., 2000, Particle segregation in granular flows down chutes, *in* Rosato, A.D., and Blackmore, D.L., eds. Segregation in granular flows: Dordrecht, Kluwer, p. 31–51.
- Waitt, R.B., 1995, Hybrid wet flows formed by hot pyroclasts interacting with snow during the 1992 eruption of Crater Peak, Mount Spurr Volcano, Alaska, *in* Kieth, T.E.C., ed., U.S. Geological Survey Bulletin 2139, p. 107–118.
- Waitt, R.B., 2010, Ejecta and landslides from Augustine Volcano before 2006, *in* Power, J.A., Coombs, M.L., and Freymueller, J.T., eds., The 2006 eruption of Augustine Volcano, Alaska: U.S. Geological Survey Professional Paper 1769 (this volume).
- Waitt, R.B., and Begét, J.E., 1996, Provisional geologic map of Augustine Volcano, Alaska: U.S. Geological Survey Open-File Report 96-0516, 44 p.
- Waitt, R.B., and Begét, J.E., 2009, Volcanic processes and geology of Mount Augustine, Alaska: U.S. Geological Survey Professional Paper 1762, 78 p.
- Waitt, R.B., Gardner, C.A., Pierson, T.C., Major, J.J., and Neal, C. A., 1994, Unusual ice diamicts emplaced during the December 15, 1989 eruption of Redoubt Volcano, Alaska: Journal of Volcanology and Geothermal Research, v. 62, p. 409–428.
- Walder, J.S., 2000a, Pyroclast/snow interactions and thermally driven slurry formation; part 1, theory for monodisperse grain beds: Bulletin of Volcanology, v. 62, p. 105–118.
- Walder, J.S., 2000b, Pyroclast/snow interactions and thermally driven slurry formation; part 2, experiments and theoretical extension to polydisperse tephra: Bulletin of Volcanology, v. 62, p. 119–129.
- Wallace, K., Neal, C.A., and McGimsey, R.G., 2010, Timing, distribution and character of tephra fall from the 2005-2006 eruption of Augustine Volcano, Alaska, *in* Power, J.A., Coombs, M.L., and Freymueller, J.T., eds., The 2006 eruption of Augustine Volcano, Alaska: U.S. Geological Survey Professional Paper 1769 (this volume).
- Widiwijayanti, C., Voight, B., Hidayat, D., and Schilling, S.P., 2009, Objective delineation of areas at risk from block-and-ash pyroclastic flows and surges: Bulletin of Volcanology, v. 71, p. 687–703, doi:10.1007/s00445-008-0254-6.

260 The 2006 Eruption of Augustine Volcano, Alaska

Table 2. Samples taken and analyses performed for pyroclastic-flow, lahar, and mixed-avalanche deposits of the 2006 eruption of Augustine Volcano, Alaska.

[Samples are sorted by event and sector]

| Sample Number | Latitude (decimal degrees) | Longitude (decimal degrees) | Sector 1=ESE- 2=NE- WNW 3=SSE- SW | Unit | Phase | Emplacement Date | Event | Sample Type | Grain size | Sedi-graph | Com po nen try |
|---------------|----------------------------|-----------------------------|--|-------------------|-----------|------------------|----------|-----------------------------------|------------|------------|----------------|
| V021A | 59.366 | -153.410 | 1 | Expct | Explosive | 1/13/06 | 3-4 | Bulk | X | | |
| V033A | 59.368 | -153.394 | 1 | Expct | Explosive | 1/13/06 | 3-4 | Bulk | X | | X |
| V096 | 59.371 | -153.407 | 1 | Expct | Explosive | 1/14/06 | 3-4, 6-7 | Bulk | X | X | X |
| V281A | 59.363 | -153.404 | 1 | Expct | Explosive | 1/13/06 | 3-4 | Bulk | X | | |
| V281B | 59.363 | -153.404 | 1 | Expct | Explosive | 1/13/06 | 3-4 | Bulk | X | | |
| V283A | 59.363 | -153.402 | 1 | Expct basal | Explosive | 1/13/06 | 3-4 | Bulk | X | | |
| V283B | 59.363 | -153.402 | 1 | Expct basal | Explosive | 1/13/06 | 3-4 | Bulk | X | | |
| V283C | 59.363 | -153.402 | 1 | Expct basal | Explosive | 1/13/06 | 3-4 | Bulk | X | | |
| V283D | 59.363 | -153.402 | 1 | Expct top | Explosive | 1/13/06 | 3-4 | Bulk | X | | |
| V283E | 59.363 | -153.402 | 1 | Expct top | Explosive | 1/13/06 | 3-4 | Bulk | X | | |
| V330 | 59.367 | -153.382 | 1 | Exlh | Explosive | 1/13/06 | 3-4 | Bulk | X | | |
| B096A | 59.366 | -153.410 | 1 | Expct | Explosive | 1/13/06 | 3-4 | Bulk | | | |
| B096B | 59.366 | -153.410 | 1 | Expct | Explosive | 1/13/06 | 3-4 | Hand-picked juvenile clasts | | | |
| B106 | 59.365 | -153.409 | 1 | Expf | Explosive | 1/13/06 | 3-4 | Bulk | X | | X |
| B184A | 59.363 | -153.403 | 1 | Expct | Explosive | 1/13/06 | 3-4 | Bulk | X | X | X |
| B184B | 59.363 | -153.403 | 1 | Expct | Explosive | 1/13/06 | 3-4 | Bulk | X | X | X |
| B184C | 59.363 | -153.403 | 1 | Expct | Explosive | 1/13/06 | 3-4 | Bulk | X | | |
| B102 | 59.346 | -153.429 | 1 | Expf | Explosive | 1/13-14/06 | 3-7 | Bulk | X | | X |
| C120 | 59.351 | -153.406 | 3 | Expct | Explosive | 1/13-14/06 | 3-8 | Bulk | X | | |
| V117 | 59.369 | -153.447 | 2 | Expf | Explosive | 1/13/06 | 5 | Bulk | X | | |
| B176 | 59.404 | -153.449 | 2 | Expf | Explosive | 1/13-14/06 | 5 | Bulk | X | X | |
| V270A | 59.384 | -153.399 | 2 | Exma | Explosive | 1/13-14/06? | 7? | Bulk | X | | |
| V270B | 59.384 | -153.399 | 2 | Exlh | Explosive | 1/13-14/06 | 7 | Bulk | X | | |
| V272 | 59.386 | -153.397 | 2 | Exlh | Explosive | 1/13-14/06 | 7 | Bulk | X | | |
| V275A | 59.387 | -153.391 | 2 | Exlh | Explosive | 1/13-14/06 | 7 | Bulk | X | | X |
| V275B | 59.387 | -153.391 | 2 | Exlh | Explosive | 1/13-14/06 | 7 | Bulk | X | | X |
| V275C | 59.387 | -153.391 | 2 | Exlh | Explosive | 1/13-14/06 | 7 | Bulk | X | | |
| V237 | 59.388 | -153.385 | 2 | Exlh | Explosive | 1/14/06 | 7 | Bulk | X | | |
| V258 | 59.366 | -153.398 | 3 | Exma | Explosive | 1/13-14/06 | 7 | Bulk | X | | |
| V199 | 59.336 | -153.410 | 3 | Exma | Explosive | 1/14/06 | 8 | Bulk | X | | |
| V256A | 59.344 | -153.418 | 3 | Expf-top | Explosive | 1/14/06 | 8 | Bulk | X | X | |
| V256B | 59.344 | -153.418 | 3 | Expf-mid | Explosive | 1/14/06 | 8 | Bulk | X | X | |
| V256C | 59.344 | -153.418 | 3 | Expf-base | Explosive | 1/14/06 | 8 | Bulk | X | | |
| V256D | 59.344 | -153.418 | 3 | Expf-base | Explosive | 1/14/06 | 8 | Bulk | X | X | |
| V256E | 59.344 | -153.418 | 3 | Expf | Explosive | 1/14/06 | 8 | Bulk | X | | |
| V257 | 59.344 | -153.416 | 3 | Exma | Explosive | 1/14/06 | 8 | Bulk | X | | |
| V264 | 59.345 | -153.420 | 3 | Expf- reworked | Explosive | 1/13-14/06 | 8 | Bulk | | | |

Table 2. Samples taken and analyses performed for pyroclastic-flow, lahar, and mixed-avalanche deposits of the 2006 eruption of Augustine Volcano, Alaska.—Continued

[Samples are sorted by event and sector]

| Sample Number | Latitude (decimal degrees) | Longitude (decimal degrees) | Sector 1=ESE- ENE 2=NE- WNW 3=SSE- SW | Unit | Phase | Emplacement Date | Event | Sample Type | Grain size | Sedi-graph | Compo- nen- try |
|---------------|----------------------------|-----------------------------|---|-----------|------------|------------------|-------|-----------------------------------|------------|------------|-----------------------|
| V276A | 59.333 | -153.399 | 3 | Exlh-base | Explosive | 1/13-14/06 | 8 | Bulk | X | X | X |
| V276B | 59.333 | -153.399 | 3 | Exlh-top | Explosive | 1/13-14/06 | 8 | Bulk | X | X | |
| V278 | 59.333 | -153.400 | 3 | Exma | Explosive | 1/13-14/06 | 8 | Bulk | X | X | X |
| V280 | 59.333 | -153.400 | 3 | Exlh | Explosive | 1/13-14/06 | 8 | Bulk | X | | |
| B230 | 59.343 | -153.455 | 3 | Expf | Explosive | 1/13-14/06 | 8 | Bulk | X | | X |
| C025A | 59.329 | -153.468 | 3 | Exlh | Explosive | 1/13-14/06 | 8 | Bulk | | | |
| B129 | 59.360 | -153.436 | 3 | Expf | Explosive | 1/17/09 | 9 | Bulk | | | |
| V254 | 59.350 | -153.487 | 3 | Expf | Explosive | 1/17/06 | 9 | Bulk | X | | |
| V019 | 59.352 | -153.477 | 2 | Expf | Explosive | 1/17/06 | 9 | Bulk | X | | X |
| V297 | 59.386 | -153.442 | 2 | Expc | Explosive | 1/27/06 | 10 | Bulk | X | | |
| V311 | 59.376 | -153.439 | 2 | Expc | Explosive | 1/27/06 | 10 | Bulk | | | |
| V312A | 59.376 | -153.440 | 2 | Expc | Explosive | 1/27/06 | 10 | Bulk | X | | |
| V312B | 59.376 | -153.440 | 2 | Expc | Explosive | 1/27/06 | 10 | Bulk | X | | |
| V312C | 59.376 | -153.440 | 2 | Expc | Explosive | 1/27/06 | 10 | Bulk | | | |
| V312D | 59.376 | -153.440 | 2 | Expc | Explosive | 1/27/06 | 10 | Bulk | X | | |
| V313 | 59.377 | -153.439 | 2 | Expc | Explosive | 1/27/06 | 10 | Bulk | X | | X |
| V315 | 59.379 | -153.442 | 2 | Expc | Explosive | 1/27/06 | 10 | Bulk | X | | |
| B215A | 59.371 | -153.437 | 2 | Expc | Explosive | 1/27/06 | 10 | Bulk | X | X | X |
| B216 | 59.373 | -153.439 | 2 | Expc | Explosive | 1/27/06 | 10 | Bulk | X | | |
| B217 | 59.374 | -153.440 | 2 | Expc | Explosive | 1/27/06 | 10 | Bulk | X | | |
| C259C | 59.385 | -153.438 | 2 | Expc | Explosive | 1/27/06 | 10 | Bulk | X | X | X |
| B173 | 59.404 | -153.439 | 2 | RPpf | Explosive | 1/27/06 | 10 | Bulk | X | X | X |
| B222 | 59.390 | -153.439 | 2 | RPpf | Explosive | 1/27/06 | 10 | Bulk | X | | X |
| B223 | 59.394 | -153.434 | 2 | RPpf | Explosive | 1/27/06 | 10 | Bulk | X | | |
| B224 | 59.400 | -153.425 | 2 | RPpf | Explosive | 1/27/06 | 10 | Bulk | X | X | |
| B225 | 59.403 | -153.435 | 2 | RPpf | Explosive | 1/27/06 | 10 | Bulk | X | X | |
| C259B | 59.385 | -153.438 | 2 | RPpf | Explosive | 1/27/06 | 10 | Bulk | X | | |
| B218 | 59.377 | -153.436 | 2 | Cpf | Continuous | >1/27/2006 | >14 | Bulk | X | | |
| V224 | 59.383 | -153.395 | 2 | Cpf | Continuous | >1/28/06 | >14 | Bulk | X | | |
| LC259A | 59.385 | -153.438 | 2 | Cpf | Continuous | >1/28/06 | >14 | Bulk | X | X | |
| B143 | 59.369 | -153.446 | 2 | Cpf | Continuous | >1/28/06 | >14 | Hand-picked juvenile clasts | | | |
| B149A | 59.371 | -153.432 | 2 | Cpf | Continuous | >1/28/06 | >14 | Hand-picked juvenile clasts | | | |
| B155A | 59.376 | -153.429 | 2 | Cpf | Continuous | >1/28/06 | >14 | Bulk | | | |
| B203 | 59.384 | -153.409 | 2 | Cpf | Continuous | >1/28/06 | >14 | Bulk | X | X | X |
| V101 | 59.372 | -153.405 | 2 | Cpc | Continuous | >1/28/06 | >14 | Bulk | X | | X |
| C294 | 59.375 | -153.445 | 2 | Cpfw | Continuous | 1/30/06 | Windy | Bulk | X | | |
| V022A | 59.363 | -153.405 | 1 | Efba | Effusive | 3/3-16/06 | >14 | Bulk | X | | X |

Table 3. Grain-size distribution for samples of clastic-flow deposits of the 2006 eruption of Augustine Volcano, Alaska.

[Samples sorted by map unit¹. Data are obtained by sieve analysis and given in weight percent. Data for grain sizes <0.063 mm obtained by sedigraph. Fine-ash totals from sedigraph-measured samples are calculated from sedigraph data, not weighed. All samples analyzed at the Cascades Volcano Observatory]

| Sample Number | Unit | 31.5 mm | 16.0 mm | 8.0 mm | 4.0 mm | 2.0 mm | 1.0 mm | 0.50 mm | 0.25 mm | 0.125 mm | 0.063 mm | Fine ash (<0.063 mm) | 31 µm | 16 µm | 8 µm | 4 µm | 2 µm | 1 µm |
|---------------|-------------|---------|---------|--------|--------|--------|--------|---------|---------|----------|----------|----------------------|-------|-------|------|------|------|------|
| V021A | Expct | 0.0 | 5.4 | 10.0 | 7.1 | 4.7 | 8.8 | 11.4 | 14.6 | 15.6 | 10.2 | 12.2 | | | | | | |
| V033A | Expct | 16.4 | 9.0 | 8.0 | 7.9 | 6.0 | 9.8 | 11.3 | 12.4 | 9.4 | 4.9 | 4.9 | | | | | | |
| V096 | Expct | 4.2 | 7.4 | 4.6 | 4.2 | 4.0 | 7.5 | 11.5 | 15.1 | 15.1 | 11.8 | 14.0 | 6.3 | 4.0 | 2.1 | 1.0 | 0.4 | 0.2 |
| V281A | Expct | 0.0 | 0.0 | 2.2 | 2.6 | 6.3 | 12.4 | 18.3 | 19.1 | 19.1 | 12.9 | 6.9 | | | | | | |
| V315 | Expct | 2.5 | 10.9 | 9.5 | 9.4 | 6.8 | 10.0 | 13.9 | 15.6 | 12.2 | 6.6 | 2.5 | | | | | | |
| V283D | Expct | 16.0 | 0.6 | 2.1 | 3.9 | 4.9 | 9.6 | 14.4 | 17.4 | 14.7 | 10.0 | 6.4 | | | | | | |
| V283E | Expct | 2.8 | 11.7 | 7.1 | 6.9 | 5.6 | 8.8 | 10.8 | 13.0 | 13.3 | 9.6 | 10.3 | | | | | | |
| V283A | Expct-basal | 0.0 | 0.0 | 3.0 | 4.9 | 8.1 | 13.4 | 18.2 | 20.6 | 16.8 | 10.6 | 4.4 | | | | | | |
| V283B | Expct-basal | 0.0 | 4.9 | 8.0 | 8.0 | 7.5 | 10.3 | 14.9 | 18.4 | 14.9 | 8.7 | 4.3 | | | | | | |
| V283C | Expct-basal | 18.5 | 7.6 | 7.2 | 7.2 | 6.1 | 10.4 | 12.1 | 13.1 | 10.0 | 4.8 | 3.0 | | | | | | |
| B184A | Expct | 0.0 | 1.9 | 3.4 | 6.7 | 7.2 | 13.6 | 18.0 | 21.6 | 16.3 | 8.1 | 3.2 | 1.9 | 0.6 | 0.3 | 0.2 | 0.1 | 0.0 |
| B184B | Expct | 1.9 | 2.7 | 3.0 | 5.1 | 6.0 | 9.9 | 15.1 | 19.5 | 18.1 | 11.0 | 7.7 | 3.9 | 1.7 | 1.0 | 0.7 | 0.3 | 0.2 |
| B184C | Expct | 0.0 | 0.0 | 0.3 | 1.0 | 3.2 | 10.5 | 19.1 | 26.1 | 24.1 | 11.9 | 4.0 | | | | | | |
| C120 | Expct | 0.0 | 3.9 | 21.6 | 16.5 | 7.7 | 8.3 | 11.6 | 12.8 | 9.1 | 5.0 | 3.6 | | | | | | |
| V117 | Expf | 7.7 | 14.0 | 8.4 | 8.0 | 8.3 | 11.0 | 13.9 | 14.5 | 9.1 | 3.7 | 1.3 | | | | | | |
| B102 | Expf | 3.8 | 9.1 | 10.3 | 9.1 | 8.7 | 10.6 | 13.2 | 14.6 | 10.2 | 5.5 | 4.8 | | | | | | |
| B176 | Expf | 0.0 | 1.3 | 3.5 | 5.5 | 7.5 | 10.8 | 15.6 | 19.7 | 18.7 | 10.9 | 6.3 | 2.6 | 1.5 | 1.1 | 0.7 | 0.3 | 0.1 |
| V256A | Expf-top | 23.8 | 8.5 | 4.6 | 4.1 | 3.8 | 7.0 | 9.0 | 10.7 | 8.1 | 5.7 | 6.2 | 2.4 | 1.8 | 1.1 | 0.6 | 0.2 | 0.1 |
| V256B | Expf-middle | 17.0 | 7.8 | 7.8 | 7.2 | 5.0 | 6.7 | 7.6 | 7.9 | 6.0 | 3.7 | 5.5 | 2.0 | 1.6 | 1.0 | 0.5 | 0.2 | 0.1 |
| V256C | Expf-base | 0.0 | 7.5 | 7.4 | 7.7 | 6.2 | 11.5 | 14.1 | 15.8 | 13.1 | 7.6 | 9.0 | | | | | | |
| V256D | Expf-base | 0.0 | 0.0 | 1.9 | 2.1 | 3.9 | 9.3 | 18.6 | 23.5 | 19.0 | 10.8 | 10.3 | 3.8 | 2.8 | 2.0 | 1.1 | 0.5 | 0.2 |
| V256E | Expf | 0.0 | 2.3 | 1.8 | 1.3 | 1.8 | 6.6 | 12.2 | 18.4 | 20.4 | 15.3 | 19.9 | | | | | | |
| V019 | Expf | 2.5 | 3.6 | 4.0 | 6.3 | 9.5 | 13.7 | 15.6 | 14.4 | 12.3 | 8.0 | 10.1 | | | | | | |
| B230 | Expf | 13.9 | 5.1 | 5.8 | 7.2 | 5.9 | 12.6 | 13.9 | 15.4 | 12.1 | 5.5 | 2.6 | | | | | | |
| V237 | Exlh | 3.1 | 5.6 | 9.2 | 11.8 | 11.8 | 14.8 | 15.3 | 13.0 | 8.0 | 3.7 | 3.7 | | | | | | |
| V270B | Exlh | 0.0 | 7.8 | 12.2 | 10.8 | 8.2 | 11.0 | 12.0 | 12.0 | 9.5 | 6.5 | 10.0 | | | | | | |
| V275B | Exlh | 2.1 | 2.2 | 6.3 | 8.3 | 10.5 | 17.1 | 18.2 | 15.8 | 9.4 | 5.1 | 5.0 | | | | | | |
| V275C | Exlh | 0.0 | 2.8 | 5.8 | 8.1 | 7.7 | 13.6 | 21.0 | 20.4 | 11.7 | 4.8 | 4.1 | | | | | | |
| V280 | Exlh | 0.0 | 16.8 | 22.0 | 11.2 | 6.3 | 7.6 | 8.6 | 9.5 | 7.0 | 5.1 | 5.8 | | | | | | |
| V330 | Exlh | 0.0 | 4.0 | 8.4 | 9.1 | 8.6 | 11.9 | 12.8 | 14.9 | 14.3 | 9.4 | 6.5 | | | | | | |

| | | | | | | | | | | | | | | | | | | |
|-------|----------|------|------|------|------|------|------|------|------|------|------|------|-----|-----|-----|-----|-----|-----|
| V276A | Exlh-hcf | 5.9 | 15.3 | 17.5 | 13.9 | 8.9 | 8.7 | 8.8 | 7.9 | 5.2 | 2.9 | 4.8 | 1.6 | 1.4 | 1.0 | 0.5 | 0.2 | 0.1 |
| V276B | Exlh-hcf | 0.0 | 0.4 | 7.3 | 15.7 | 14.8 | 17.5 | 15.2 | 12.7 | 6.9 | 3.8 | 5.3 | 1.8 | 1.7 | 1.0 | 0.5 | 0.2 | 0.1 |
| V272 | Exlh-hcf | 0.0 | 3.6 | 4.4 | 5.0 | 5.7 | 12.8 | 16.5 | 17.0 | 15.1 | 10.7 | 9.2 | | | | | | |
| V275A | Exlh-hcf | 0.0 | 3.2 | 16.8 | 17.7 | 13.8 | 12.9 | 12.0 | 10.2 | 6.4 | 3.4 | 3.6 | | | | | | |
| V199 | Exma | 0.0 | 84.1 | 11.9 | 0.2 | 0.2 | 0.4 | 0.6 | 0.6 | 0.6 | 0.6 | 0.8 | | | | | | |
| V257 | Exma | 0.0 | 8.2 | 11.1 | 8.8 | 7.2 | 10.3 | 14.2 | 13.3 | 9.0 | 6.2 | 11.7 | | | | | | |
| 0V258 | Exma | 5.6 | 5.3 | 6.2 | 7.2 | 3.0 | 48.7 | 6.0 | 6.1 | 4.1 | 3.2 | 4.6 | | | | | | |
| V254 | Exma | 0.0 | 0.0 | 0.0 | 0.0 | 0.7 | 0.7 | 2.3 | 9.5 | 23.0 | 22.4 | 41.4 | | | | | | |
| V270A | Exma | 4.8 | 2.9 | 10.0 | 11.4 | 11.3 | 16.8 | 15.2 | 12.2 | 7.0 | 4.5 | 4.0 | | | | | | |
| V278 | Exma | 13.5 | 3.2 | 5.5 | 6.4 | 5.1 | 9.1 | 13.6 | 15.4 | 11.8 | 6.3 | 9.6 | 3.6 | 2.8 | 1.7 | 0.9 | 0.3 | 0.3 |
| V297 | Expc | 3.9 | 9.5 | 12.6 | 8.3 | 7.7 | 10.1 | 14.3 | 15.8 | 12.0 | 4.9 | 1.0 | | | | | | |
| V312A | Expc | 0.0 | 1.0 | 6.8 | 9.8 | 8.8 | 18.2 | 20.4 | 16.1 | 10.4 | 5.0 | 3.5 | | | | | | |
| V312B | Expc | 0.0 | 0.0 | 0.0 | 9.7 | 13.9 | 20.0 | 25.8 | 19.4 | 7.7 | 2.4 | 1.1 | | | | | | |
| V312C | Expc | 0.0 | 0.0 | 16.4 | 29.0 | 11.2 | 10.7 | 8.8 | 9.1 | 7.6 | 4.3 | 2.9 | | | | | | |
| V313 | Expc | 0.0 | 0.0 | 3.0 | 7.3 | 14.9 | 19.9 | 20.6 | 16.2 | 8.6 | 4.2 | 5.4 | | | | | | |
| B215A | Expc | 10.4 | 3.2 | 7.7 | 8.4 | 10.5 | 12.6 | 10.4 | 9.4 | 8.7 | 7.9 | 10.7 | 5.3 | 3.1 | 1.3 | 0.6 | 0.3 | 0.1 |
| B216 | Expc | 2.5 | 8.3 | 5.6 | 6.7 | 8.4 | 13.2 | 17.0 | 18.5 | 13.0 | 6.1 | 0.8 | | | | | | |
| B217 | Expc | 0.0 | 20.3 | 8.8 | 11.1 | 9.5 | 12.7 | 14.2 | 12.3 | 6.8 | 2.7 | 1.7 | | | | | | |
| C259C | Expc | 0.0 | 8.6 | 13.9 | 14.1 | 8.3 | 13.0 | 13.4 | 12.2 | 7.2 | 4.2 | 5.0 | 2.3 | 1.5 | 0.7 | 0.3 | 0.1 | 0.1 |
| B173 | RPpf | 2.0 | 1.2 | 4.6 | 6.4 | 6.6 | 12.1 | 14.4 | 15.3 | 12.7 | 10.3 | 13.9 | 5.1 | 3.7 | 2.5 | 1.6 | 0.7 | 0.4 |
| B222 | RPpf | 9.8 | 10.5 | 9.6 | 7.4 | 6.9 | 10.2 | 11.7 | 12.1 | 9.5 | 5.6 | 6.7 | | | | | | |
| B223 | RPpf | 17.1 | 9.6 | 7.2 | 7.1 | 6.5 | 9.8 | 10.8 | 10.5 | 7.6 | 5.7 | 8.1 | | | | | | |
| B224 | RPpf | 0.0 | 9.7 | 8.9 | 8.2 | 4.9 | 11.4 | 13.8 | 15.6 | 11.8 | 7.9 | 7.5 | 2.6 | 2.0 | 1.4 | 0.9 | 0.4 | 0.2 |
| B225 | RPpf | 12.2 | 6.0 | 6.9 | 7.3 | 7.1 | 10.2 | 12.4 | 12.8 | 9.7 | 6.1 | 8.9 | 3.2 | 2.4 | 1.6 | 1.1 | 0.5 | 0.3 |
| C259B | RPpf | 0.0 | 0.0 | 1.9 | 5.1 | 6.1 | 8.5 | 15.0 | 21.7 | 21.3 | 14.3 | 6.1 | | | | | | |
| B218 | Cpf | 2.7 | 10.5 | 6.1 | 8.1 | 10.6 | 13.4 | 14.1 | 12.0 | 8.4 | 6.4 | 7.4 | | | | | | |
| B203 | Cpf | 13.6 | 3.5 | 6.8 | 6.3 | 6.4 | 11.4 | 13.2 | 12.6 | 9.0 | 7.0 | 9.9 | 3.4 | 2.7 | 1.9 | 1.0 | 0.6 | 0.2 |
| C259A | Cpf | 10.2 | 10.9 | 8.4 | 7.5 | 8.4 | 11.5 | 13.9 | 14.2 | 9.6 | 4.0 | 1.3 | 0.7 | 0.2 | 0.2 | 0.1 | 0.0 | 0.0 |
| V224 | Cpf | 9.7 | 1.5 | 3.8 | 5.9 | 8.3 | 11.7 | 14.4 | 14.9 | 12.3 | 9.9 | 7.8 | | | | | | |
| C294 | Cpf | 24.9 | 7.6 | 4.0 | 4.0 | 5.5 | 7.4 | 10.5 | 11.2 | 10.0 | 8.3 | 6.5 | | | | | | |
| V101 | Cpc | 6.8 | 9.4 | 5.2 | 5.4 | 5.7 | 11.2 | 13.4 | 15.2 | 12.9 | 8.5 | 6.3 | | | | | | |
| V022A | Efba | 11.7 | 13.4 | 10.0 | 10.6 | 9.7 | 14.1 | 14.0 | 9.0 | 4.6 | 1.8 | 1.2 | | | | | | |

¹ Map units defined in figure 2. Expct, Explosive-phase pyroclastic-current deposit, thin; Expf, pyroclastic-flow deposit; Expc, pyroclastic-current deposit; Exlh, lahar deposit (hcf,hyperconcentrated flow deposit); Exma, mixed-avalanche deposit; RPpf, Rocky Point pyroclastic-flow deposit; Cpf, Continuous-phase pyroclastic-flow deposit; Cpfw, pyroclastic-flow of Windy Creek; Cpc, pyroclastic-current deposit; Efba, Effusive-phase block-and-ash-flow deposit.

Table 4. Statistics of grain-size analyses for samples of pyroclastic-flow, lahar, and mixed-avalanche deposits from the 2006 eruption of Augustine Volcano, Alaska.

[All values in phi units. Statistics calculated by using software courtesy of Sebastien Darteville, Los Alamos National Laboratories. Units defined in figure 2]

| Sample | Unit | Mean | Median | Sorting | Mode | Skewness | Kurtosis |
|--------|-----------------------|-------|--------|---------|------|----------|----------|
| V021A | Expct | 0.60 | 1.19 | 3.14 | 2.5 | -0.16 | 0.96 |
| V033A | Expct | -1.14 | -0.70 | 3.27 | -5.5 | -0.11 | 0.70 |
| V096 | Expct | 0.72 | 1.42 | 3.31 | 1.5 | -0.25 | 1.08 |
| V281A | Expct | 1.38 | 1.42 | 2.15 | 2.5 | 0.05 | 1.23 |
| V315 | Expct | -0.42 | 0.07 | 2.78 | 1.5 | -0.20 | 0.75 |
| V283D | Expct | -0.36 | 0.91 | 3.76 | 1.5 | -0.30 | 1.22 |
| V283E | Expct | 0.08 | 0.68 | 3.41 | 2.5 | -0.13 | 0.85 |
| V283A | Expct-basal | 1.01 | 1.12 | 1.94 | 1.5 | -0.12 | 0.97 |
| V283B | Expct-basal | 0.31 | 0.78 | 2.52 | 1.5 | -0.24 | 0.87 |
| V283C | Expct-basal | -1.24 | -0.64 | 3.23 | -5.5 | -0.17 | 0.67 |
| B184A | Expct-basal | 0.73 | 0.96 | 2.04 | 1.5 | -0.18 | 1.03 |
| B184B | Expct-basal | 1.05 | 1.33 | 2.44 | 1.5 | -0.20 | 1.18 |
| B184C | Expct-basal | 1.56 | 1.61 | 1.43 | 1.5 | -0.06 | 0.94 |
| V117 | Expf | -1.07 | -0.64 | 2.83 | 1.5 | -0.16 | 0.70 |
| B102 | Expf | -0.48 | -0.14 | 2.84 | 1.5 | -0.13 | 0.79 |
| B176 | Expf | 1.06 | 1.30 | 2.20 | 1.5 | -0.16 | 1.05 |
| V256A | Expf-top | -1.66 | -1.85 | 3.64 | -5.5 | 0.12 | 0.64 |
| V256B | Expf-mid | -2.41 | -3.04 | 3.65 | -6.5 | 0.28 | 0.71 |
| V256D | Expf-base | -0.48 | 0.02 | 3.46 | 1.5 | -0.12 | 0.89 |
| V256E | Expf | 2.83 | 2.28 | 2.70 | 2.5 | 0.09 | 1.28 |
| B230 | Expf | -0.77 | -0.04 | 3.09 | 1.5 | -0.27 | 0.80 |
| V019 | Expf | 1.34 | 1.64 | 2.07 | 3.5 | -0.28 | 0.94 |
| V256C | Expf-base | 0.30 | 0.70 | 3.05 | 1.5 | -0.09 | 1.07 |
| V297 | Expc | -0.60 | -0.18 | 2.69 | 1.5 | -0.19 | 0.71 |
| V312A | Expc | 0.11 | 0.27 | 2.15 | 0.5 | -0.08 | 1.04 |
| V312B | Expc-base | 0.15 | 0.26 | 1.58 | 0.5 | -0.08 | 0.97 |
| V312C | Expc-top | -0.92 | -1.60 | 2.29 | -2.5 | 0.42 | 0.82 |
| V313 | Expc | 0.30 | 0.25 | 2.21 | 0.5 | 0.18 | 1.34 |
| B215A | Expc | -0.20 | -0.24 | 3.36 | -0.5 | 0.01 | 0.91 |
| B216 | Expc | -0.16 | 0.33 | 2.53 | 1.5 | -0.27 | 0.93 |
| B217 | Expc | -1.24 | -0.97 | 2.58 | -4.5 | -0.04 | 0.68 |
| C120 | Expc | -0.75 | -0.95 | 2.53 | -3.5 | 0.16 | 0.69 |
| C259C | Expc | -0.67 | -0.60 | 2.65 | -2.5 | 0.03 | 0.83 |
| B173 | RPpf | 1.07 | 1.17 | 2.82 | 1.5 | -0.02 | 1.10 |
| B222 | RPpf | -0.75 | -0.41 | 3.47 | 1.5 | -0.02 | 0.89 |
| B223 | RPpf | -1.05 | -0.73 | 3.70 | -5.5 | 0.02 | 0.81 |
| B224 | RPpf | 0.05 | 0.51 | 2.99 | 1.5 | -0.14 | 0.88 |
| B225 | RPpf | -0.48 | 0.02 | 3.46 | 1.5 | -0.12 | 0.89 |
| V022A | Efba | 0.46 | 0.78 | 2.55 | 3.5 | -0.22 | 0.86 |
| V237 | Exlh | -0.56 | -0.42 | 2.51 | 0.5 | -0.05 | 0.91 |
| V270B | Exlh | -0.09 | 0.00 | 3.16 | -3.5 | 0.06 | 0.91 |
| V275B | Exlh | 0.07 | 0.20 | 2.34 | 0.5 | -0.06 | 1.06 |
| V275C | Exlh | 0.27 | 0.57 | 2.20 | 0.5 | -0.17 | 1.09 |
| V280 | Exlh | -1.27 | -2.01 | 3.16 | -3.5 | 0.43 | 0.88 |
| V330 | Exlh | 0.34 | 0.64 | 2.88 | 1.5 | -0.04 | 1.01 |
| V276A | Exlh-hcf ¹ | -1.65 | -2.23 | 2.85 | -3.5 | 0.32 | 0.86 |
| V276B | Exlh-hcf ¹ | -0.27 | -0.34 | 2.25 | -0.5 | 0.13 | 0.96 |
| V272 | Exlh-hcf ¹ | 1.00 | 1.12 | 2.65 | 1.5 | -0.03 | 1.28 |
| V275A | Exlh-hcf ¹ | -0.88 | -1.12 | 2.35 | -2.5 | 0.20 | 0.84 |
| V199 | Exma | -4.40 | -4.49 | 0.43 | -4.5 | 0.47 | 3.34 |
| V257 | Exma | 0.09 | 0.31 | 3.21 | 0.5 | 0.00 | 0.93 |
| V258 | Exma | -0.74 | -0.38 | 2.47 | -0.5 | -0.15 | 2.21 |
| V254 | Exma | 3.91 | 3.61 | 1.69 | 5.5 | 0.12 | 0.56 |
| V270A | Exma | -0.55 | -0.43 | 2.58 | -0.5 | -0.06 | 0.99 |
| V278 | Exma | -0.23 | 0.53 | 3.45 | 1.5 | -0.22 | 0.93 |
| B218 | Cpf | -0.32 | -0.11 | 3.18 | 0.5 | 0.02 | 1.08 |
| B203 | Cpf | -0.35 | 0.14 | 3.54 | -5.5 | -0.12 | 0.92 |
| C259A | Cpf | -1.04 | -0.58 | 2.89 | 1.5 | -0.18 | 0.72 |
| V224 | Cpc | 0.34 | 0.65 | 3.22 | 1.5 | -0.11 | 1.23 |
| C259B | RPpf | 1.42 | 1.62 | 2.22 | 1.5 | -0.06 | 1.36 |
| C294 | Cpfw | -1.00 | -0.43 | 3.84 | -5.5 | -0.06 | 0.68 |
| V101 | Cpc | -0.22 | 0.49 | 3.42 | 1.5 | -0.17 | 1.01 |

¹Hyperconcentrated-flow lahars

Table 6. Lithologic components in pyroclastic-current, lahar, and mixed-avalanche samples from the 2006 eruption of Augustine Volcano, Alaska.

[All values in weight percent. Components: low-silica andesite scoria (LSAS), dense low-silica andesite (DLSA), dense intermediate-silica andesite (DIA), high-silica andesite (HSA), high-silica andesite pumice (HSAP), and mixtures (banded) and defined in table 5. Phases and units (after Coombs and others, this volume), are defined in figure 2]

| Sample | Unit ¹ | Event | Size ² (mm) | Clasts counted ³ | LSAS | DLSA | DIA | Banded | HSA | HSAP | Oxidized | Crystals | Non- crystals |
|---------|-------------------|-------|---------------------------|--------------------------------|------|------|------|--------|------|------|----------|----------|------------------|
| V033A | Expct | 3–4 | 8 | 171 | 43.9 | 22.2 | 10.5 | 2.3 | 13.5 | 0.0 | 7.6 | 0.0 | 0.0 |
| | | | 4 | 395 | 43.3 | 22.8 | 11.1 | 1.8 | 14.7 | 0.0 | 6.3 | 0.0 | 0.0 |
| | | | 1 | 509 | 46.8 | 6.3 | 10.8 | 0.0 | 13.9 | 1.6 | 5.7 | 14.9 | 0.0 |
| | | | 32 | 3 | 66.7 | 0.0 | 0.0 | 0.0 | 33.3 | 0.0 | 0.0 | 0.0 | 0.0 |
| | | | 16 | 14 | 21.4 | 21.4 | 7.1 | 21.4 | 21.4 | 0.0 | 7.1 | 0.0 | 0.0 |
| V096 | Expct | 3–4 | 8 | 70 | 47.1 | 10.0 | 17.1 | 2.9 | 18.6 | 0.0 | 4.3 | 0.0 | 0.0 |
| | | | 4 | 513 | 50.5 | 15.2 | 12.3 | 1.6 | 15.4 | 0.0 | 5.1 | 0.0 | 0.0 |
| | | | 2 | 223 | 32.3 | 17.0 | 18.8 | 0.0 | 21.5 | 0.0 | 8.1 | 2.2 | 0.0 |
| | | | 1 | 660 | 44.7 | 5.9 | 6.1 | 0.0 | 18.8 | 0.0 | 10.2 | 14.4 | 0.0 |
| | | | 0.5 | 1,158 | 26.2 | 6.4 | 7.0 | 0.0 | 8.7 | 0.2 | 9.9 | 41.7 | 0.0 |
| | | | 0.25 | 465 | 26.5 | 3.7 | 0.0 | 0.0 | 13.8 | 0.0 | 8.2 | 48.0 | 0.0 |
| | | | 0.125 | 1,248 | 0.0 | 0 | 0 | 0 | 0.0 | 0.0 | 7.3 | 56.7 | 36.0 |
| Average | Expct | -- | -- | -- | 40.8 | 10.9 | 8.4 | 6.0 | 17.6 | 0.1 | 6.6 | 14.8 | 3.0 |
| B184A | Expct basal | 3–4 | 8 | 51 | 49.0 | 21.6 | 17.6 | 0.0 | 11.8 | 0.0 | 0.0 | 0.0 | 0.0 |
| | | | 4 | 728 | 44.2 | 23.2 | 9.5 | 0.3 | 15.7 | 0.1 | 7.0 | 0.0 | 0.0 |
| | | | 1 | 744 | 55.2 | 2.8 | 8.5 | 0.0 | 12.6 | 0.0 | 8.9 | 12.0 | 0.0 |
| B184B | Expct basal | 3–4 | 8 | 52 | 53.8 | 17.3 | 15.4 | 3.8 | 9.6 | 0.0 | 0.0 | 0.0 | 0.0 |
| | | | 4 | 305 | 48.9 | 13.8 | 8.2 | 1.6 | 20.0 | 0.7 | 6.9 | 0.0 | 0.0 |
| | | | 1 | 441 | 53.3 | 2.9 | 14.7 | 0.2 | 10.4 | 0.0 | 9.3 | 9.1 | 0.0 |
| Average | Expct basal | -- | -- | -- | 50.7 | 13.6 | 12.3 | 1.0 | 13.4 | 0.2 | 5.3 | 3.5 | 0.0 |
| B102 | Expf | 3–7 | 8 | 286 | 50.0 | 13.3 | 14.7 | 2.1 | 11.9 | 0.0 | 8.0 | 0.0 | 0.0 |
| | | | 4 | 609 | 53.5 | 11.8 | 14.4 | 0.0 | 11.2 | 0.8 | 8.2 | 0.0 | 0.0 |
| | | | 1 | 537 | 30.9 | 1.5 | 11.0 | 0.0 | 21.4 | 0.0 | 11.4 | 23.8 | 0.0 |
| B230 | Expf | 8 | 8 | 72 | 73.6 | 8.3 | 5.6 | 2.8 | 9.7 | 0.0 | 0.0 | 0.0 | 0.0 |
| | | | 4 | 703 | 56.8 | 5.3 | 16.4 | 0.1 | 15.4 | 2.4 | 3.7 | 0.0 | 0.0 |
| V019 | Expf | 9 | 8 | 147 | 48.3 | 9.5 | 12.2 | 7.5 | 17 | 0 | 5.4 | 0 | 0.0 |
| Average | Expf | -- | -- | -- | 53.0 | 8.0 | 12.4 | 13.0 | 13.9 | 0.8 | 6.3 | -- | 0.0 |
| V278 | Exma | 8 | 8 | 76 | 47.4 | 10.5 | 6.6 | 2.6 | 18.4 | 9.2 | 5.3 | 0.0 | 0.0 |
| | | | 4 | 649 | 47.8 | 10.9 | 12.3 | 1.7 | 13.3 | 2.2 | 11.9 | 0.0 | 0.0 |
| V275A | Exlh | 7 | 8 | 138 | 40.6 | 29.7 | 7.2 | 0.0 | 12.3 | 0.0 | 10.1 | 0.0 | 0.0 |
| | | | 4 | 705 | 38.2 | 15.5 | 14.6 | 0.0 | 20.4 | 0.0 | 11.3 | 0.0 | 0.0 |
| | | | 1 | 344 | 39.0 | 0.3 | 9.0 | -- | 19.5 | 0.0 | 13.1 | 19.2 | 0.0 |
| V275B | Exlh-levee | 7 | 8 | 131 | 58.8 | 11.5 | 5.3 | 0.8 | 19.1 | 0.0 | 4.6 | 0.0 | 0.0 |
| | | | 4 | 352 | 53.7 | 9.9 | 10.5 | 0.3 | 17.0 | 0.0 | 8.5 | 0.0 | 0.0 |
| | | | 1 | 671 | 31.0 | 2.5 | 6.7 | 0.0 | 20.0 | 0.0 | 14.2 | 25.6 | 0.0 |

Table 6. Lithologic components in pyroclastic-current, lahar, and mixed-avalanche samples from the 2006 eruption of Augustine Volcano, Alaska.—Continued

[All values in weight percent. Components: low-silica andesite scoria (LSAS), dense low-silica andesite (DLSA), dense intermediate-silica andesite (DIA), high-silica andesite (HSA), high-silica andesite pumice (HSAP), and mixtures (banded) and defined in table 5. Phases and units (after Coombs and others, this volume), are defined in figure 2]

| Sample | Unit ¹ | Event | Size ² (mm) | Clasts counted ³ | LSAS | DLSA | DIA | Banded | HSA | HSAP | Oxidized | Crystals | Non- crystals |
|---------|-------------------|-------|---------------------------|--------------------------------|------|-------|------|--------|------|------|----------|----------|------------------|
| V276A | Exlh | 8 | 8 | 250 | 24.0 | 17.2 | 29.6 | 1.2 | 15.6 | 0.0 | 12.4 | 0.0 | 0.0 |
| | | | 4 | 327 | 38.8 | 15.9 | 15.9 | 0.9 | 15.9 | 0.0 | 12.5 | 0.0 | 0.0 |
| | | | 1 | 402 | 43.0 | 3.7 | 10.9 | 0.0 | 12.9 | 0.0 | 15.2 | 14.2 | 0.0 |
| Average | Exlh | -- | -- | -- | 42.0 | 11.6 | 11.7 | 0.9 | 16.8 | 1.0 | 10.8 | 5.4 | 0.0 |
| B215A | Expc | 10 | 8 | 114 | 9.6 | 3.5 | 28.1 | 1.8 | 48.2 | 0.0 | 8.8 | 0.0 | 0.0 |
| | | | 4 | 959 | 9.7 | 9.2 | 38.5 | 0.0 | 39.0 | 0.0 | 2.5 | 1.1 | 0.0 |
| | | | 1 | 808 | 14.5 | 5.3 | 7.3 | 0.0 | 32.9 | 0.0 | 7.1 | 32.9 | 0.0 |
| C259C | Expc | 10 | 8 | 279 | 13.6 | 44.4 | 9.7 | 6.8 | 24.0 | 0.0 | 1.4 | 0.0 | 0.0 |
| | | | 4 | 2,080 | 35.3 | 39.3 | 9.8 | 1.2 | 11.4 | 0.0 | 2.9 | 0.0 | 0.0 |
| V313 | Expc | 10 | 8 | 10 | 0.0 | 40.0 | 30.0 | 0.0 | 30.0 | 0.0 | 0.0 | 0.0 | 0.0 |
| | | | 4 | 179 | 0.0 | 29.6 | 20.1 | 0.6 | 44.1 | 1.7 | 3.9 | 0.0 | 0.0 |
| Average | Expc | -- | -- | -- | 11.8 | 24.5 | 20.5 | 1.7 | 32.8 | 0.2 | 3.8 | 4.9 | 0.0 |
| B173 | RPpf | 10 | 8 | 78 | 9.0 | 9.0 | 19.2 | 1.3 | 56.4 | 1.3 | 3.8 | 0.0 | 0.0 |
| | | | 4 | 330 | 2.4 | 9.1 | 10.6 | 0.0 | 73.9 | 0.9 | 3.0 | 0.0 | 0.0 |
| | | | 2 | 214 | 4.2 | 10.7 | 9.8 | 0.0 | 71.5 | 0.0 | 0.5 | 3.3 | 0.0 |
| | | | 32 | 2 | 0.0 | 100.0 | 0.0 | 0.0 | 0.0 | 0.0 | 0.0 | 0.0 | 0.0 |
| | | | 16 | 13 | 38.5 | 46.2 | 7.7 | 0.0 | 7.7 | 0.0 | 0.0 | 0.0 | 0.0 |
| B222 | RPpf | 10 | 8 | 105 | 8.6 | 12.4 | 8.6 | 0.0 | 67.6 | 0.0 | 2.9 | 0.0 | 0.0 |
| | | | 4 | 723 | 5.8 | 7.9 | 3.3 | 0.0 | 79.8 | 0.0 | 3.0 | 0.1 | 0.0 |
| | | | 2 | 373 | 5.4 | 6.7 | 5.9 | 0.3 | 67.6 | 0.0 | 4.6 | 9.7 | 0.0 |
| | | | 1 | 820 | 2.7 | 3.9 | 8.3 | 0.0 | 31.7 | 18.0 | 7.0 | 28.4 | 0.0 |
| | | | 0.5 | 1282 | 0.9 | 1.6 | 9.2 | 0.0 | 19.6 | 0.0 | 6.9 | 61.8 | 0.0 |
| | | | 0.25 | 907 | 0.7 | 4.0 | 0.0 | 0.0 | 11.1 | 0.0 | 2.5 | 81.7 | 0.0 |
| | | | | | 7.1 | 19.2 | 7.5 | 0.2 | 44.3 | 2.2 | 3.1 | 16.8 | 0.0 |
| B203 | Cpf | ≥14 | 8 | 95 | 0.0 | 33.7 | 31.6 | 0.0 | 28.4 | 0.0 | 6.3 | 0.0 | 0.0 |
| | | | 4 | 641 | 0.0 | 42.6 | 7.2 | 0.0 | 46.6 | 0.0 | 3.6 | 0.0 | 0.0 |
| V101 | Cpc | ≥14 | 8 | 73 | 0.0 | 1.4 | 50.7 | 11.0 | 28.8 | 0.0 | 8.2 | 0.0 | 0.0 |
| | | | 4 | 589 | 0.0 | 4.9 | 40.6 | 0.2 | 45.7 | 0.0 | 8.7 | 0.0 | 0.0 |
| Average | Cpf | | | | 0.0 | 20.6 | 32.5 | 2.8 | 37.4 | 0.0 | 6.7 | 0.0 | 0.0 |
| V22A | Efba | | 8 | 108 | 9.0 | 63.1 | 9.0 | 0.0 | 3.6 | 0.0 | 15.3 | 0.0 | 0.0 |

¹ Units after Coombs and others (this volume), same as in table 1.

² Size is defined as particles remaining on sieve indicated; for larger size classes (≥1.0 mm), grains were sorted by using a hand lens and binocular microscope, and commonly the lithologic differences were best determined by using wetted clasts (which represented the most common field conditions). Clast-type groups were then dried, counted, weighed, and normalized to 100 percent. For smaller size classes (≤0.50 mm), sorting was done by using a single paintbrush hair under a binocular microscope. Clast types were sorted by lithology or oxidation for most size classes. The samples whose small grains were sorted had them divided among crystals, noncrystals, and oxidation. Lithologies are described in table 3.

³ Not all size classes were counted for all samples. Clasts from each size class were initially sorted from 32 mm to 0.125 mm to assess the similarity in clast-type proportions between size classes. The 4- and 8-mm size classes were deemed representative of the proportions of lithologies for many samples.

Table 8. Parameters and analysis-of-variance statistics for alternative linear models of log-transformed volume versus planimetric area for pyroclastic-current deposits worldwide and those from the 2006 eruption of Augustine Volcano, Alaska.

| Variable | Best-fit regression | Specified 2/3 slope | Specified zero slope |
|---|---------------------|---------------------------------|----------------------|
| Dome-collapse pyroclastic flows | | | |
| Slope of line | 0.659 | 0.667 | 0 |
| Intercept of line at $\log V=0$ | 1.612 | 1.5661 = $\log 37$ | 5.530 |
| Number of data pairs (N) | 21 | 21 | 21 |
| Residual degrees of freedom (DF) | 19 | 20 | 20 |
| Residual sum of squares (SS) | 0.800 | 0.801 | 5.133 |
| Residual mean square (MS) | 0.042 | 0.042 | 0.257 |
| Standard error of model (sigma) | 0.205 | 0.200 | 0.507 |
| Coefficient of determination (r^2) | 0.844 | 0.844 | 0 |
| F statistic comparison to best-fit regression | Not applicable | 0.017 | 102.9 |
| Null hypothesis | Not applicable | Accepted, 0.99-confidence level | Rejected |
| Column-collapse pyroclastic currents | | | |
| Slope of line | 0.736 | 0.667 | 0 |
| Intercept of line at $\log V=0$ | 1.779 | 2.1717 = $\log 150$ | 5.943 |
| Number of data pairs (N) | 14 | 14 | 14 |
| Residual degrees of freedom (DF) | 12 | 13 | 13 |
| Residual sum of squares (SS) | 0.110 | 0.151 | 4.731 |
| Residual mean square (MS) | 0.009 | 0.012 | 0.364 |
| Standard error of model (sigma) | 0.095 | 0.108 | 0.603 |
| Coefficient of determination (r^2) | 0.977 | 0.968 | 0 |
| F statistic comparison to best-fit regression | Not applicable | 4.493 | 547.9 |
| Null hypothesis | Not applicable | Accepted, 0.99-confidence level | Rejected |
| Surge-like pyroclastic currents | | | |
| Slope of line | 0.653 | 0.667 | 0 |
| Intercept of line at $\log V=0$ | 2.794 | 2.718 = $\log 520$ | 6.509 |
| Number of data pairs (N) | 4 | 4 | 4 |
| Residual degrees of freedom (DF) | 2 | 3 | 3 |
| Residual sum of squares (SS) | 0.008 | 0.008 | 0.444 |
| Residual mean square (MS) | 0.004 | 0.003 | 0.148 |
| Standard error of model (sigma) | 0.064 | 0.053 | 0.385 |
| Coefficient of determination (r^2) | 0.981 | 0.981 | 0 |
| F statistic comparison to best-fit regression | Not applicable | 0.045 | 105.5 |
| Null hypothesis | Not applicable | Accepted, 0.99-confidence level | Rejected |